TRIBHUVAN UNIVERSITY

INSTITUTE OF ENGINEERING

PULCHOWK CAMPUS

THESIS NO: PUL079MSPSE006

"Assessment of Voltage Stability Using Non-Linear Control of Distributed Power Flow Controller in Multi-Machine Power System"

By

Bimal Adhikari

A THESIS

SUBMITTED TO THE DEPARTMENT OF ELECTRICAL ENGINEERING IN PARTIAL FULFILLMENT OF THE REQUIREMENTS FOR THE DEGREE OF MASTER OF SCIENCE IN POWER SYSTEM ENGINEERING

DEPARTMENT OF ELECTRICAL ENGINEERING

LALITPUR, NEPAL

April 2025

Assessment of Voltage Stability Using Non-Linear Control of Distributed Power Flow Controller in Multi-Machine Power System

By

Bimal Adhikari

C.R.N.: PUL079MSPSE006

Thesis Supervisor

Associate Professor Jeetendra Chaudhary

Department of Electrical Engineering

Pulchowk Campus, IOE, TU

A Thesis

submitted to the Department of Electrical Engineering in partial fulfillment of the requirements for the Degree of Master of Science in Power System Engineering

Department of Electrical Engineering

Institute of Engineering, Pulchowk Campus

Tribhuvan University

Lalitpur, Nepal

April 2025

COPYRIGHT©

त्रिभुवन विश्वविद्यालय
TRIBHUVAN UNIVERSITY
इञ्जिनियरिङ्ग अध्ययन संस्थान
INSTITUTE OF ENGINEERING
पुल्चोक क्याम्पस
PULCHOWK CAMPUS
DEPARTMENT OF ELECTRICAL ENGINEERING
Pulchowk, Lalitpur

Accredited by University Grants Commission (UGC) Nepal 2020

Institute of Engineering Electrical Engineering Department Pulchowk Campus

CERTIFICATE OF APPROVAL

The undersigned certify that they have read, and recommended to the Institute of Engineering for acceptance, a thesis entitled **"Assessment of Voltage Stability using Non-Linear Control of Distributed Power Flow Controller in Multi-Machine Power System"** submitted by **Bimal Adhikari** in partial fulfilment of the requirements for the degree of **Master of Science in Power System Engineering**.

.....

Assoc. Prof. Jeetendra Chaudhary
Department of Electrical Engineering
Pulchowk Campus, Lalitpur
(Supervisor)

.....

Dr. Laxman Maharjan
Former Assistant Manager, Corporate R&D
Headquarters, Fuji Electric Co., Ltd., Japan
(External Examiner)

.....

Asst. Prof. Dr. Bishal Silwal
Program Coordinator
MSc. in Power System Engineering
Department of Electrical Engineering
Pulchowk Campus, Lalitpur

.....

Assoc. Prof. Dr. Basanta Kumar Gautam
Head of Department
Department of Electrical Engineering
Pulchowk Campus, Lalitpur

April 2025

Tel: +977-1-5443081, Email: doee@pcampus.edu.np, Website: www.doee.pcampus.edu.np

DECLARATION AND AUTHORIZATION

This statement formally certifies that the enclosed thesis represents the candidate's authentic and independent research, undertaken solely by them and not previously presented for any other academic qualification or used to obtain a prior degree. It further grants the Institute of Engineering, Pulchowk Campus, explicit permission to disseminate this work for scholarity purposes, including lending copies to other institutions or individuals, and reproducing it through photocopying or other means, in its entirety or in part, ensuring its availability for academic research.

……..

Candidate

Bimal Adhikari

PUL079MSPSE006

Department of Electrical Engineering

Pulchowk Campus, Lalitpur

……..

Supervisor

Assoc. Prof. Jeetendra Chaudhary

Department of Electrical Engineering

Pulchowk Campus, Lalitpur

ACKNOWLEDGEMENT

I would like to extend my heartfelt gratitude to a number of individuals and institutions whose support and encouragement have been instrumental in the completion of this thesis. First and foremost, I owe a profound debt of gratitude to my supervisor, **Assoc. Prof. Jeetendra Chaudhary**, whose exceptional guidance, insightful feedback, and unwavering commitment have shaped this research from its inception to its final form. His expertise in electrical engineering and his willingness to provide constructive advice during every stage of this journey have been invaluable, inspiring me to push the boundaries of my understanding and refine my work to meet the highest academic standards.

I am also deeply thankful to the entire faculty and staff of the **Department of Electrical Engineering** at the Institute of Engineering (IoE), Pulchowk Campus. Their creation of a good and supportive academic environment has greatly enriched my learning experience and enabled me to conduct this research effectively. I am particularly grateful to my colleagues and peers within the department, whose collaborative spirit and intellectual exchanges have broadened my perspective and motivated me to excel.

Beyond the academic sphere, I wish to express my sincere appreciation to my friends, who have offered endless encouragement, shared in my challenges, and celebrated my progress. Their companionship has been a vital source of motivation during moments of doubt. Above all, I am immensely indebted to my family, whose unconditional love, patience, and understanding have sustained me through the demanding phases of this endeavor. Their belief in my abilities and their constant moral support have been the bedrock of my perseverance.

This thesis stands as a testament to the collective efforts and belief of all those mentioned above. I am truly honored to have been supported by such a remarkable network of individuals and institutions. Thank you all for being an integral part of this rewarding academic journey and for helping me turn my aspirations into reality

- Bimal Adhikari

ABSTRACT

Voltage stability is a critical aspect of secure and reliability power system operation, particularly under high loading and contingency conditions. This study begins with the development of a methodology for assessing voltage stability in a multi-machine power system using a proposed Voltage Stability Index (VSI) and Voltage Collapse Proximity Index (VCPI). Subsequently, a methodology is proposed for enhancing both voltage stability and power flow indices by deploying Distributed Power Flow Controller (DPFC) at optimally located buses. The optimal location and sizing of the DPFC are determined using a metaheuristic optimization technique – the Multi-Objective Grey Wolf Optimization (MOGWO) algorithm.

Nepal's grid system experiences voltage stability issues due to remotely located generation sources, short transmission lines, and inadequate reactive power support. Therefore, the assessment of voltage stability in Integrated Nepal Power System (INPS) is essential to identify the buses most prone to voltage instability. The results of the assessment revealed that bus 14 in Kathmandu, bus 39 in Hetauda, and bus 104 in Attaria grid division are the most vulnerable load buses in their respective regions. Conversely, bus 85 in Pokhara grid division was found to be the most stable, due to its lesser sensitivity to reactive power variation.

To address the challenges posed by weak buses that are prone to voltage collapse and overload, a FACTS device – DPFC is proposed. DPFC's capability to independently control series and shunt parameters enhances both voltage regulation and power flow flexibility. Also, due to modular structure, lower cost, reliable and ability to operate without DC link, favors DPFC an effective solution for INPS, which is characterized by short and spatially dispersed transmission lines.

Non-linear DPFC system control the output of series converter ($V_{se,1}\angle\delta_{se,1}$) by feedback linearization method referencing the load on the line. This regulates the power flow on DPFC compensated line. This enables effective voltage and power angle regulation based on the inductive and capacitive mode of operation.

Deploying DPFC in a multi-machine power system presents challenges, particularly for real-world implementation in the INPS. In this study, the DPFC is deployed in the IEEE 118 standard test system by optimizing its location and sizing in three selected regions – between buses 6-5, 59-60, and 110-109.

The MOGWO is used to determine the optimal placement and sizing of the DPFC, with multi-objectives of maximizing total VSI, minimizing total line losses and VCPI, increased system loadability, and reduction of voltage deviation across buses. Comparative analysis of DPFC compensated system with uncompensated system showed a significant improvement in both voltage stability and power flow performance.

Keywords: Voltage Collapse Proximity Index, Voltage Stability Index, Integrated Nepal Power System, Distributed Power Flow Controller, Multi-Objective Grey Wolf Optimizer, Non-linear System, Optimal Location, Optimal Sizing.

ABBREVIATIONS

IEEE:	**Institute of Electrical and Electronics Engineers**
DOED:	**Department of Electricity Development**
NEA:	**Nepal Electricity Authority**
VSI:	**Voltage Stability Index**
VCPI:	**Voltage Collapse Proximity Index**
FACTS:	**Flexible AC Transmission System**
UPFC:	**Unified Power Flow Controller**
DPFC:	**Distributed Power Flow Controller**
MOGWO:	**Multi-Objective Grey Wolf Optimizer**
ULTC:	**Under-Load Tap Changers**
INPS:	**Integrated Nepal Power System**
IPPs:	**Independent Power Producers**
PSOD:	**Power System Operation Directorate**
LDC:	**Load Dispatch Centre**
SSSC:	**Static Synchronous Series Compensator**
SVC:	**Static Var Compensator**
STATCOM:	**Static Compensator**
TCSC:	**Thyristor Controlled Series Capacitor**
MOGWO:	**Multi-Objective Grey Wolf Optimization**
WECS:	**Water and Energy Commission Secretariat**

TABLE OF CONTENTS

LIST OF TABLES

LIST OF FIGURES

CHAPTER ONE: INTRODUCTION

1.1 Background

Growing demand, unequal generation distribution, and inadequate reactive power support have made it more difficult to ensure the steady and dependable operation of electric power systems. Voltage instability, a common consequence of such operating conditions, poses a significant threat to system security. It is characterized by an uncontrollable drop in voltage levels, often leading to voltage collapse and widespread blackouts. Key contributors to voltage instability include high line loading, long-distance or remote generation, insufficient reactive compensation, and low sending-end voltages.

Voltage stability assessment, therefore, is a fundamental aspect of planning and operation of power system. It involves determining proximity of a system to instability and identifying critical locations (buses or lines) vulnerable to voltage collapse. Analytical tools such as the VSI and VCPI provide quantitative measures for identifying weak points within the grid and are central to the methodology adopted in this study.

To improve voltage stability and power flow control of multi-machine power system, FACTS have been widely adopted. Among them, the DPFC offers distinct advantages, particularly for systems like the INPS. Unlike the UPFC, the DPFC eliminates the need for a common DC link by utilizing third-harmonic components for active power exchange between shunt and series converters. This not only enhances modularity and reduces cost but also simplifies insulation and maintenance—making DPFC highly suitable for Nepal's predominantly short-line and resource-constrained transmission network.

Given the nonlinear dynamics introduced by power electronic devices like the DPFC, conventional linear control strategies fall short in ensuring reliable operation under varying grid conditions. This is addressed in the current study by adopting nonlinear control via state feedback linearization, which is a technique that changes the control and state variables to convert a nonlinear system into an equivalent linear one. This enables decoupled control of power components, offering improved responsiveness and robustness.

However, for effective deployment, the location and capacity of the DPFC must be optimally selected. Arbitrary placement can lead to underutilization or system inefficiencies. Hence, this study integrates the MOGWO, a nature-inspired metaheuristic algorithm, to identify optimal DPFC placement and sizing. The optimization process simultaneously considers multiple objectives such as minimization of voltage deviation, power losses, and shunt device size, ensuring a balanced technical and economic solution.

By integrating nonlinear control with optimal placement and sizing, this research aims to enhance voltage stability and controllability of power flow in a multi-machine environment, validated modified IEEE standard test system providing a clear roadmap to implementation of DPFC in real-world systems for future work.

1.2 Problem Statement

The INPS, although advancing in generation capacity and electrification coverage, is facing persistent challenges related to voltage instability, particularly during peak loading conditions, contingencies, and seasonal variations. Buses such as bus 14 (Kathmandu), bus 39 (Hetauda), and bus 104 (Attaria) frequently experience poor voltage profiles, which can escalate into voltage collapse if not mitigated effectively.

Traditional voltage control methods using fixed or switched capacitor banks, under-load tap changers (ULTCs), and load shedding offer limited dynamic response and are often inadequate in real-time grid operations. Moreover, the integration of intermittent renewable energy sources, growing regional imbalances in load-generation patterns, and insufficient reactive power support exacerbate system instability.

While FACTS devices like UPFCs have been proposed for enhancing voltage stability, their centralized architecture and high cost make them less feasible for geographically diverse and economically constrained systems like the INPS. In contrast, the DPFC offers a promising alternative due to its modular design, cost-efficiency, and ability to control power flow independently.

Despite this, the existing body of work has largely overlooked two critical aspects:

1. The optimal siting and sizing of DPFC for maximum voltage support and cost-effectiveness.
2. The application of nonlinear control strategies, such as feedback linearization, to exploit the full dynamic potential of DPFC in complex, multi-machine environments.

This research addresses these gaps by implementing a nonlinear control strategy for DPFC and determining its optimal configuration using the MOGWO, aiming to provide a technically robust and economically viable solution for enhancing voltage stability in the INPS.

1.3 Objectives

The primary objective of this study is to develop a comprehensive framework for assessment and enhancement of voltage stability using nonlinear control of a DPFC in a multi-machine power system. The specific objectives are:

1. **Voltage Stability Assessment**:

   To evaluate the voltage stability of the INPS under stressed conditions using analytical techniques, particularly the VSI and VCPI.

2. **Nonlinear Control Implementation**:

   To design and implement a nonlinear controller based on feedback linearization for the DPFC, enabling precise regulation of power flow and voltage support across a multi-machine environment.

3. **Optimization of DPFC Location and Capacity**:

   To optimize location and capacity of DPFC units using meta-heuristic optimization tool MOGWO considering multiple objectives for enhancement of system efficiency and reliability.

4. **System Performance Evaluation**:

   To evaluate the impact of optimally located and controlled DPFC on voltage profiles, power flow, and overall system stability of DPFC compensated IEEE 118-bus.

1.4 Scope of the Study

This study is conducted within the following technical and methodological boundaries:

- The system under investigation is a multi-machine power system modeled using MATLAB, with particular emphasis on voltage stability analysis under varying operating scenarios.
- DPFC dynamic modeling includes both the series and shunt-side converters, along with third harmonic power flow interactions.
- A nonlinear system of DPFC controls the output of series DPFC based on state feedback linearization technique.
- The MOGWO is employed optimize location and capacity of the DPFC device using a set of predefined technical objectives.
- DPFC based multi-machine power system validated on standard IEEE 118 bus test system focusing on steady-state stability.

1.5 Limitations of the Study

While the study provides a comprehensive analysis and simulation-based validation, it has the following limitations:

- **Applicability to Short Transmission Lines**:

  Although DPFC are typically designed for long transmission corridors, this study implementation for short and medium-length lines, which dominate the INPS. The results are therefore context-specific.

- **Exclusion of Real-Time Hardware Testing**:

  The study is limited to offline simulations and does not include hardware-in-the-loop (HIL) or real-time implementation, which would be required for practical deployment.

- **Simplified Load Modeling and Forecasting**:

  The demand-side variations are modeled as static loads. Advanced load forecasting techniques and dynamic models of distributed energy resources are not considered.

- **No Economic Cost-Benefit Analysis**:

  While optimization includes size minimization as a surrogate for cost, a full economic feasibility study of DPFC deployment in Nepal's grid is beyond the scope of this work.

- **Limited Contingency Scenarios**:

  Only selected N-1 contingency and loading conditions are simulated. Broader system security assessments, including protection coordination, are not within the current scope.

1.6 Report Structure

This report is organized into five chapters, each systematically addressing the assessment and enhancement of voltage stability using nonlinear control of DPFC in a multi-machine power system:

Chapter One: Introduction outlines the context and motivation for the study, describing the increasing challenges of assessment of voltage stability in multi-machine power system through and introducing role of DPFC in the relevant field. It further states the problem, research objectives, scope, and limitations of the study, setting a clear direction for the reader.

Chapter Two: Literature Review provides a comprehensive review of existing work and developments related to voltage stability, the operation of the NEA, and the application of FACTS devices. It discusses previous research findings on voltage stability assessment methods and the use of nonlinear control strategies in power systems, especially the potential of DPFC for the INPS.

Chapter Three: Methodology is technical and detailed, presenting the mathematical foundations of the research, including power equations and voltage stability indices such as the VSI and VCPI. It also explains the load flow analysis in systems with DPFC integration, harmonic power flow, and nonlinear control strategies based on feedback linearization. This chapter describes how the DPFC is modeled, analyzed, and optimized using algorithms like the MOGWO.

Chapter Four: Results and discussions contain the detailed simulation result of voltage stability assessment of INPS, optimal location and sizing of the DPFC using MOGWO. The compensated and uncompensated test systems are further made comparative analysis with different indices for optimal and maximum control strategy of nonlinear system of DPFC.

Chapter Five: Conclusion and Recommendations summarizes the key findings of the study, concludes the impact of DPFC on voltage stability enhancement, and provides recommendations for future work and practical implementation within Nepal's power system context.

CHAPTER TWO: LITERATURE REVIEW

2.1 Introduction to Voltage Instability

Voltage instability primarily arises from excessive loading of transmission lines, long distances between generation sources and load centers, low source voltages, and inadequate reactive power support at load points. The use of transmission system V–P (voltage vs. active power) and Q–V (reactive power vs. voltage) characteristics illustrates the core mechanisms behind voltage instability. Although these characteristics can be derived using conventional power-flow methods, such approaches may not be the most efficient for in-depth voltage stability studies. Voltage stability analysis typically involves assessing the system's proximity to voltage collapse and understanding the underlying mechanisms, including contributing factors, weak voltage areas, and effective corrective measures.

2.2 Overview of NEA's Operations and Achievements [2]

The NEA, in its 39th year of operation, has continued to fulfill its mandate of ensuring the generation, transmission, and distribution of reliable, high-quality, and economically viable electrical energy to consumers across Nepal. In the post–load shedding era, NEA has demonstrated substantial progress across multiple operational domains. Notable achievements include a significant reduction in system losses, augmentation of generation capacity, expansion of the national transmission network, accelerated electrification efforts, and the initiation of cross-border electricity exports. During the fiscal year under review, NEA recorded the lowest transmission and distribution (T&D) losses in its operational history. The total installed generation capacity reached 3,157 MW, with an additional 473 MW integrated into the system through the commissioning of new hydropower and other generation projects.

The number of electricity consumers has shown a steady upward trend, reaching 5.46 million in fiscal year (FY) 2023/24—an annual growth of 6.33% compared to 5.14 million in FY 2022/23. The total energy available in the national system rose from 12,369 GWh in the previous fiscal year to 13,966 GWh during the same time, representing an increase of 12.91%. NEA and its affiliated businesses provided 39.42% of this total energy availability, with domestic IPPs contributing 47.00% and imports from India making up the remaining 13.57%.

Domestic electricity consumption for FY 2023/24 rose to 10,243 GWh, reflecting a 9.46% increase from 9,358 GWh recorded in FY 2022/23. Energy exports to India experienced a notable surge, reaching 1,946 GWh—an increase of 44.57% over the 1,346 GWh exported in the previous year. Additionally, NEA achieved further improvements in system efficiency, reducing system losses from 13.46% in FY 2022/23 to 12.73% in FY 2023/24.

Significant advancements were also made in transmission infrastructure. The total length of high-voltage transmission lines increased from 5,742 circuit kilometers to 6,508 circuit

kilometers. Similarly, the total installed substation capacity rose from 8,867 MVA to 13,050 MVA. Over the past eight years, NEA has successfully added 3,597 circuit kilometers of transmission lines and expanded substation capacity by 10,826 MVA—an achievement that underscores the authority's continued commitment to strengthening Nepal's power system infrastructure.

2.2.1 TRANSMISSION DIRECTORATE:

Under the direction of the Deputy Managing Director, the NEA's Transmission Directorate is principally in charge of the nation's high-voltage transmission infrastructure's design, construction, modernization, operation, and maintenance. Existing high voltage transmission lines includes a total of 514.6, 3967.87, 1105 and 384 circuit kilometers of 66, 132, 220 and 400 kV line

2.2.2 Power System Operation Directorate (PSOD)

The PSOD, functioning under the Transmission Directorate of the NEA, serves as the central authority for overseeing the coordinated and integrated operation of Nepal's national power system. Commonly referred to as the LDC, it operates as the principal control hub, responsible for real-time monitoring, control, and optimization of the national grid. By continuously evaluating system parameters, network constraints, and operational limits, PSOD ensures the secure, stable, and efficient functioning of the grid. Its primary mandate is to maintain a reliable and uninterrupted supply of high-quality electrical power to consumers across the country.

Highlights of LDC's Performance in FY 2080/81

2.2.2.1 Voltage and Frequency Control

Voltage and frequency are essential markers of power quality. In FY 2080/81, the system frequency was well maintained around 50 Hz. Most substations operated within the voltage limits set by the Nepal Electricity Grid Code — ± 10% for up to 132 kV and ± 5% for 220 kV and above. However, some substations in the Central Terai, Mid-Western, and Eastern regions experienced low voltage during peak summer demand. While capacitor banks and reactors installed by the Grid Operation Department helped mitigate the issue, additional reinforcement is needed to maintain voltage stability during critical periods.

2.2.2.2 Partial System Tripping

Proactive system monitoring and timely interventions by system operators during faults and abnormal conditions significantly contributed to minimizing partial system tripping incidents in FY 2080/81. The number of partial trippings decreased to 66, down from 72 in the previous fiscal year, with a total interruption duration of 7 hours and 38 minutes—also reflecting a reduction in outage time. Most of these events were attributed to ongoing transmission line constraints and insufficient contingency provisions. Nonetheless, system

restoration times were notably reduced due to the efficient and prompt actions of the operating personnel.

2.2.3 Challenges

With the continued integration of substantial generation capacities into the national grid, the existing, aging transmission infrastructure has become increasingly inadequate for efficient power evacuation to major load centers. Despite the accelerated expansion of transmission networks, progress remains behind schedule relative to the operational requirements dictated by current generation and load growth dynamics.

System behavior is subject to seasonal variability, driven by fluctuations in temperature and precipitation patterns, which in turn impact the loading levels of transmission lines, power transformers, and the overall performance of critical infrastructure at various times. Key 132 kV transmission corridors—such as Matatirtha-Hetauda, Damauli-Bharatpur, Marsyangdi-New Bharatpur, Duhabi-Damak, Dhalkebar-Nawalpur-Chapur, and Bhaktapur-Lamosanghu—routinely operate near or at their thermal limits during specific periods. This persistent overloading has frequently led to equipment stress and partial outages across the network.

Further compounding operational challenges are transformer capacity constraints at major substations including New-Khimti, Hetauda, Syuchatar, and Balaju, which significantly hinder load dispatch flexibility and voltage stability. The absence of sufficient *n-1* contingency provisions exacerbates the vulnerability of the power system, placing sustained operational pressure on the System Operation Department and threatening both supply reliability and power quality.

The western region of the country continues to experience supply deficits due to limited local generation capacity, which is insufficient to meet the increasing regional demand. Meanwhile, transmission bottlenecks prevent the transfer of surplus power generated in the eastern region to the west, often resulting in voltage regulation issues and system instability.

The evacuation of energy from newly commissioned IPPs is constrained by existing transmission capacity limitations and systemic network bottlenecks, representing a significant operational challenge for the LDC. These issues are particularly pronounced during the monsoon season, where frequent unplanned outages and emergency tripping events of generating stations and transmission lines disrupt system balance, intermittently affecting cross-border import-export schedules and domestic supply continuity.

Additionally, unanticipated fluctuations in the consumption patterns of large and bulk consumers create operational uncertainty, complicating real-time balancing and network management. These irregularities frequently cause deviations from scheduled transactions, leading to overloading of transmission corridors and penal charges incurred by the NEA under the Deviation Settlement Mechanism (DSM).

Timely and strategic interventions—including transmission reinforcement, transformer augmentation, implementation of robust *n-1* criteria, and improved demand forecasting—are essential to ensure system resilience, optimal resource utilization, and the delivery of reliable, high-quality power supply to end-users.

2.2.4 Grid Connection Agreement

Completion of Grid Connection Agreements with 31 IPPs with Grid Operation Department has enabled the integration of a total generation capacity of 2,473.879 MW into the national grid. Of the total agreements, 27 IPPs are set to contribute a combined hydroelectric capacity of 2,413.879 MW, while the remaining 4 IPPs will supply a total of 60 MW through solar photovoltaic generation.

2.3 Planned Transmission Network [3]

The national transmission network has been carefully planned to guarantee dependable electricity evacuation from all hydropower stations throughout the nation, in accordance with the Transmission System Development Plan of Nepal. In addition to an anticipated peak load requirement of 18 GW by 2040, the proposed transmission system is intended to accommodate a total of 38 GW of hydropower generating that is now in service, under construction, and planned.

To facilitate efficient power flow, major hub substations have been identified in proximity to clusters of significant hydropower projects and major load centers. The transmission corridors predominantly align with major river basins, enabling the interconnection of these key substations. Furthermore, the integration of north-south transmission lines from the mid-hill to the southern Terai region creates a 400 kV backbone loop, forming a robust and redundant high-voltage transmission ring essential for national power reliability and system stability.

The national transmission network is segmented into five operational zones, each engineered to be self-sufficient in generation based on its respective regional load demands. While minimal inter-zonal power exchange is anticipated under normal operating conditions, each zone retains the capability for inter-area power transfer, enhancing national grid flexibility and resilience.

2.4 Assessment of Voltage Stability

Several voltage stability indices have been presented to evaluate the voltage stability of a multi-machine power system. Haque (1995) introduced the Thevenin equivalent methodology to transform a multi-machine power system into a two-bus network in order to accomplish the assessment more quickly and effectively [4]. VCPI was introduced by Balamourougan et al. (2004) to identify buses that are susceptible to voltage instability [5]. Maharjan et al. (2015) present a novel form of VSI that evaluates the voltage stability of primarily two test bus systems, the IEEE 39 bus and IEEE 118 bus test system [6]. This method is contrasted with the VCPI [4] and the p-v curve [1].

2.5 FACTS Devices for Voltage Stability Improvement

Through reactive power control and voltage profile regulation, FACTS devices are essential for improving voltage stability. Pioneers of FACTS technology, Hingorani and Gyugyi (2000), highlighted the importance of power electronics-based controllers in enhancing power systems' dynamic and steady-state performance. FACTS devices are classified into shunt, series, and combined types—such as SVC, STATCOM, TCSC, and UPFC. Shunt devices like SVC and STATCOM provide fast-acting reactive power support at critical buses, improving voltage levels and increasing system loadability. [7]

Gadal et al. (2023) further reviewed various VSIs and compared the effectiveness of FACTS devices in mitigating voltage instability. Their study shows that FACTS devices, when properly placed and selected, can significantly enhance voltage margins and delay voltage collapse during contingencies. Among them, STATCOM and UPFC demonstrated superior performance in maintaining stable voltage profiles under stressed system conditions. [8]

2.6 Distributed Power Flow Controller

According to Yuan et al. (2010), DPFC is a novel idea that uses the same line but a different frequency to transfer active power between shunt and series converters, giving it the same level of control as UPFC. [9]

Gedam et al. (2018) compared UPFC and DPFC for power quality enhancement and found that DPFC provides higher operational reliability, better electrical efficiency, and improved power quality. They noted that while UPFC uses two three-phase converters linked by a DC bus, the DPFC architecture distributes the series converters and uses a single shunt converter, enhancing scalability and fault tolerance. [10]

Qian et al. (2021) described the deployment of DPFC technology on the 220 kV Gan Quan–Xiang Fu lines in China demonstrated its effectiveness in managing power flow under N-1 contingency scenarios. When one line was out of service, DPFC reduced the overload from 589 MW to below 450 MW, keeping the system within safe operating limits. [11,12]

Additionally, Qian et al. have shown that as load, receiving power, and new energy generation increase, power flow imbalance—that is, the mismatch between line power flow and current-carrying capacity—becomes increasingly severe during power grid operation, leading to low operating efficiency of power grid assets. The DPFC, which has the benefits of being compact, light, and inexpensive, is used to regulate the power flow. [11]

2.7 Applicability of DPFC in INPS under N-1 Contingency

Similarly, the INPS faces risks of line overload and instability under N-1 conditions, especially on key 132 kV and 220 kV corridors. DPFC can be a practical solution for dynamic power flow control in such cases, improving reliability without major infrastructure upgrades.

With trends in device miniaturization, increased compensation capacity, and applicability to higher voltage levels, DPFC is well-suited for future deployment in INPS to enhance system security and operational flexibility.

Though DPFC was initially developed with long-distance transmission applications in mind, its modular nature and independent series control can also benefit short transmission lines found in INPS. Unlike UPFC, which applies centralized voltage control, DPFC can regulate local segments of the grid, which is highly beneficial for voltage regulation and power flow optimization in a system with short, overloaded lines, such as in the hilly and rural terrains of Nepal.

Moreover, DPFC's lower cost and modular deployment make it suitable for Nepal, where budget constraints and geographical challenges limit the installation of centralized FACTS devices. As noted, Yuan et al, the absence of a high-rating DC link in DPFC reduces insulation requirements and eases maintenance, which is a practical advantage for INPS substation operators with limited resources.

2.8 DPFC for Voltage Stability and Power System Enhancement

Reddy (2015) emphasizes how DPFC distributes several single-phase converters throughout the network, doing away with the common DC link utilized in UPFC. This design enhances system reliability through redundancy, reduces insulation requirements due to its floating configuration, and lowers overall system cost. Simulation studies verified DPFC's ability to improve power system performance under various conditions. [13]

Aali and Maghouli (2016) looked into incorporating an adaptive neuro-fuzzy inference system (ANFIS) into the auxiliary control scheme of the DPFC in a different study. Across a broad range of operating conditions, the ANFIS-based controller effectively enhanced system damping and maintained stability using wide-area data from Phasor Measurement Units (PMUs). Under dynamic disturbances, this hybrid intelligent controller outperformed conventional control techniques. [14]

Nascimento and Gouvêa (2017) addressed the need of placement of FACTS devices optimally in power systems, including DPFC, for voltage stability enhancement. They proposed an automatic allocation method using evolutionary algorithms. The approach was tested on IEEE standard systems, showing effective enhancement in voltage stability compared to conventional optimization methods. [15]

The use of DPFC in a 14-bus test system exposed to transmission line disruptions was investigated by Bahmani et al. (2017). According to their investigation, DPFC was successful in preserving system stability and power quality during line interruptions by bringing voltage, active power, and reactive power levels back to levels that were nearly normal. [16]

Dai et al. (2019) presented an optimization framework using Mixed Integer Linear Programming (MILP) to determine the most cost-effective configuration of DPFCs. Their approach considered both economic factors and technical performance, identifying the optimal number, location, and settings of DPFC units. Simulation results on the IEEE RTS-79 system confirmed that this method successfully enhanced system loadability while minimizing investment costs. [17]

2.9 DPFC Non-Linear Control System

Godbole and George (2023) proposed an optimal harmonic load flow algorithm that highlights the importance of accurate harmonic modeling and compensation. [18] Through series and shunt converters, the DPFC, an improved version of the UPFC, enables separate regulation of active and reactive power. Its modularity, dependability, and control capabilities over a broad operating range are improved by doing away with a common DC link and using third-harmonic current for power exchange (Ramesh & Reddy, 2015). [19]

For robust performance in multi-machine power systems, nonlinear behaviors of DPFC must be addressed. Traditional linear controllers often fail under wide variations of system conditions. Tang et al. (2019) proposed a nonlinear control approach by deriving exact feedback linearization of DPFC's 5th-order nonlinear model. This transformation allows a decoupled control design where nonlinear system dynamics are mapped into a linear control framework, ensuring stability and fast response across varying grid scenarios. [20]

Further, Yan et al. (2019) demonstrated that nonlinear optimal control using Lyapunov-based functions and state feedback improves the effectiveness of DPFC in damping power oscillations. Similarly, the feedback linearization control strategy offers greater flexibility and precision than conventional methods, validating its suitability for real-time grid stability enhancement. [21]

Moreover, the hierarchical control method proposed by Xiao and Wang (2018) enables coordinated regulation among multiple DPFC units, ensuring accurate power flow control in multi-machine systems. This is vital for engineering-scale implementations. [22]

Jin et al. (2017) expanded DPFC capabilities by integrating Modular Multilevel Converter (MMC) topologies to the shunt side, improving voltage levels and scalability. To support practical application and testing, Tang et al. [23] (2021) developed a closed-loop real-time digital/analog simulation platform using ADPSS and dSPACE, enabling dynamic validation of DPFC models under transient and steady-state conditions. [24]

2.10 DPFC Optimal Location and Capacity Evaluation

The optimal placement of DPFCs plays a vital role in improving voltage stability, reducing power losses, and managing power flow in transmission networks. Unlike UPFCs, DPFCs eliminate the need for a common DC link, providing structural simplicity and cost-effectiveness.

Venkatesh et al. (2014) applied a Bang-Bang control approach to compare UPFC, IPQC, and DPFC on the IEEE 14-bus system. Their study found that DPFC provided better efficiency and voltage regulation when optimally placed. [25]

Chakravorty and Saraswat (2019) used the Artificial Algae Algorithm (AAA) to determine optimal DPFC placement. Testing with one and two DPFCs on the IEEE 14-bus system showed improved transmission capacity and system stability. [26]

Ismail et al. (2020) reviewed various optimization techniques for reactive power compensation devices. Although not focused on DPFCs, the study emphasized the importance of optimal location and sizing using hybrid and metaheuristic methods for improving power system performance. [27]

Designing the capacity and internal parameters of the DPFC is also crucial. Pi et al. (2014) proposed a method to size the series and shunt converters based on power flow variations and voltage levels to ensure compatibility and efficiency. [28] Zhai et al. (2020) extended this by introducing a systematic approach for designing converter capacities and filter parameters. Their PSCAD simulations showed over 70% capacity utilization and stable voltage performance, validating DPFC's suitability in real-world systems. [29]

A novel MOGWO technique was presented by Mirjalili et al. and evaluated on ten benchmark issues. Both the qualitative and quantitative results demonstrated better convergence and solution variety than MOEA/D and MOPSO. [30]

The MOGWO has been successful in resolving the multi-objective placement challenge. It is a good approach for DPFC optimal location studies because it strikes a balance between competing objectives including stability improvement, voltage profile improvement, and loss reduction.

CHAPTER THREE: METHODOLOGY

3.1 Research Methodology

The research methodology is systematically structured to evaluate the voltage stability of the INPS and to enhance the voltage stability of a multi-machine power system through the application of a DPFC. The key steps involved in the methodology are as follows:

1. **Problem Identification**

   The study begins by identifying the primary challenges affecting the INPS, including voltage instability, inefficient power flow management, and energy losses. These issues serve as the motivation for exploring advanced control strategies.

2. **Literature Review**

   A detailed review of relevant literature is conducted to build foundational knowledge on voltage stability analysis, FACTS devices, and specifically, DPFC technology. This review provides insights into existing methodologies and identifies research gaps.

3. **Modeling and Simulation**

   The INPS is modeled using MATLAB/Simulink to analyze its voltage stability characteristics under various conditions. A dynamic model of the DPFC, incorporating its nonlinear control strategy, is also developed and integrated into the system.

4. **Voltage Stability Assessment**

   VSIs are utilized to evaluate the voltage stability performance of the INPS. These indices help identify weak buses and critical conditions under different loading scenarios.

5. **Optimal Placement and Sizing of DPFC**

   A MOGWO algorithm is employed to determine the optimal location and sizing of the DPFC within the INPS. The optimization process considers multiple objectives, including the maximization of voltage stability margins and minimization of active power losses.

6. **Implementation of Nonlinear Control**

   Advanced nonlinear control techniques are applied to the DPFC to enhance its operational effectiveness in voltage regulation and power flow control. The control strategy is designed to improve dynamic response and stability.

7. **Performance Evaluation**

   The performance of the DPFC is evaluated by analyzing its impact on the INPS. Key performance indicators such as voltage profiles, power flows, and system losses are examined through detailed simulations.

8. **Analysis and Conclusion**

   The simulation results are analyzed to assess the effectiveness of the DPFC in improving voltage stability. Based on these findings, practical recommendations are provided for the deployment of DPFC technology in real-world power systems.

3.2 Power Equations

A simplified single-line depiction of a transmission line linking two buses, designated bus m and bus k, is shown in Figure 3.1. This type of representation is frequently used in power system analysis. V_m is the voltage of the sending end (bus m), and $V_k$is the voltage of the receiving end (bus k). I_{km} is a representation of the current moving via the transmission line from bus m to bus k. In order to represent the impedance characteristics of the transmission line, a passive element with admittance Y_{km} is used. This element usually consists of both reactive and resistive components. The complex power used at receiving bus k is $P_k + jQ_k$, where P_k and Q_k is the real and reactive power.

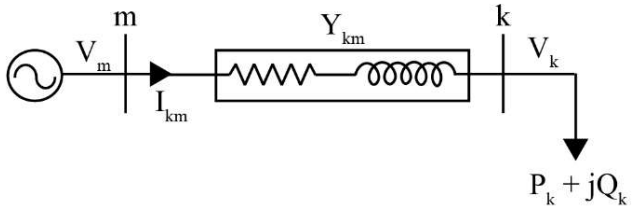

Figure 3.1: Two Bus Network

In a power system network, the active power at bus k can be shown as follows:

$$P_k = \sum_{m=1}^{n} |V_k||V_m||Y_{km}| \cos(\delta_m - \delta_k + \theta_{km}) \tag{3.1}$$

The reactive power at bus k in a power system network can be represented as:

$$Q_k = -\sum_{m=1}^{n} |V_k||V_m||Y_{km}| \sin(\delta_m - \delta_k + \theta_{km}) \tag{3.2}$$

The above formulation provides a foundational mathematical basis for calculating active power injection at a bus, which is essential for understanding power flow behavior and system performance under various operating conditions.

3.3 Voltage Stability Assessment

The following section describes a voltage stability assessment technique based on the Thevenin equivalent methodology, which evaluates the system's proximity to voltage collapse by modeling the network and load behavior using an equivalent circuit approach.

3.3.1 Thevenin Equivalent Methodology

The Thevenin equivalent voltage V_{th} at a load bus, typically referred to as the no-load voltage, can be derived directly from the results of a standard power flow (load flow) analysis. To determine the Thevenin equivalent parameters—namely the equivalent voltage and impedance—a slight modification of the conventional load flow solution is performed. Specifically, this involves modifying the diagonal elements of the system impedance matrix (Z-matrix) to eliminate or minimize the influence of the actual load impedance present at the candidate bus under consideration. By effectively isolating the load, this process enables the estimation of the equivalent source voltage and impedance that would be observed from the load bus under no-load conditions. This Thevenin model is essential for assessing voltage stability because it looks at the relationship between the load impedance and the Thevenin impedance to determine how close the system is to voltage collapse.

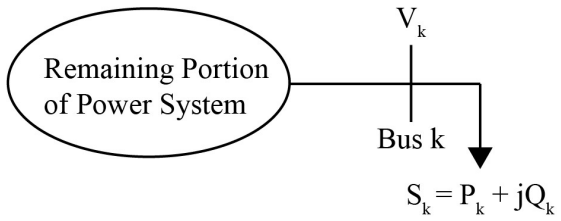

Figure 3.2: Load at Bus k to the remaining portion of a Power System

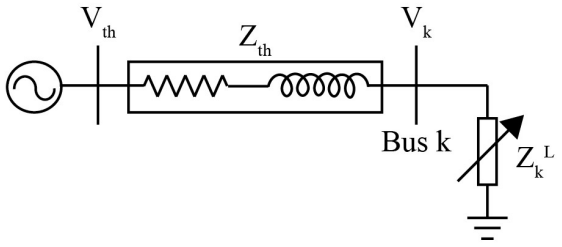

Figure 3.3: Equivalent Thevenin Representation of Power System at Load Bus k

As seen in Figure 3.2, a load at bus k is connected to the rest of the power system. The complex power used by the load is expressed as $S_k = P_k + jQ_k$, and the associated bus voltage is shown as V_k. This general depiction shows how the load and the network as a whole interact without going into specifics about the system's internal organization.

The power system's Thevenin equivalent model as viewed from bus k is displayed in figure 3.3. In this case, the complete power system is reduced to an ideal voltage source V_{th} connected to the load Z_k^L at bus k in series with the Thevenin equivalent impedance Z_{th}. The voltage drops across Z_{th} affects the voltage at the load bus, which stays at V_k. This analogous circuit is essential for evaluating voltage stability since it enables examination of the system's behavior under various load scenarios. The system achieves the maximum power transfer limit, beyond which voltage instability or collapse may occur, namely when the size of the load impedance Z_k^L equals the magnitude of Z_{th}.

$$Z_k^L = \frac{|V_k|^2}{P_k - jQ_k} \tag{3.3}$$

Figure 3.4 represents the schematic of a power system model where generators are connected at buses 1 to m, and loads are connected at buses m+1 to n. The generators are modeled with constant terminal voltages, and the internal series reactance jX_g of the generator model is assumed to be zero, i.e., $jX_{g1} = jX_{gm} = 0$, simplifying the equivalent source impedance.

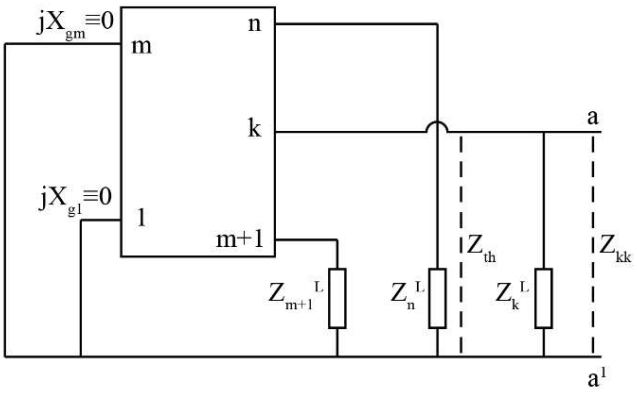

Figure 3.4: Schematic Diagram of Generator Model and Thevenin Impedance Extraction in Power System

The load buses m+1, n, k are represented by their respective load impedances Z_{m+1}^L, Z_n^L, Z_k^L, and the Thevenin equivalent impedance Z_{th} is in parallel with the load impedance Z_k^L at bus k and addition of Z_{th} and Z_k^L can be summed to get kth diagonal element of impedance matrix Z_{kk}. In other words, the Z_{th} can be calculated by removing the influence of the load from the total bus impedance Z_{kk}, which includes both the system and load impedances.

Therefore, the expression for Thevenin impedance at bus k is:

$$Z_{th} = \left(\frac{1}{Z_{kk}} - \frac{1}{Z_k^L}\right)^{-1} \tag{3.4}$$

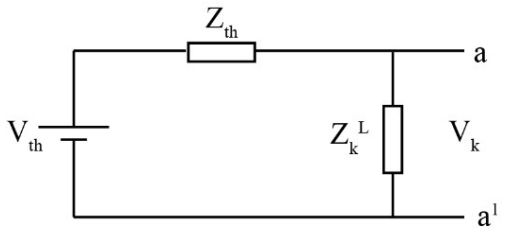

Figure 3.5: Thevenin Equivalent Circuit as observed from Bus k of the Power System

Now, referring to Figure 3.5, the schematic illustrates the Thevenin equivalent circuit as observed from bus k of given power system. In this representation, the complex power system is simplified to a series combination of Thevenin voltage with the Thevenin impedance Z_{th}, supplying to load Z_k^L. V_k is the actual voltage at bus k appearing across load under normal operating conditions.

Now V_{th} can obtained by using the voltage divider principle across the series combination of Z_{th} and Z_k^L. The total voltage across the circuit is V_{th}, and then voltage across load impedance is V_k. Rearranging voltage divider equation, the Thevenin voltage is expressed in equation (3.5):

$$V_{th} = \left(1 + \frac{Z_{th}}{Z_k^L}\right) V_k \tag{3.5}$$

Equation (3.5) implies that the Thevenin voltage is a scaled version of the actual load bus voltage V_k, adjusted by the ratio of Z_{th} to Z_k^L. This expression is particularly useful in voltage stability studies, as it helps determine how close the system is to instability by analyzing changes in V_k with respect to changes in load Z_k^L. When the load impedance approaches the magnitude of Z_{th}, the system operates near its maximum power transfer point, beyond which voltage collapse can occur.

In the next section, a derivation of a proposed Voltage Stability Index (VSI) is presented using fundamental power flow equations (3.1) and (3.2) along with the Thevenin equivalent parameters V_{th} and Z_{th}. The formulation involves expressing the load bus voltage in terms of these Thevenin parameters and substituting into the active and reactive power equations to derive a quadratic expression. By manipulating this expression, a discriminant-based index is obtained, which serves as a mathematical indicator of voltage stability margin. The resulting VSI expression, represented in the form of a quadratic equation, incorporates system voltages, admittances, and power injections to analytically assess the system's proximity to voltage collapse.

3.3.2 Voltage Stability Index

The derivation begins with the standard active and reactive power equations for a two-bus system, which are manipulated and squared to eliminate angular dependencies. This leads to a quadratic equation in terms of the squared of the bus voltage magnitude V_k^2. The discriminant of this quadratic expression $(b^2 - 4ac)$ must be non-negative to ensure a physical meaningful (real) solution for voltage. This condition is the basis of voltage stability criterion.

Power flow equations for a two-bus network illustrated in Figure 3.1 can be derived from the general equation (3.1) and are expressed in equation (3.6):

$$P_k = V_k^2 Y_{kk} \cos\theta_{kk} + V_k V_m Y_{km} \cos(\delta_m - \delta_k + \theta_{km}) \tag{3.6}$$

Rearranging terms leads to:

$$P_k - V_k^2 Y_{kk} \cos\theta_{kk} = V_k V_m Y_{km} \cos(\delta_m - \delta_k + \theta_{km}) \tag{3.7}$$

Similarly, reactive power equations at bus k becomes:

$$Q_k = -V_k^2 Y_{kk} \sin\theta_{kk} - V_k V_m Y_{km} \sin(\delta_m - \delta_k + \theta_{km}) \tag{3.8}$$

Rewriting equation (3.8) yields:

$$V_k^2 Y_{kk} \sin\theta_{kk} + Q_k = -V_k V_m Y_{km} \sin(\delta_m - \delta_k + \theta_{km}) \tag{3.9}$$

To simplify, both equations (3.7) and (3.9) are squared individually:

$$P_k^2 + V_k^4 Y_{kk}^2 \cos^2\theta - 2V_k^2 Y_{kk} \cos\theta\, P_k = (V_k V_m Y_{km})^2 \cos^2(\delta_m - \delta_k + \theta_{km}) \tag{3.10}$$

$$V_k^4 Y_{kk}^2 \sin^2\theta + Q_k^2 + 2V_k^2 Y_{kk} \sin\theta\, Q_k = (V_k V_m Y_{km})^2 \sin(\delta_m - \delta_k + \theta_{km}) \tag{3.11}$$

By summing equations (3.10) and (3.11), and applying the trigonometric identity $\cos^2 x + \sin^2 x = 1$, the result is:

$$V_k^4 Y_{kk}^2 + P_k^2 + Q_k^2 - 2V_k^2 Y_{kk}(P_k \cos\theta - Q_k \sin\theta) = (V_k V_m Y_{km})^2 \tag{3.12}$$

Rearranging equation (3.12) gives a quadratic form in V_k^2:

$$V_k^4 Y_{kk}^2 - V_k^2\big((V_m Y_{km})^2 + 2Y_{kk}(P_k \cos\theta - Q_k \sin\theta)\big) + (P_k^2 + Q_k^2) = 0 \tag{3.13}$$

$$Y_{kk}^2 (V_k^2)^2 - V_k^2\big((V_m Y_{km})^2 + 2Y_{kk}(P_k \cos\theta - Q_k \sin\theta)\big) + (P_k^2 + Q_k^2) = 0 \tag{3.14}$$

This can be further compacted to equation (3.15):

$$a(V_k^2)^2 + bV_k^2 + c = 0 \tag{3.15}$$

Where the coefficients are defined as:

$$a = Y_{kk}^2 \tag{3.16}$$

$$b = -(V_m^2 Y_{km}^2 + 2Y_{kk}(P_k \cos\theta - Q_k \sin\theta) \quad (3.17)$$

$$c = (P_k^2 + Q_k^2) \quad (3.18)$$

Solving this quadratic equation gives:

$$V_k^2 = \frac{-b \pm \sqrt{(b^2 - 4ac)}}{2a} \quad (3.19)$$

To ensure the existence of a real solution, the discriminant must be non-negative:

$$(b^2 - 4ac) \geq 0 \quad (3.20)$$

For voltage stability analysis under constant power factor assumption, the complex power $P_k + jQ_k$ is scaled by a voltage stability index (VSI), leading to:

$$[V_m^2 Y_{km}^2 + 2Y_{kk}(P_k \cos\theta\, VSI - Q_k \sin\theta\, VSI)]^2 - 4Y_{kk}^2 VSI^2 (P_k^2 + Q_k^2) = 0 \quad (3.21)$$

Expanding and simplifying the expression, the resulting quadratic form becomes:

$$4VSI^2 Y_{kk}^2 [(P_k \cos\theta - Q_k \sin\theta)^2 - (P_k^2 + Q_k^2)] + VSI\ 4V_m^2 Y_{km}^2 Y_{kk}(P_k \cos\theta - Q_k \sin\theta) + V_m^4 Y_{km}^4 = 0 \quad (3.22)$$

The solution of the above expression in terms of VSI is obtained using the quadratic formula:

$$VSI = \frac{-b \pm \sqrt{b^2 - 4ac}}{2a} \geq 0 \quad (3.23)$$

Where the coefficients are redefined for VSI calculation as:

$$a = 4Y_{kk}^2 [\big(P_k Cos(\theta) - Q_k Sin(\theta)\big)^2 - (P_k^2 + Q_k^2) \quad (3.24)$$

$$b = 4V_m^2 Y_{km}^2 Y_{kk}\big(P_k Cos(\theta) - Q_k Sin(\theta)\big) \quad (3.25)$$

$$c = V_m^4 Y_{km}^4 \quad (3.26)$$

In larger power networks, the sending-end voltage V_m and admittance Y_{km} are replaced by the Thevenin equivalents V_{th} and Z_{th}, resulting in:

$$a = 4Y_{kk}^2 [(P_k \cos\theta - Q_k \sin\theta)^2 - (P_k^2 + Q_k^2)] \quad (3.27)$$

$$b = 4V_{th}^2 Z_{th}^{-2} Y_{kk}(P_k \cos\theta - Q_k \sin\theta) \quad (3.28)$$

$$c = V_{th}^4 Z_{th}^{-4} \quad (3.29)$$

The larger the VSI of a bus, the higher its voltage stability. A steeper slope of the VSI with respect to changes in reactive power injection indicates greater sensitivity, suggesting that the bus is more vulnerable to voltage instability. Maximum loadability occurs when the VSI reaches zero, i.e., when the Thevenin impedance equals the load impedance ($Z_{th} =$

Z_k^L). Beyond this point, the system experiences voltage collapse, and no further power transfer is possible.

3.3.3 Voltage Collapse Proximity Index

The VCPI determined by Balamourougan et al. (2004) is a scalar indicator used in power system stability studies to quantify how close a bus (in this case, bus k) is to voltage collapse. It is particularly useful in online voltage stability assessment, helping operators identify weak buses and take preventive actions. [5]

$$VCPI_{kth\ bus} = \left| 1 - \frac{\sum_{\substack{m=1 \\ m \neq k}}^{N} V'_m}{V_k} \right| \leq 1 \tag{3.30}$$

where,

$$V'_m = \frac{Y_{km}}{\sum_{\substack{j=1 \\ j \neq k}}^{N} Y_{kj}} \tag{3.31}$$

In the VCPI expression (3.30) for the kth bus, the term V_k represents the complex voltage at bus k, while V'_m denotes the normalized admittance-based contribution of neighboring bus m to bus k. The normalized voltage V'_m is calculated as the ratio of mutual admittance Y_{km} between buses k and m to the sum of all admittances Y_{kj} connecting bus k to other buses $j \neq k$. This ratio reflects how strongly bus m is electrically coupled to bus k. The summation $\sum_{\substack{m=1 \\ m \neq k}}^{N} V'_m$ represents the collective influence of all other buses on bus k. The entire VCPI expression $\left|1 - \frac{\sum V'_m}{V_k}\right|$ quantifies the deviation of the normalized admittance environment from the actual voltage at bus k. A value close to zero indicates a stable condition, while values approaching one suggest that the bus is nearing voltage collapse. This index is bounded by 1 and provides a useful indication of voltage stability in power system networks.

3.3.4 Power-Voltage (P-V) Curve

The fluctuation of active power supply with respect to voltage at a load bus with a constant power factor ϕ is described by the P–V curve equation. To make analysis easier, it is normalized using Thevenin equivalent parameters. The normalized voltage v is the ratio of the load bus voltage V_k to the Thevenin voltage V_{th}, and the normalized power p is the actual power P_k divided by the Thevenin maximum power transfer limit V_{th}^2/Z. A nonlinear relationship with a distinct nose point showing the maximum real power that may be given without running the danger of voltage instability is shown by the resulting equation (3.32). In voltage stability analysis, this model is frequently used to assess how close a power system operating point is to voltage collapse.

For $\tan\phi = \frac{P_k}{Q_k}$, a relation for power-voltage curve equation [1] is obtained as:

$$p = -v^2 \sin\phi \cos\phi + v \cos\phi \sqrt{1 - v^2 \cos^2\phi} \tag{3.32}$$

where,

$$p = \frac{P_k}{\left(\frac{V_{th}^2}{Z}\right)} \tag{3.33}$$

$$v = \frac{V_k}{V_{th}} \tag{3.34}$$

3.3.5 Voltage Stability Assessment Flowchart

The flowchart illustrates a systematic procedure for assessing voltage stability at a load bus in a power system using key indicators such as the VSI, VCPI, and the P–V curve. The process begins by selecting a load bus with specified active and reactive power demands. A power flow analysis is performed to calculate the Thevenin impedance by extraction of load impedance from the corresponding diagonal element of the impedance matrix to the selected bus given in equation (3.4). Then Thevenin voltage is obtained from equation (3.5), which are essential for deriving the VSI and VCPI from equations (3.23) and (3.30) respectively. These indices help quantify the close of the system voltage collapse. The next step involves plotting the VSI, VCPI, and P–V curve to visualize the system's behavior under increased loading. The load at the selected bus is then incrementally increased, and for each increment, the convergence of the power flow is checked. If convergence is achieved, new VSI and VCPI values are calculated; if not, the process stops, and the system's voltage stability performance is assessed. This iterative procedure provides valuable insights into the critical loading point and helps in identifying weak buses, thereby aiding in system planning and preventive control strategies.

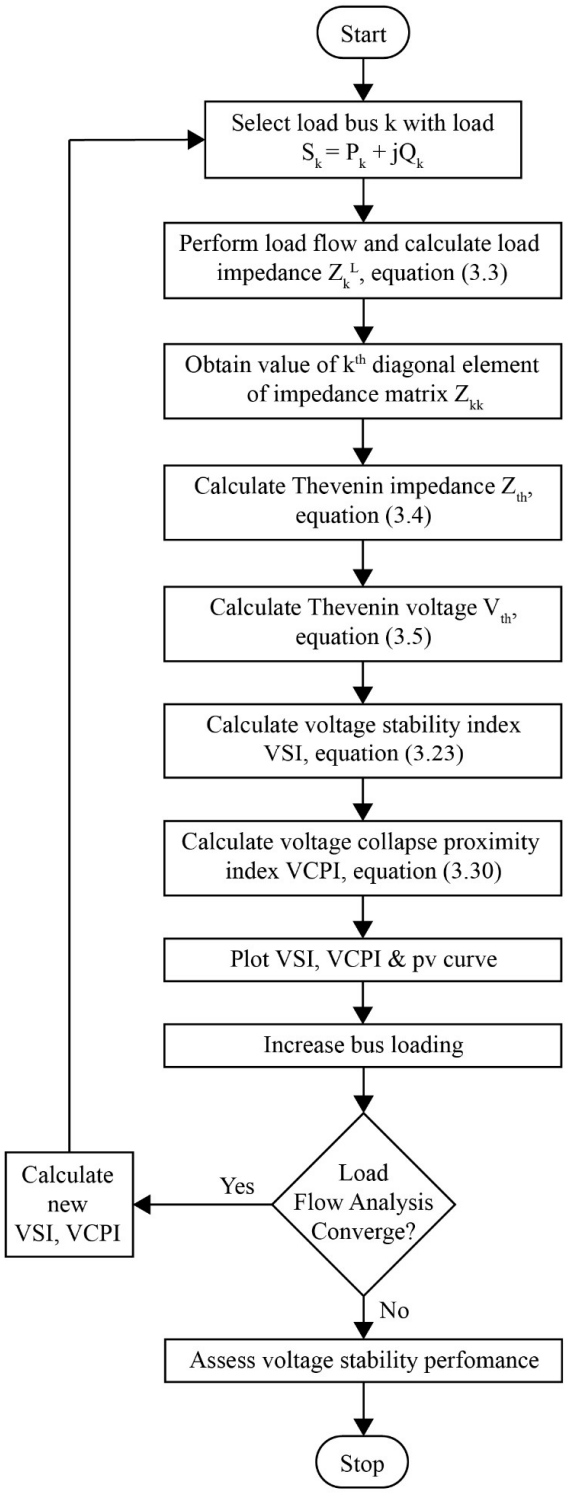

Figure 3.6: Flowchart for Online Voltage Assessment

3.4 Load Flow Analysis with DPFC

3.4.1 Harmonic Power Flow Equations

The formulation essential for performing load flow analysis in a power system incorporating a DPFC requires harmonic power flows significantly influence the overall system behavior. The total active and reactive powers at the ith bus, denoted by equations (3.35) and (3.36), respectively, are calculated by summing contributions from the fundamental as well as higher-order harmonic components up to a specified maximum harmonic order h_{max} [18]. The presence of DPFC, which injects voltage at third harmonic frequency, necessitates a harmonic power flow framework that accurately models the interactions of voltage and current phasors at various harmonic frequencies.

The total power including fundamental and harmonic powers calculated at the ith bus is:

$$P_{i,t} = \sum_{h=1}^{h_{max}} \left(|V_{i,h}| \sum_{k=1}^{n} |V_{k,h}||Y_{i.k,h}| \cos(\theta_{i.k,h} - \delta_{i,h} + \delta_{k,h}) \right) \tag{3.35}$$

$$Q_{i,t} = - \sum_{h=1}^{h_{max}} \left(|V_{i,h}| \sum_{k=1}^{n} |V_{k,h}||Y_{i.k,h}| \sin(\theta_{i.k,h} - \delta_{i,h} + \delta_{k,h}) \right) \tag{3.36}$$

In equations (3.35) and (3.36), $V_{i,h}$ is the voltage at i^{th} bus corresponding to h^{th} harmonic component, and $V_{k,h}$ is the voltage at k^{th} bus for same harmonic order. The term $Y_{ik,h}$ represents element of the bus admittance matrix at harmonic order h between buses i and k, with magnitude $|Y_{ik,h}|$ and phase angle $\theta_{ik,h}$. $\delta_{i,h}$ and $\delta_{k,h}$ are phase angles of voltages $V_{i,h}$ and $V_{k,h}$, respectively. These variables collectively account for the impact of harmonic propagation and phase interactions in the network. The inner summation over k computes the net power interaction between the i^{th} bus and all other buses for each harmonic, while the outer summation over h aggregates the effects of all considered harmonic orders. In systems with DPFC, where voltage injections at particular harmonic frequencies impact not only the power flow but also the network's voltage stability and harmonic performance, this thorough modeling technique is essential.

3.4.2 Power Equations of Sending End

Figure 3.7 illustrates the concept of harmonic components in an electrical waveform, showing a comparison between fundamental and third harmonic component.

Fundamental waveform, shown in dark blue, represents the primary sine wave of the power system, typically at 50 or 60 Hz depending on the region. This is the basic frequency at which electrical power is generated and consumed.

Superimposed on this is a third harmonic waveform, shown in light blue, which completes three cycles in the same time that the fundamental completes one. This higher-frequency component distorts the original sine wave, leading to a waveform that deviates from a pure sinusoid when both components are present.

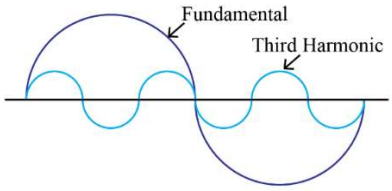

Figure 3.7: Fundamental and Third Harmonic Wave

The extended expressions from equations (3.35) and (3.36) provide a refined formulation for the total active and reactive power at the i^{th} bus by considering only the fundamental (1st harmonic) and third harmonic components.

$$P_{i,t} = |V_{i,1}| \sum_{k=1}^{n} |V_{k,1}||Y_{i.k,1}| \cos(\theta_{i.k,1} - \delta_{i,1} + \delta_{k,1}) + |V_{i,3}| \sum_{k=1}^{n} |V_{k,3}||Y_{i.k,3}| \cos(\theta_{i.k,3} - \delta_{i,3} + \delta_{k,3}) \quad (3.37)$$

Equation 3.37 adds the contributions of both fundamental and third harmonic components of total active power at bus i. Total reactive power also includes the impact of third harmonic interactions, which become significant in systems with nonlinearities or harmonic injections given by equation 3.38.

$$Q_{i,t} = -|V_{i,1}| \sum_{k=1}^{n} |V_{k,1}||Y_{i.k,1}| \sin(\theta_{i.k,1} - \delta_{i,1} + \delta_{k,1}) - |V_{i,3}| \sum_{k=1}^{n} |V_{k,3}||Y_{i.k,3}| \sin(\theta_{i.k,3} - \delta_{i,3} + \delta_{k,3}) \quad (3.38)$$

Third harmonic active power flow from sending-end bus to series voltage source converter of DPFC, which operates at third harmonic frequency for decoupled power injection is given in equation (3.39):

$$P_{s.se,3} = |V_{s,3}| \sum_{se=1}^{n} |V_{se,3}||Y_{s.se,3}| \cos(\theta_{s.se,3} - \delta_{s,3} + \delta_{se,3}) \quad (3.39)$$

Therefore, total active power drawn at sending-end bus, which now includes both power exchanged via fundamental component and third harmonic power supplied to series VSC of DPFC is:

$$P_{s,t} = |V_{s,1}| \sum_{k=1}^{n} |V_{k,1}||Y_{s.k,1}| \cos(\theta_{s.k,1} - \delta_{s,1} + \delta_{k,1}) + |V_{s,3}| \sum_{se=1}^{n} |V_{se,3}||Y_{s.se,3}| \cos(\theta_{s.se,3} - \delta_{s,3} + \delta_{se,3}) \quad (3.40)$$

3.4.3 Total Power at the Receiving End

In a typical uncompensated transmission line, real and reactive power at receiving end is governed by voltage phasors between sending and receiving ends and line impedance. When a DPFC is introduced, series converter injects a controllable fundamental voltage $\dot{V}_{se,1}$ into the line. This modifies the voltage drop across transmission line and consequently alters power flow.

Transmitted active power P_r and reactive power $-jQ_r$, delivered to receiving end after compensation, is expressed in equation (3.41):

$$P_{r,1} + jQ_{r,1} = \dot{V}_{r,1} \left(\frac{\dot{V}_{s,1} + \dot{V}_{se,1} - \dot{V}_{r,1}}{R + jX_1} \right)^* \quad (3.41)$$

Where symbol * means conjugate of a complex number and $j = e^{j\pi/2} = \sqrt{-1}$. If there is no series voltage injection (i.e., $\dot{V}_{se1} = 0$), then equation (3.41) is simplified to the conventional power flow expression for an uncompensated line:

$$P_{r,1} + jQ_{r,1} = \dot{V}_{r,1} \left(\frac{\dot{V}_{s,1} - \dot{V}_{r,1}}{R + jX_1} \right)^* \quad (3.42)$$

Thus, with $\dot{V}_{se} \neq 0$, total active and reactive power can be written in the form

$$P_{r,1} + jQ_{r,1} = \dot{V}_{r,1} \left(\frac{\dot{V}_{s,1} - \dot{V}_{r,1}}{R + jX_1} \right)^* + \frac{\dot{V}_{r,1}\dot{V}^*_{se,1}}{R - jX_1} \quad (3.43)$$

It is evident that the fundamental voltage V_{se} , which is produced by the series side converter, is directly correlated with the power flow between DPFC and the systems. We can only modify the transmission line's power flow in accordance with dispatching center's system instructions by regulating amplitude and phase angle of $\dot{V}_{se}$.

$$P_{r.se,1} = |V_{r,1}||V_{se,1}||Y_{r.se,1}| \cos(\theta_{r.se,1} - \delta_{r,1} + \delta_{r.se,1}) \quad (3.44)$$

$$Q_{r.se,1} = -|V_{r,1}||V_{se,1}||Y_{r.se,1}| \sin(\theta_{r.se,1} - \delta_{r,1} + \delta_{r.se,1}) \quad (3.45)$$

After including effect of series converter, net active and reactive power at receiving-end bus is modified as follows:

Total fundamental active power at receiving end after compensation is:

$$P_{r,t} = |V_{r,1}| \sum_{k=1}^{n} |V_{r,1}||Y_{r.k,1}| \cos(\theta_{r.k,1} - \delta_{r,1} + \delta_{k,1})$$
$$-|V_{r,1}| \sum_{se=1}^{n} |V_{se,1}||Y_{r.se,1}| \cos(\theta_{r.se,1} - \delta_{r,1} + \delta_{se,1}) \quad (3.46)$$

Total fundamental reactive power at receiving end after compensation is:

$$Q_{r,t} = -|V_{r,1}| \sum_{k=1}^{n} |V_{r,1}||Y_{r.k,1}| \sin(\theta_{r.k,1} - \delta_{r,1} + \delta_{k,1})$$
$$+|V_{r,1}| \sum_{se=1}^{n} |V_{se,1}||Y_{r.se,1}| \sin(\theta_{r.se,1} - \delta_{r,1} + \delta_{se,1}) \quad (3.47)$$

The above equations show that the DPFC's injected voltage subtracts from the load flow as an additional component, modifying power balance at receiving end.

3.4.4 DPFC Performance Metrices: Voltage and Angle Deviation

To ensure the operation of DPFC as per the control setpoints, the following error functions are defined for voltage and phase angle deviations:

Power angle deviation on DPFC is:

$$F_{\delta se,1} = |\delta_{se,1.cal}| - |\delta_{se,1.sp}| \quad (3.48)$$

Voltage deviation on DPFC is:

$$F_{Vse,1} = |V_{se,1.cal}| - |V_{se,1.sp}| \quad (3.49)$$

These serves as control objectives or constraints in optimization and regulation frameworks to maintain desired power flow behavior through DPFC adjustment.

3.4.5 Mismatch Matrix

In the context of load flow analysis with a DPFC, the mismatch matrix represents the deviation between the specified (desired) and calculated quantities during iterative solution of the power flow equations. This matrix includes both power mismatches at the buses and control mismatches associated with the DPFC.

3.4.5.1 Active and Reactive Power Mismatches:

Active power mismatch (dP) and reactive power mismatch (dQ) at system buses are given by difference between specified and calculated values obtained from current iteration:

$$dP = P_{sp} - P_{cal} \tag{3.50}$$

$$dQ = Q_{sp} - Q_{cal} \tag{3.51}$$

Where:

P_{sp}, Q_{sp} are specified active and reactive power values,

P_{cal}, Q_{cal} are calculated active and reactive power from current iteration.

3.4.5.2 Control Mismatches of DPFC:

The mismatch in the DPFC control objectives – namely voltage magnitude and angle at series converter – is handled as:

$$dF_{\delta se,1} = -F_{\delta se,1} \tag{3.52}$$

$$dF_{Vse,1} = -F_{Vse,1} \tag{3.53}$$

The negative signs in equations (3.52) and (3.53) indicate that the goal is to minimize these deviations, i.e., drive them towards zero.

3.4.5.3 Mismatch Vector

The complete mismatch vector, combining power mismatches and DPFC control mismatches, is constructed as:

$$M = \begin{bmatrix} dP \\ dQ \\ dF_{\delta se,1} \\ dF_{Vse,1} \end{bmatrix} \tag{3.54}$$

This vector serves as the residual input for Newton-Raphson load flow algorithm used in solving the power system equations with DPFC integration.

3.4.6 Correction Matrix

The correction matrix contains the incremental updates of the state variables required to reduce the mismatch vector towards zero.

Control and State Variable Updates:

For PV bus, both power angle δ and voltage magnitude V are adjusted.

For PQ bus, only voltage magnitude V is corrected.

For DPFC series converter, corrections are applied to both voltage angle $\delta_{se,1}$ and voltage magnitude $V_{se,1}$.

Thus, overall correction vector is expressed as:

$$C = \begin{bmatrix} \Delta\delta \\ \Delta V \\ \Delta\delta_{se,1} \\ \Delta V_{se,1} \end{bmatrix} \tag{3.55}$$

This vector is used to iteratively update the respective state variables during the numerical solution of the power flow equations, ultimately ensuring system convergence.

3.4.7 Jacobian Matrix

In the context of load flow analysis with inclusion of a DPFC, the Jacobian matrix represents the sensitivity of the system's mismatches to variations in state variables. These state variables include both the conventional power system variables (voltage magnitude V and angle δ) and the control parameters of DPFC (magnitude $V_{se,1}$ and phase $\delta_{se,1}$ of series converter at fundamental frequency).

$$J = \begin{bmatrix} \frac{\partial P}{\partial \delta} & \frac{\partial P}{\partial V} & \frac{\partial P}{\partial \delta_{se,1}} & \frac{\partial P}{\partial V_{se,1}} \\ \frac{\partial Q}{\partial \delta} & \frac{\partial Q}{\partial V} & \frac{\partial Q}{\partial \delta_{se,1}} & \frac{\partial Q}{\partial V_{se,1}} \\ 0 & 0 & 1 & 0 \\ 0 & 0 & 0 & 1 \end{bmatrix} \tag{3.56}$$

The last two rows of the matrix are associated with the DPFC control equations defined by the mismatch in angle and voltage magnitude, effectively enforcing the constraints for the series converter.

Using this Jacobian matrix, the mismatch vector M and correction vector C are related by the following matrix equation:

$$M = J.C \tag{3.57}$$

Expanded form:

$$\begin{bmatrix} dP \\ dQ \\ dP_{dpfc} \\ dF \end{bmatrix} = \begin{bmatrix} \frac{\partial P}{\partial \delta} & \frac{\partial P}{\partial V} & \frac{\partial P}{\partial \delta_{se1}} & \frac{\partial P}{\partial V_{se1}} \\ \frac{\partial Q}{\partial \delta} & \frac{\partial Q}{\partial V} & \frac{\partial Q}{\partial \delta_{se}} & \frac{\partial Q}{\partial V_{se}} \\ 0 & 0 & 1 & 0 \\ 0 & 0 & 0 & 1 \end{bmatrix} \begin{bmatrix} d\delta \\ dV \\ d\delta_{se,1} \\ dV_{se,1} \end{bmatrix} \tag{3.58}$$

From this, the correction vector can be obtained through:

$$C = J^{-1}.M \tag{3.59}$$

3.4.8 Update in Variables

After computing the correction vector C, the state variables are updated iteratively. These updates refine the estimates of bus voltages and DPFC parameters in order to minimize mismatch and converge toward power flow solution.

$$\left.\begin{aligned} \delta_{new} &= \delta_{old} + d\delta \\ V_{new} &= V_{old} + dV \\ \delta_{se,1.new} &= \delta_{se,1.old} + d\delta_{se,1} \\ V_{se,1.new} &= V_{se,1.old} + dV_{se,1} \end{aligned}\right\} \tag{3.60}$$

This completes one iteration of the proposed load flow algorithm with DPFC, which considers both fundamental and third harmonic power flow components. Iterations continue until all mismatch values fall within an acceptable tolerance, ensuring convergence of the load flow solution.

3.5 Non-Linear Control of DPFC

3.5.1 Power Balance in the Series Side Converter

The operation of the DPFC's series converter is governed by the energy exchange between fundamental and third harmonic components. Specifically, power injected at fundamental frequency must be equal in magnitude and opposite in sign to power absorbed at third harmonic frequency:

$$P_{se,1} = -P_{se,3} \tag{3.61}$$

Here, $P_{se,1}$ is the fundamental active power supplied to network, while $P_{se,3}$ denotes third harmonic active power drawn from the system.

3.5.2 Dynamic Modeling of the DPFC Series Converter

The equivalent dynamic model of the DPFC series converter is constructed by considering three distinct subsystems: the AC fundamental network, the AC third harmonic network, and the DC link capacitor C_{se}, as illustrated in Figure 3.8.

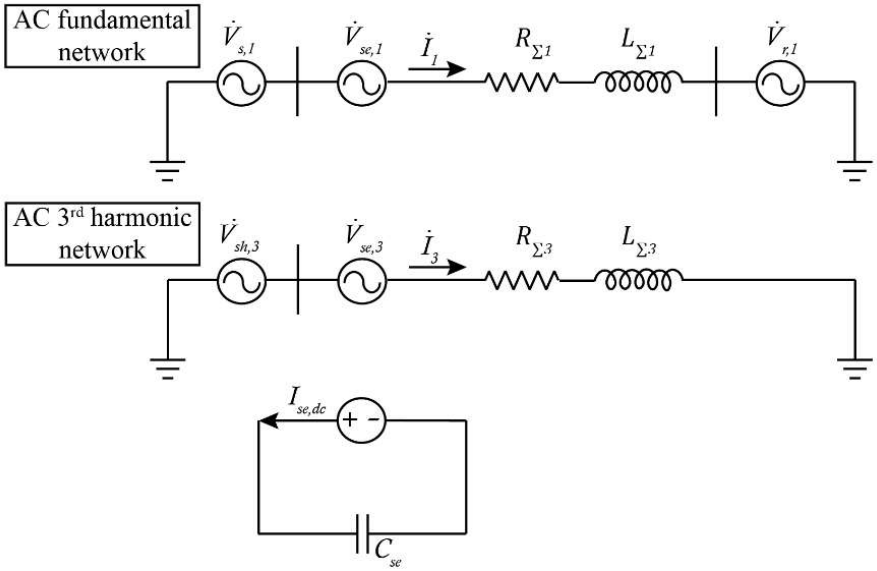

Figure 3.8: Equivalent Circuit of the DPFC Series Side

In this configuration:

- $\dot{V}_{s,1}$ and $\dot{V}_{r,1}$ denote the fundamental voltages at the sending and receiving ends, respectively.
- $\dot{V}_{se,1}$ and $\dot{V}_{se,3}$ represent the equivalent fundamental and third harmonic voltages across the series converter.
- I_1 and I_3 are the respective currents at fundamental and third harmonic frequencies.

- $I_{se,dc}$ and $V_{se,dc}$ are the current and voltage across the DC link capacitor.
- $R_{\sum 1}$, $L_{\sum 1}$ and $R_{\sum 3}$, $L_{\sum 3}$ refer to the aggregate resistance and inductance in the respective frequency domains.

The energy relationships governing the dynamic behavior of the series side of the DPFC involve the power interactions at the DC link and both the fundamental and third harmonic components. These relationships are formulated as follows:

$$\left.\begin{aligned} P_{Cse} &= I_{se,dc} \cdot V_{se,dc} \\ P_{se,1} &= \frac{1}{2}\left(V_{se,1.d} \cdot I_{1.d} + V_{se,1.q} \cdot I_{1.q}\right) \\ P_{se,3} &= \frac{1}{2}\left(V_{se,3.d} I_{3.d} + V_{se,3.q} I_{3.q}\right) \\ P_{Cse} &= P_{se,3} - P_{se,1} \end{aligned}\right\} \tag{3.62}$$

In this formulation:

- $I_{1.d}, I_{1.q}$ and $I_{3.d}, I_{3.q}$ represent the direct and quadrature axis components of the fundamental and third harmonic currents, respectively.
- $V_{se,1.d}, V_{se,1.q}$ and $V_{se,3.d}, V_{se,3.q}$ denote the corresponding dq-axis components of the fundamental and third harmonic series voltages.
- P_{Cse} is the power exchange across the DC-link capacitor C_{se}, while $P_{se,1}$ and $P_{se,3}$ represent the power at fundamental and third harmonic frequencies, respectively.

Based on the system configuration depicted in figure 3.8, the dynamic behavior of the series converter is described by the following set of differential equations:

$$\left.\begin{aligned} L_{\sum 1}\frac{dI_{1.d}}{dt} &= -R_{\sum 1} I_{1.d} + \omega L_{\sum 1} I_{1.q} + V_{s,1.d} - V_{r,1.d} + m_{se,1.d} V_{se,dc} \\ L_{\sum 1}\frac{dI_{1.q}}{dt} &= -R_{\sum 1} I_{1.q} - \omega L_{\sum 1} I_{1.d} + V_{s,1.q} - V_{r,1.q} + m_{se,1.q} V_{se,dc} \\ L_{\sum 3}\frac{dI_{3.d}}{dt} &= -R_{\sum 3} I_{3.d} + 3\omega L_{\sum 3} I_{3.q} + V_{s,3.d} + m_{se,3.d} V_{se,dc} \\ L_{\sum 3}\frac{dI_{3.q}}{dt} &= -R_{\sum 3} I_{3.q} - 3\omega L_{\sum 3} I_{3.d} + V_{s,3.q} + m_{se,3.q} V_{se,dc} \\ C_{se}\frac{dV_{se,dc}}{dt} &= \frac{1}{2}\left(m_{se,1.d} I_{3,d} + m_{se,1.q} I_{3,q}\right) - \frac{1}{2}\left(m_{se,3.d} I_{1.d} + m_{se,3.q} I_{1.q}\right) \end{aligned}\right\} \tag{3.63}$$

Here:

- $V_{s,1.d}$, $V_{s,1.q}$ and $V_{r,1.d}, V_{r,1.q}$ are the dq-axis components of the sending and receiving end voltages at the fundamental frequency, respectively.
- $V_{s,3.d}, V_{s,3.q}$ are the third harmonic voltage components at the sending end.

- $m_{se,1.d}, m_{se,1.q}, m_{se,3.d}, m_{se,3.q}$ are the modulation terms associated with the converter's output in both the fundamental and third harmonic domains.
- $L_{\sum 1}, R_{\sum 1}$ and $L_{\sum 3}, R_{\sum 3}$ are the equivalent inductance and resistance seen by the converter at the fundamental and third harmonic frequencies, respectively.
- ω is the system angular frequency.

The modulation signals for the converter are derived based on amplitude and phase parameters, expressed as:

$$\left.\begin{aligned} m_{se,1.d} &= k_1 \cos \delta_1 \\ m_{se,1.q} &= k_1 \sin \delta_1 \\ m_{se,3.d} &= k_3 \cos \delta_3 \\ m_{se,3.q} &= k_3 \sin \delta_3 \end{aligned}\right\} \tag{3.64}$$

These relations indicate how the series converter's modulation indices are calculated from the reference magnitudes k_1, k_3 and phase angles δ_1, δ_3, which are the principal control variables in regulating power flow and maintaining system stability.

The dynamic mathematical model of DPFC series side is composed of (3.62), (3.63) and (3.64).

3.5.3 Controller Design for the DPFC

The amplitude and phase angle of the fundamental voltage output at the series side of the DPFC can be modulated to control the power flow along the transmission line. **By applying the feedback linearization technique for nonlinear systems**, the following system variables are selected for controller design:

State vector: $x = \begin{bmatrix} I_{se,1.d} \\ I_{se,1.q} \end{bmatrix}$

Control input: $v = \begin{bmatrix} v_1 \\ v_2 \end{bmatrix} = \begin{bmatrix} m_{se,1.d} \\ m_{se,1.q} \end{bmatrix}$

Output vector: $y_1 = h_1(x) = I_{se,1.d}, y_2 = h_2(x) = I_{se,1.q}$

This leads to a two-input two-output (TITO) nonlinear control model, which is represented as:

$$\dot{x} = f(x) + g_1(x)v_1 + g_2(x)v_2 \tag{3.65}$$

$$y_1 = h_1(x) \tag{3.66}$$

$$y_2 = h_2(x) \tag{3.67}$$

Where the nonlinear functions are defined as:

$$f(x) = \begin{bmatrix} \omega I_{1.q} + \frac{V_{s,1.d} - V_{r,1.d}}{L_{\sum 1}} \\ -\omega I_{1.d} + \frac{V_{s,1.q} - V_{r,1.q}}{L_{\sum 1}} \end{bmatrix}, g_1(x) = \begin{bmatrix} \frac{V_{se,dc}}{L_{\sum 1}} \\ 0 \end{bmatrix}, g_2(x) = \begin{bmatrix} 0 \\ \frac{V_{se,dc}}{L_{\sum 1}} \end{bmatrix}$$

Here, the series arm's internal resistance is neglected for simplification.

Applying a **nonlinear coordinate transformation**, the transformed variables are defined as:

$$z = \begin{bmatrix} z_1 \\ z_2 \end{bmatrix} = \begin{bmatrix} L_f^{r_1 - 1} h_1(x) \\ L_f^{r_2 - 1} h_2(x) \end{bmatrix} = \begin{bmatrix} h_1(x) \\ h_2(x) \end{bmatrix} = \begin{bmatrix} I_{1.d} \\ I_{1.q} \end{bmatrix} \tag{3.68}$$

Where $L_f h(x) = \frac{\partial h[f(x)]}{\partial x}$ and the relative degrees are $r_1 = r_2 = 1$.

Using the model equations and system structure (refer to Figure 3.8), the inputs u_1 and u_2 , representing the desired state derivatives, are obtained as:

$$u_1 = \omega \,.\, z_2 + \frac{1}{L_{\sum 1}} \left(V_{s,1.d} - V_{r,1.d} \right) + \frac{m_{se,1.d}}{L_{\sum 1}} V_{se,dc} \tag{3.69}$$

$$u_2 = -\omega \,.\, z_1 + \frac{1}{L_{\sum 1}} \left(V_{s,1.d} - V_{r,1.d} \right) + \frac{m_{se,1.q}}{L_{\sum 1}} V_{se,dc} \tag{3.70}$$

Solving for the control inputs v_1 and v_2 (which correspond to modulation indices $m_{se,1.d}$ and $m_{se,1.q}$), we get:

$$v = \begin{bmatrix} v_1 \\ v_2 \end{bmatrix} = \begin{bmatrix} m_{se,1.d} \\ m_{se,1.q} \end{bmatrix} = \frac{1}{V_{se,dc}} \begin{bmatrix} L_{\sum 1}.u_1 - V_{s,1.d} + V_{r,1.d} - \omega L_{\sum 1}.z_2 \\ L_{\sum 1}.u_2 - V_{s,1.q} + V_{r,1.q} + \omega L_{\sum 1}.z_1 \end{bmatrix} \tag{3.71}$$

From these control variables, the output voltage phase angle and magnitude of the series converter at the fundamental frequency can be computed as:

$$\delta_{se,1} = \tan^{-1}\left(\frac{v_1}{v_2}\right) \tag{3.72}$$

$$V_{se,1} = \sqrt{v_1^2 + v_2^2} \tag{3.73}$$

Let $P_{L,ref}$ and $Q_{L,ref}$ denote the reference values of active power and reactive power at the load side. The corresponding current references in the dq frame, $I_{1.d,ref}$ and $I_{1.q,ref}$, can be derived as:

$$x_{1,ref} = I_{1.d,ref} = \frac{2}{3}\frac{\left(P_{L,ref}V_{r,1.d} + Q_{L,ref}V_{r,1.q}\right)}{\left(V_{r,1.d}^2 + V_{r,1.q}^2\right)} \tag{3.74}$$

$$x_{2,ref} = I_{1.q,ref} = \frac{2}{3}\frac{\left(P_{L,ref}V_{r,1.q} + P_{L,ref}V_{r,1.d}\right)}{\left(V_{r,1.d}^2 + V_{r,1.q}^2\right)} \tag{3.75}$$

It is important to note that the series converter is primarily responsible for the absorption of third harmonic active power. To avoid excessive reactive power loss associated with harmonics, the quadrature component of the third harmonic voltage, $V_{se,3.q}$, is set to zero as a control strategy.

3.5.4 Non-linear Optimal Control System

The block diagram in figure 3.9 represents a non-linear optimal control system applied to a single-phase series converter in a DPFC. The goal of this control strategy is to optimally regulate active and reactive power flow through a transmission line, enhancing system stability and performance. The control operates in the dq reference frame using a single-phase Park transform to simplify AC signal control into steady-state quantities.

The control begins by generating reference currents $I_{1.d,ref}$ and $I_{1.q,ref}$ based on desired active $P_{L,ref}$ and reactive $Q_{L,ref}$ power. These references are compared to the actual dq-axis currents $I_{1,d}$ and $I_{1,q}$, which are obtained from measured voltages and currents transformed via the single-phase park transform. The errors are fed into PI controllers, which output control variables u_1 and u_2.

The core of the system lies in the non-linear optimal control law, which computes the control voltages v_1 and v_2 using a mathematical model of the system that incorporates non-linear terms such as cross-coupling effects, system inductance, and angular frequency. These voltages are then transformed back into the stationary reference frame via a single-phase park inverse transform, generating the final modulation signal for the series converter.

The system includes a filter to eliminate high-frequency switching noise before injecting the control voltage into the grid. By continuously adjusting the injected voltage, the controller ensures optimal power flow and voltage stability. This non-linear optimal control approach provides better dynamic performance, robustness, and decoupled control of active and reactive power, compared to traditional linear control methods.

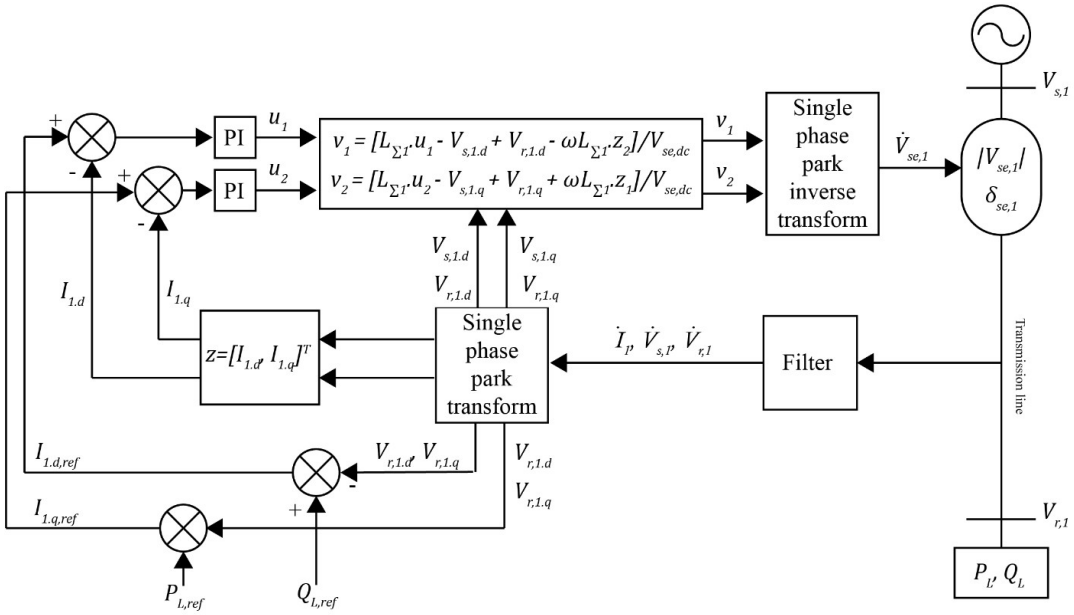

Figure 3.9: Non-Linear System Control Block Diagram of DPFC Series Side

3.6 DPFC Location and Capacity

3.6.1 Parallel Side Device Capacity Design [29]

The capacity design of the DPFC involves determining the required ratings of the series and parallel side converters with the power flow adjustment range of ±25%. This subsection focuses on the design of the parallel side converter capacity, based on the fundamental and third harmonic power exchange characteristics.

3.6.1.1 Series Side Capacity for Fundamental Frequency

With Q_N unchanged, when the active power flow is $1.25P_N$, there exists the following equation: $V_r' = 0.99V_r$ and $\delta_{max} = \delta_2 = 13.9°$. The maximum fundamental voltage output from a single-phase series converter is given by:

$$V_{se,1.max} = 0.0445V_r \tag{3.76}$$

The maximum current flowing through the line is:

$$I_{max} = \frac{0.241V_r}{X} \tag{3.77}$$

Consequently, the apparent power handled by the fundamental wave on the series side is:

$$S_{se,1} = \frac{V_{se,1.max}I_{max}}{\sqrt{3}} = \frac{0.011V_r^2}{\sqrt{3}X} \tag{3.78}$$

3.6.1.2 Third Harmonic Current Constraints

To ensure operational safety and economic feasibility, the third harmonic current I_3 must satisfy the following constraint:

$$\frac{P_{se,3}}{3\sqrt{V_{n.max}^2 - V_{n,1.max}^2}} \leq I_3 \leq \min[I_{3.max1}, I_{3.max2}] \tag{3.79}$$

Where:

$V_{n.max}$: Insulation voltage at the neutral voltage at the neutral point of the transformer.

$V_{n,1.max}$: Maximum allowable fundamental voltage at the transformer neutral point.

The upper bounds of the third harmonic current are determined by:

$$I_{3.max1} = \sqrt{I_{max}^2 - I_{1.max}^2} \tag{3.80}$$

$$I_{3.max2} = \sqrt[4]{\frac{(1-\eta_{min}^2)P_{se,3}^2}{X_2^{*2}\eta_{min}^2}} \tag{3.81}$$

Where:

$I_{1.max}$: Maximum allowable fundamental current in the line

η_{min}: Minimum efficiency of the single-phase converter on the parallel side

X_2^*: Reactance in the third harmonic current loop

3.6.1.3 Third Harmonic Voltage on Series Side

The third harmonic voltage injected by the series side is given by:

$$V_{se,3} = \frac{P_{se,3}}{\sqrt{3}I_3} \tag{3.82}$$

3.6.1.4 Parallel Side Converter Voltage and Capacity

Assuming negligible line and transformer leakage resistances, the output voltage of the parallel-side single-phase converter for the third harmonic component becomes:

$$V_{sh,3} = \sqrt{V_{se,3}^2 + 3I_3^2(2X_T + X_L)^2} \tag{3.83}$$

Accordingly, the capacity of the parallel-side single-phase converter is determined as:

$$S_{sh,3} = \sqrt{3}I_3V_{sh,3} = \sqrt{3}I_3\sqrt{V_{se,3}^2 + 3I_3^2(2X_T + X_L)^2} \tag{3.84}$$

Where:

X_T: Transformer reactance

X_L: Line reactance

3.6.2 Optimal Location and Sizing

Optimal power system operation seeks to optimize the steady-state performance of a power system in terms of one or more objective functions while satisfying several equality and inequality constraints. The problem for optimal location and sizing of DPFC can be formulated as follows:

3.6.2.1 Objective Functions

A. Optimal Location

Five objective functions to determine optimal location of DPFC considered are the proposed voltage stability index, the total apparent power loss, the voltage collapse proximity index, the system loadability, and the bus voltage deviation. These objective functions are formulated as follows.

1) The total VSI: The first objective function is to maximize the total voltage stability index of the system that can be expressed as:

$$F_1 = \sum_{i=0}^{N_{bus}} VSI_i \tag{3.85}$$

2) The total power losses: The second objective function is to minimize the total apparent power losses in transmission lines that can be expressed as:

$$F_2 = S_{Loss}(x,u) = \sum_{l=0}^{N_l} S_l \tag{3.86}$$

Where u is a set of control variables, x is a set of dependent variables, S_l is the real power losses at line-l, and N_l is the number of transmission lines.

3) The total VCPI: The third objective function is to minimize the VCPI that can be expressed as:

$$F_3 = \sum_{i=0}^{N_{bus}} VCPI_i \tag{3.87}$$

4) The system loadability: The third objective function is to maximize the system loadability that can be described as:

$$F_4 = \rho(x,u) \tag{3.88}$$

And ρ can be obtained by assuming the constant power factor at each load in the real and reactive power balance equations as follows:

$$P_{Gi} - \rho P_{Di} = f_{Pi}(x,u) \tag{3.89}$$

$$Q_{Gi} - \rho Q_{Di} = f_{Qi}(x, u) \tag{3.90}$$

Where f_{Pi} and f_{Qi} are the real and reactive power-flow equations at bus-i where the DPFC controller parameters are considered; P_{Gi} and Q_{Gi} are the generator real and reactive power at bus-i, respectively.

5) The total voltage deviation: The fifth objective function is to minimize the total pu voltage deviation from 1 that can be expressed as:

$$F_5 = \sum_{i=0}^{N_{bus}} |1 - V_i| \tag{3.91}$$

B. Optimal Capacity

After getting the optimal location from the above objective functions, optimal capacity is determined using two objective functions: minimize size of DPFC and minimize deviation of third harmonic shunt voltage which are formulated as follows.

1) The size of DPFC: The first objective function is to minimize the size of shunt DPFC device given by equation (3.84) to minimize the installation cost of the system expressed as:

$$F_6 = -S_{sh,3} \tag{3.92}$$

2) The third harmonic shunt voltage deviation: The second objective function is to minimize the third harmonic shunt voltage deviation from the one-third of line voltage that can be expressed as:

$$F_7 = \left| \frac{V_{LL}}{3} - V_{sh,3} \right| \tag{3.93}$$

3.6.2.2 Constraints

The OPF problem is governed by two categories of constraints, equality constraints and inequality constraints, which can be defined as follows:

1) Equality constraints: These represent the power balance equations necessary for system operation. Specifically, they include the real and reactive power flow equations that ensure equilibrium at each bus, as formulated in equations (3.37) and (3.38).

2) Inequality constraints: These include operational limits that the system must comply with:

Generation constraints:

The generator terminal voltage must be within prescribed limits:

$$V_{Gi}^{min} \leq V_{Gi} \leq V_{Gi}^{max}, \;\; i = 1, \dots, NG \tag{3.94}$$

The reactive power output of each generator is also limited:

$$Q_{Gi}^{min} \leq Q_{Gi} \leq Q_{Gi}^{max}, \;\; i = 1, \dots, NG \tag{3.95}$$

DPFC constraints: The DPFC must operate within the following bounds:

$$\left.\begin{array}{c} V_{se,1}^{min} \leq V_{se,1} \leq V_{se,1}^{max} \\ \delta_{se,1}^{min} \leq \delta_{se,1} \leq \delta_{se,1}^{max} \\ S_{se,1} \leq S_{se,1}^{max} \end{array}\right\} \tag{3.96}$$

3.6.2.3 Problem Statement

In general, aggregating the objectives and constraints, the problem can be mathematically formulated as follows:

A. Optimal Location

$$\left.\begin{array}{c} maximize\ F_1 \\ minimize\ F_2 \\ minimize\ F_3 \\ maximize\ F_4 \\ minimize\ F_5 \end{array}\right\} \tag{3.97}$$

B. Optimal Capacity

$$\left.\begin{array}{c} minimize\ F_6 \\ minimize\ F_7 \end{array}\right\} \tag{3.98}$$

subject to:

$$\left.\begin{array}{c} g(x,u) = 0 \\ h(x,u) \leq 0 \end{array}\right\} \tag{3.99}$$

where $g(x,u)$ and $h(x,u)$ are the set of equality and inequality constraints, respectively. The multi-objective optimization problem can be solved using MOGWO.

3.7 MOGWO Technique

The Grey Wolf Optimizer (GWO), introduced by Mirjalili, Mirjalili, and Lewis in 2014, is inspired by the leadership structure and hunting behavior of grey wolves in nature. To model this social hierarchy mathematically, the algorithm designates the best solution in the population as the alpha (α) wolf. The second and third best solutions are labeled as beta (β) and delta (δ) wolves, respectively, while the remaining candidates are categorized as omega (ω) wolves. During the optimization process, the alpha, beta, and delta wolves lead the search, guiding the omega wolves toward the optimal solution.

To simulate the encircling behavior of grey wolves during hunting, the following equations are proposed in addition to modeling social leadership:

$$\vec{D} = \left|\vec{C} \cdot \vec{X}_p(t) - \vec{X}\,(t)\right| \tag{3.100}$$

$$\vec{X}(t+1) = \vec{X}_p(t) - \vec{A} \cdot \vec{D} \tag{3.101}$$

Here t represents the current iteration, $\vec{A}$ and $\vec{C}$ are coefficients vectors, $\vec{X}_p$ is the prey's position vector, and $\vec{X}$ denotes the position vector of a grey wolf.

The formulation of vectors $\vec{A}$ and $\vec{C}$ is:

$$\vec{A} = 2\vec{a} \cdot \vec{r}_1 - \vec{a} \tag{3.102}$$

$$\vec{C} = 2 \cdot \vec{r}_2 \tag{3.103}$$

here $\vec{a}$ decreases linearly from 2 to 0 over iterations, while r_1, r_2 are random vectors in range [0,1].

The GWO algorithm draws inspiration from the social structure and hunting strategy of grey wolves to address optimization challenges. It keeps track of the top three best solutions found during the search process and uses them to guide the movement of the other candidate solutions. All remaining agents update their positions based on these leaders, enabling the group to explore and exploit the search space efficiently. The position updates are governed by specific mathematical expressions that simulate the pursuit and surrounding of prey.

$$\vec{D}_\alpha = \left|\vec{C}_1 \cdot \vec{X}_a - \vec{X}\right| \tag{3.104}$$

$$\vec{D}_\beta = \left|\vec{C}_2 \cdot \vec{X}_\beta - \vec{X}\right| \tag{3.105}$$

$$\vec{D}_\delta = \left|\vec{C}_3 \cdot \vec{X}_\delta - \vec{X}\right| \tag{3.106}$$

$$\vec{X}_1 = \vec{X}_\alpha - \vec{A}_1 \cdot \left(\vec{D}_\alpha\right) \tag{3.107}$$

$$\vec{X}_2 = \vec{X}_\beta - \vec{A}_2 \cdot \left(\vec{D}_\beta\right) \tag{3.108}$$

$$\vec{X}_3 = \vec{X}_\delta - \vec{A}_3 \cdot (\vec{D}_\delta) \tag{3.109}$$

$$\vec{X}(t+1) = \frac{\vec{X}_1 + \vec{X}_2 + \vec{X}_3}{3} \tag{3.110}$$

For solving multi-objective problems, GWO is extended with two additional strategies. First, an archive is maintained to store non-dominated (Pareto optimal) solutions. Second, a leader selection mechanism chooses the alpha, beta, and delta from this archive to lead the optimization process. These enhancements make the algorithm suitable for handling complex multi-objective optimization tasks, similar to techniques used in MOPSE.

The flowchart in figure 3.10 illustrates the methodology of the MOGWO for determining the optimal location and capacity of DPFC in a power system. The process begins with inputting system data and defining the inequality constraints of the power system, as outlined in equations (3.94) to (3.96). The grey wolf population is then initialized, along with control parameters $\vec{a}$, $\vec{A}$, and $\vec{C}$, which guide the optimizer. A Newton-Raphson load flow analysis is performed using a DPFC non-linear control technique, followed by the calculation of objective values for each search agent using equations (3.85) to (3.93). Non-dominated solutions are identified to initialize the archive, and leaders—alpha, beta, and delta wolves—are selected by temporarily excluding and then restoring them to the archive.

The iterative optimization process begins by checking if the archive is full. If it is, a grid mechanism is applied to manage the diversity of solutions; if the new solution lies outside the hypercubes, the grid is updated. Otherwise, one archive member is omitted to make space for the new solution. The positions of search agents are updated using equations (3.104) to (3.110), followed by updates to the control parameters. The Newton-Raphson load flow analysis is run again, and objective values are recalculated using equations (3.85) to (3.93), which represent the core optimization metrics such as power loss, voltage profile, and operational cost. New non-dominated solutions are identified and used to update the archive, and leaders are reselected. This loop continues until the maximum number of iterations is reached, at which point the optimization process ends. The use of the MOGWO technique allows for efficient exploration and exploitation of the solution space, providing a Pareto-optimal set of solutions for the optimal placement and sizing of DPFCs in the system.

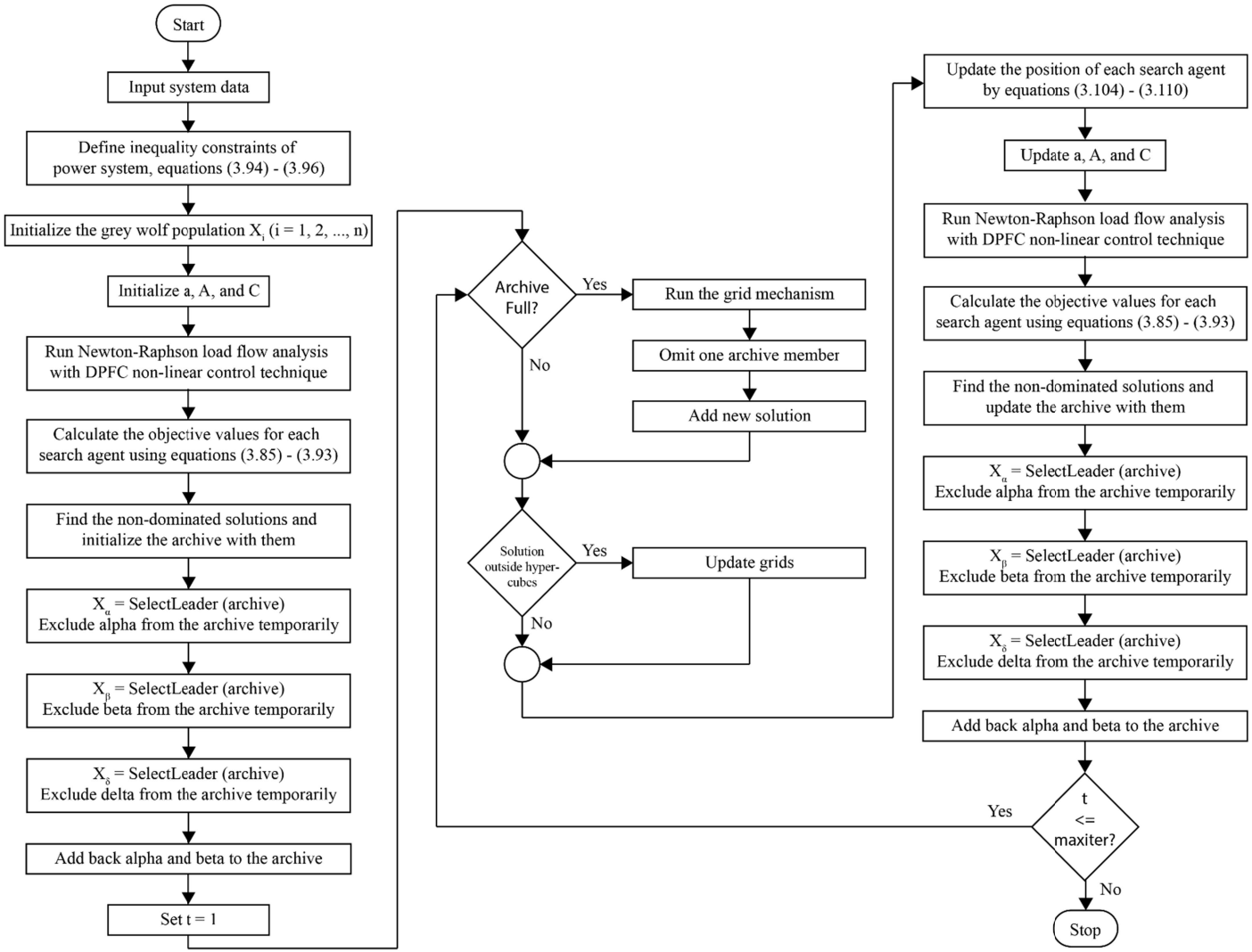

Figure 3.10: Flowchart of MOGWO to Optimize Location and Capacity of DPFC

3.8 Data Analysis

3.8.1 Steady State Load Flow Analysis

The goal of steady state load flow analysis is to ascertain the active and reactive power flows in all transmission lines under steady-state operating conditions, as well as the voltage magnitude and angles at each bus. The parameters so obtained is used to determine VSI, VCPI, system losses, voltage deviation before and after incorporating DPFC in optimal locations.

3.8.2 Maximum Loading Analysis

Maximum loading analysis determines the upper limit of power that a grid system, transmission line, or substation can handle without violating operational constraints. This analysis identifies potential bottlenecks, ensures reliability, and guides system upgrades to prevent overloading and instability.

3.9 Dataset Description

Generation Data: The generation-related information used in this study has been sourced from official government institutions, including the Department of Electricity Development (DOED) and the Annual Reports published by the NEA.

Transmission Line Data: Data related to the transmission network has been collected from the NEA Annual Reports and the Transmission System Development Plan of Nepal.

Load Data: Load demand data has been obtained from the Water and Energy Commission Secretariat (WECS) reports, the NEA Annual Reports, and the Transmission System Development Plan of Nepal.

3.10 Input Data

The system configuration, along with the location and dimensions of loads, generation, and equipment, are defined by the system information displayed on the single-line diagram. The information is shown in an easily understandable manner and is separated into different classes based on their attributes, such as line, generator, bus, and system data.

3.10.1 Bus Data:

The bus data includes information of each bus in a given system, such as:

- Bus number
- Bus name
- Bus type (e.g., slack, PV, or PQ)
- Load demand (active and reactive power)
- Shunt admittance (if any) connected to the bus

3.10.2 Generator Data:

For each generator, the following parameters are considered:

- Active power output (MW)
- Maximum reactive power capability (MVAr)
- Minimum reactive power capability (MVAr)

3.10.3 Transmission Line Data:

Following are parameters of transmission lines:

- Line resistance
- Line reactance
- Shunt charging susceptance
- Thermal ratings
- Operational status

3.11 Test Systems

3.11.1 VSI Assessment on INPS

The INPS is Nepal's main electricity network consisting of 56 generator buses, 73 load buses, 125 lines and 21 transformers which is shown in figure 3.12.

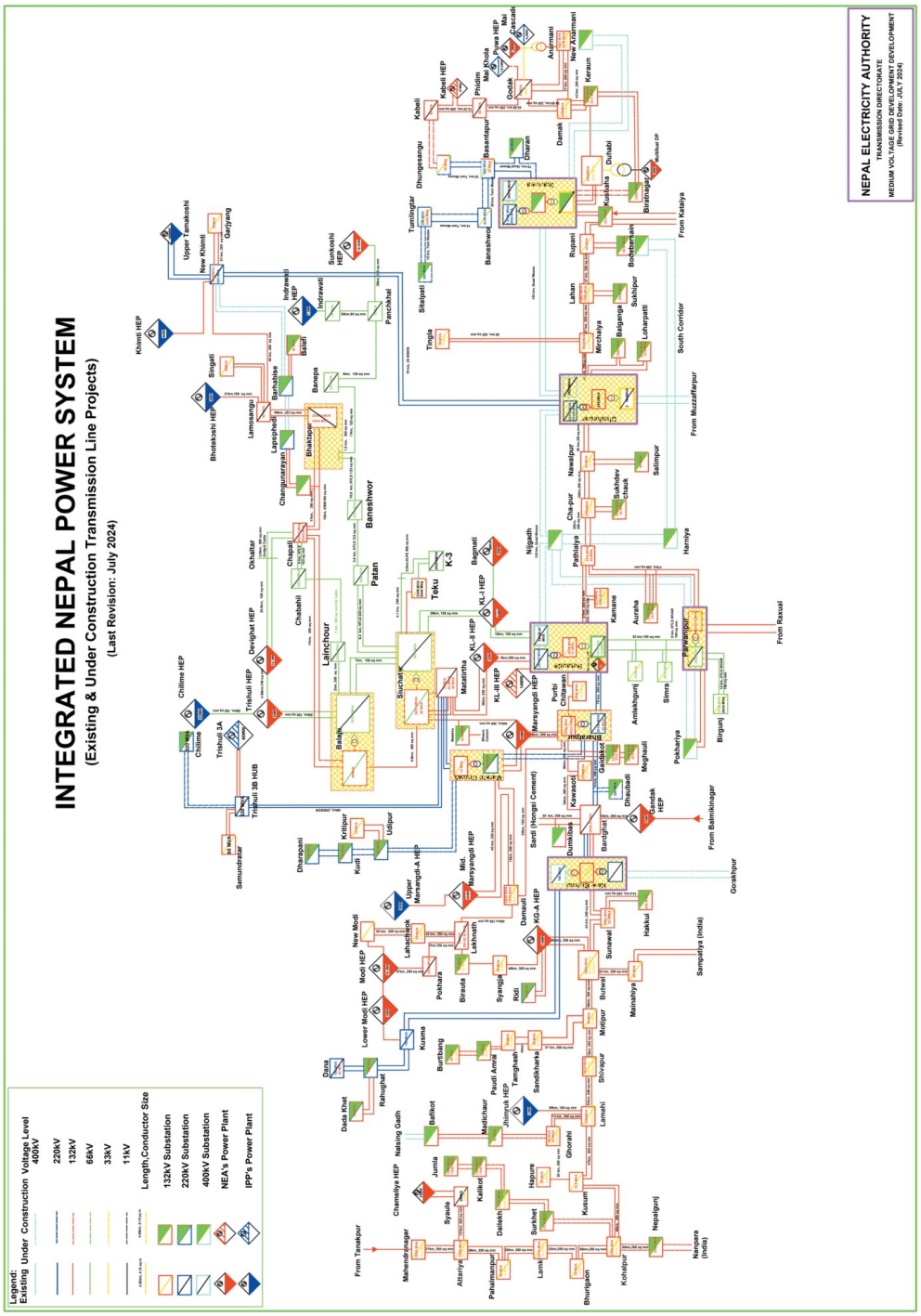

Figure 3.11: Integrated Nepal Power System

3.11.2 DPFC Modelling on IEEE 118 Test Bus System

Figure 3.13 presents the schematic layout of the IEEE 118-bus test system. In this configuration, Bus 69 (Sporn) is designated as the reference or slack bus for the power flow analysis.

IEEE 118 test bus system is divided into three regions with buses as follows:

Region 1: Buses 1-32, Buses 113-115 and Bus 117

Region 2: Buses 33-64

Region 3: Buses 65-112, Bus 116 and Bus 118.

Partition of IEEE 118 test bus system in three region is illustrated in figure

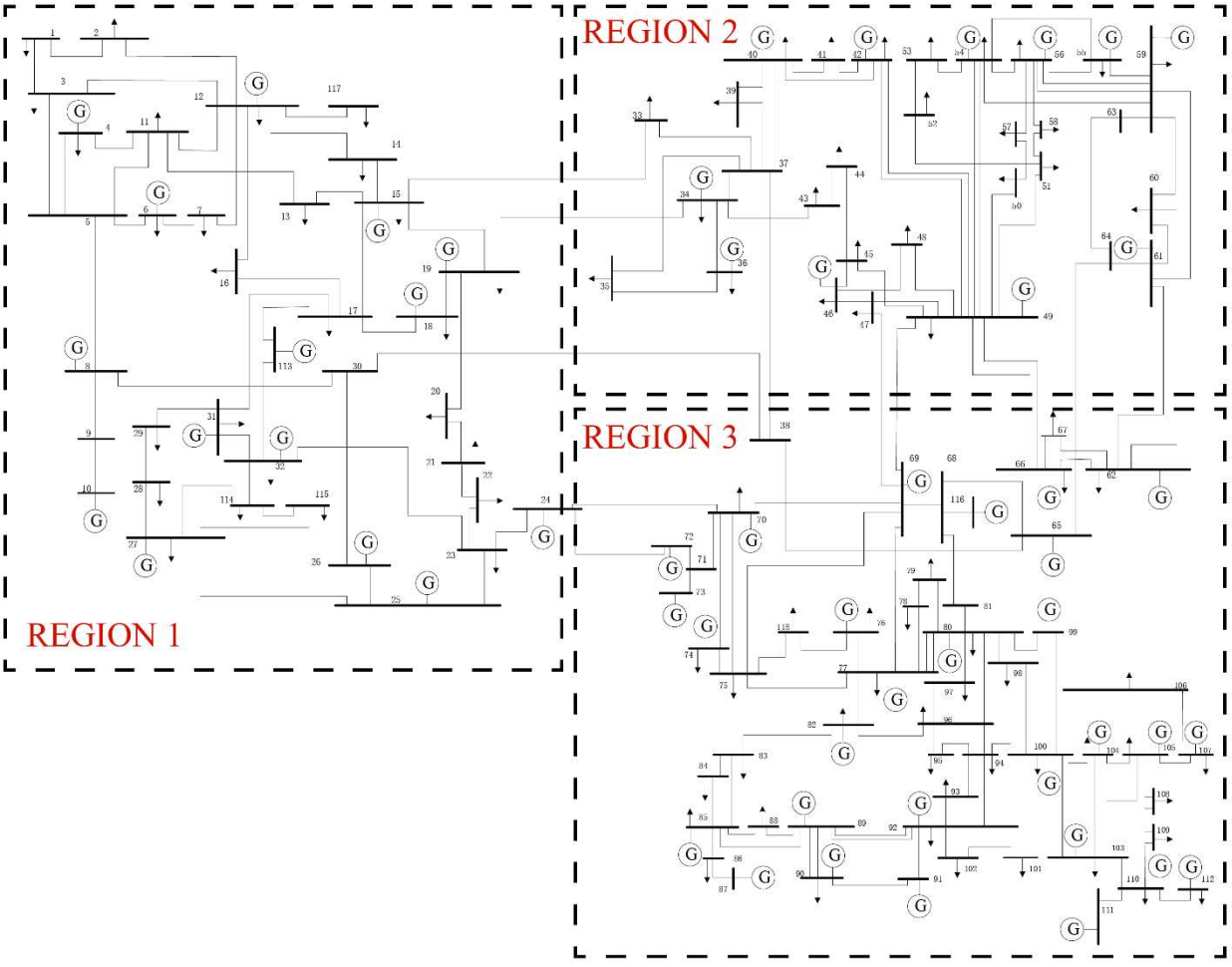

Figure 3.12: IEEE 118 Bus Partitioned Test System

The line information where DPFC are feasible to be implemented of all the three regions are provided in the table below.

Table 3.1: **Line information of all regions where DPFC can be implemented**

	Region 1		Region 2		Region 3	
S.N.	**Shunt side**	**Series end**	**Shunt side**	**Series end**	**Shunt side**	**Series end**
1	1	2	36	35	65	38
2	1	3	34	37	65	64
3	4	5	40	37	66	67
4	6	5	40	39	65	68
5	6	7	40	41	70	71
6	8	9	42	41	72	71
7	8	5	34	43	73	71
8	10	9	46	45	70	75
9	4	11	46	47	74	75
10	12	11	46	48	77	75
11	12	2	49	47	77	78
12	12	3	49	45	80	79
13	12	7	49	48	80	81
14	12	14	49	50	77	82
15	15	13	49	51	85	83
16	15	14	54	53	85	84
17	12	16	56	57	85	86
18	15	17	56	58	87	86
19	18	17	59	60	85	88
20	19	20	61	60	89	88
21	24	23	62	60	92	93
22	25	23	59	63	92	94
23	27	28	61	64	80	96
24	8	30			80	97
25	26	30			80	98
26	31	17			100	94
27	31	29			100	98
28	32	23			100	101
29	15	33			92	102
30	113	17			100	106
31	32	114			105	106
32	27	115			105	108
33	12	117			107	106
34					110	109
35					116	68
36					76	118

CHAPTER FOUR: RESULTS AND DISCUSSIONS

4.1 Voltage Stability Assessment of INPS

Voltage stability assessment of nine grid division is conducted and results and discussions of five grid division is presented in this paper as:

4.1.1 Kathmandu Grid Division

Figure 4.1 compares VSI with VCPI. When reactive power reaches 200 MVAr, VSI is 0.54, and its slope sharply decreases, while VCPI rises to 0.02. The bus's maximum loading is determined to be 1040 MVAr, where VSI drops to 0.08, VCPI increases to 0.12, and the critical voltage is 0.89. Beyond this loading point, the system collapses with no further steady-state solution.

Figure 4.2 presents the voltages at surrounding buses—bus 2, bus 4, and bus 6—when the reactive power at bus 4 is varied, while Figure 4.3 illustrates the VSI at these buses. Despite a sharp voltage drop at bus 6, its corresponding VSI remains constant well above 0, indicating that the bus is not near voltage collapse. This demonstrates that voltage monitoring alone may not provide sufficient information for predicting voltage collapse.

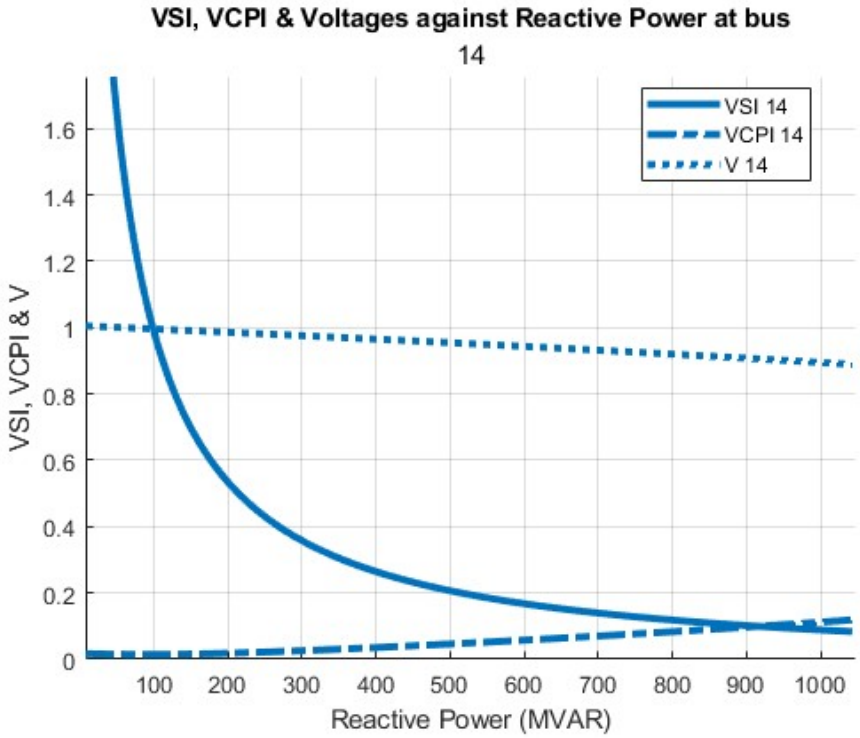

Figure 4.1: VSI, VCPI & Voltage against Reactive Power at bus 14

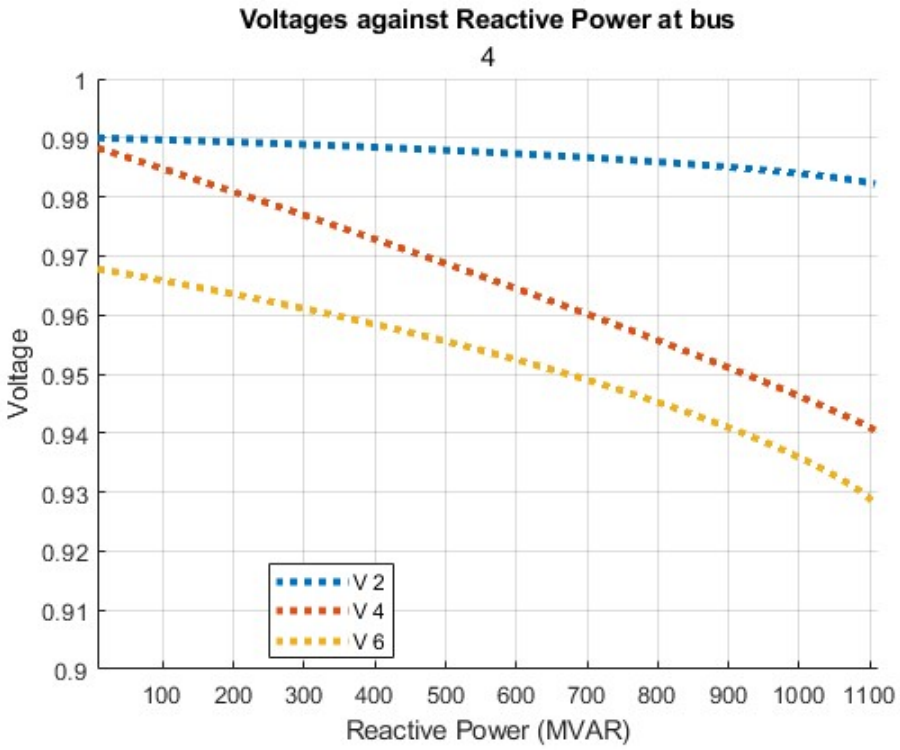

Figure 4.2: Voltages against Reactive Power at bus 4 (Suichatar)

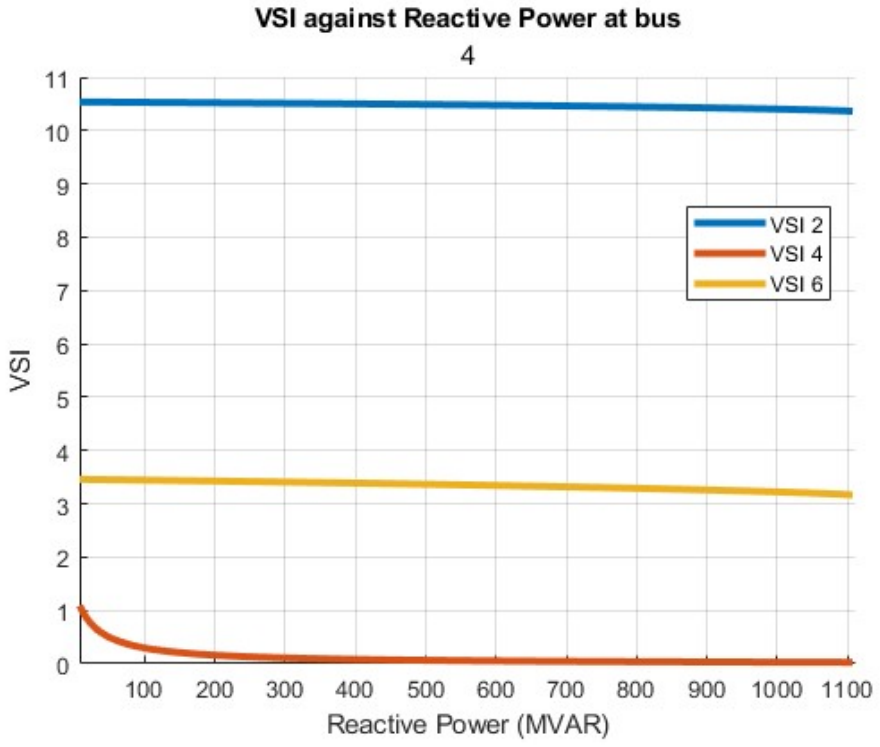

Figure 4.3: VSI against Reactive Power at bus 4

By separately increasing the load at each bus to its maximum loading and plotting the results in MATLAB, figure 4.4 presents a comparison of the VSI for load buses 4, 14, and 26 in the Kathmandu Grid Division. Based on their proximity to voltage instability, the buses are ranked as 14, 4, and 26 for a load variation ranging from 100 MVAr to 300 MVAr. The VCPI and the maximum loading approach yield the same ranking, as shown in figure 4.5.

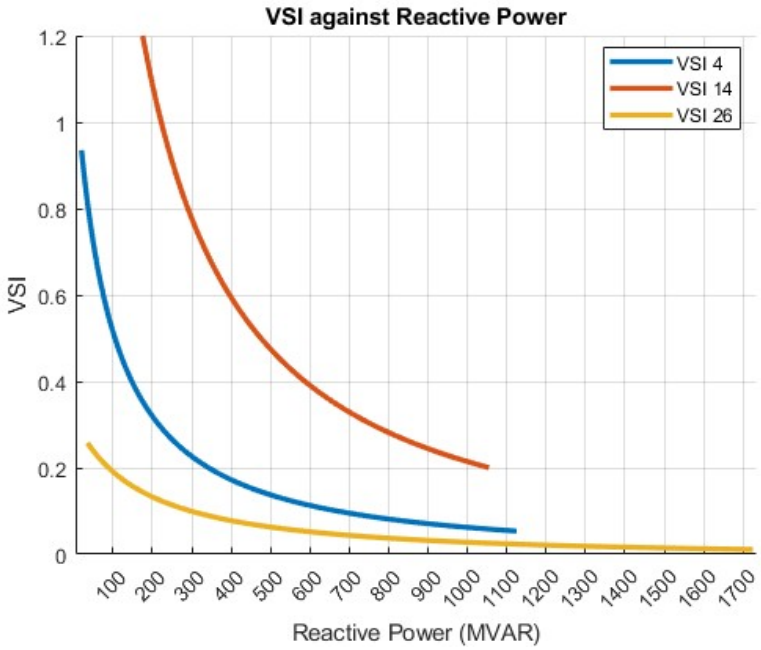

Figure 4.4: Comparison of VSI for load buses of Kathmandu Grid Division

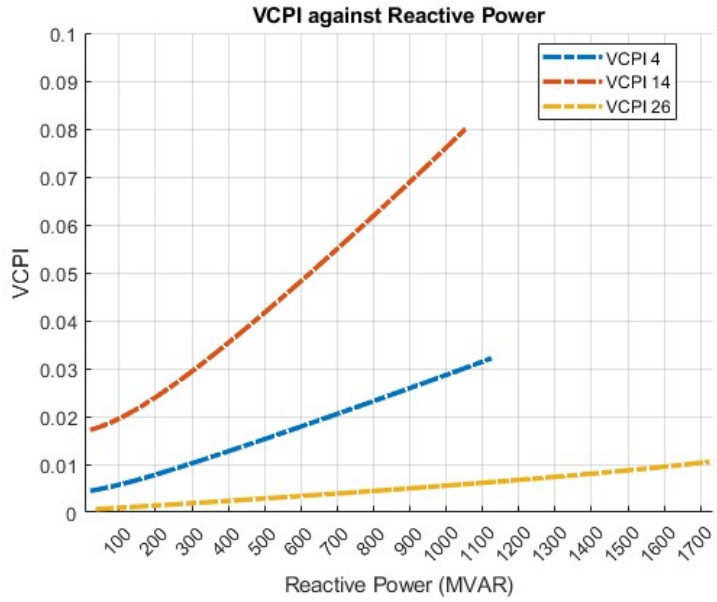

Figure 4.5: Comparison of VCPI for load buses of Kathmandu Grid Division

4.1.2 Hetauda Grid Division

Similar to figure 4.4, figure 4.6 presents the plot of VSI and voltages for various load buses in the Hetauda Grid Division with changing reactive power load. Within the range of 100 MVAr to 300 MVAr, VSI ranks the buses based on proximity to voltage instability as 39, 38 and 33.

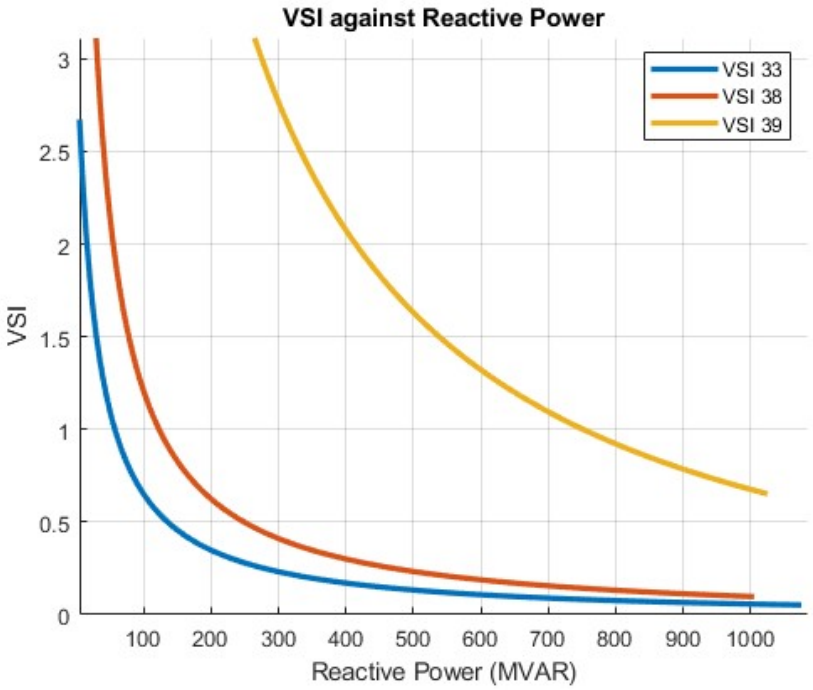

Figure 4.6: Comparison of VSI for load buses of Hetauda Grid Division

4.1.3 Attaria Grid Division

Attaria Grid Division is located at Attaria, Kailali. This division has five substations namely Attaria, Lalpur (Mahendranagar), Lamki, Pahalmanpur, and Syaule. [31] Figure 4.7 shows that bus 104 (Lamki) is the most vulnerable bus among others.

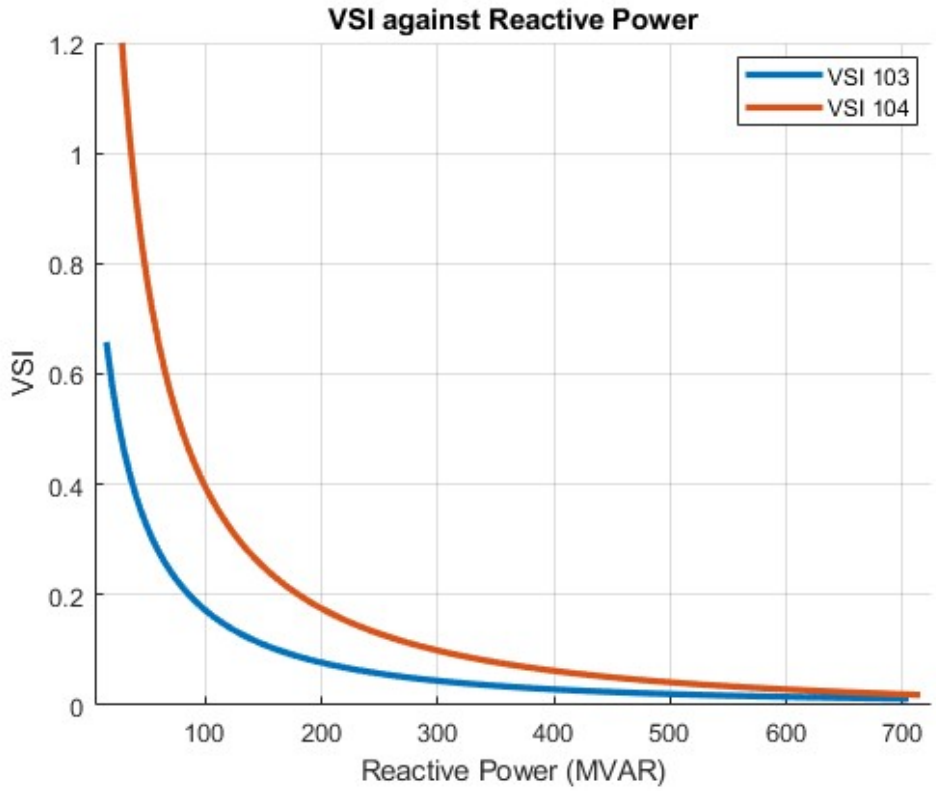

Figure 4.7: Comparison of VSI for load buses of Attaria Grid Division

4.1.4 Dhalkebar Grid Branch

Chapur, Dhalkebar, Lahan, Mirchaiya, Rupani, Tingla, and Nawalpur are major substations of the Dhalkebar Grid Division, operating at 132 kV, 220 kV, and 400 kV. This division is crucial for domestic power transmission and cross-border exchange with India. Figure 4.8 indicates that bus 45 is more stable bus than bus 53 and bus 49 due to its less sensitivity to the change in reactive power loading compared to other substation buses in the Dhalkebar Grid Division.

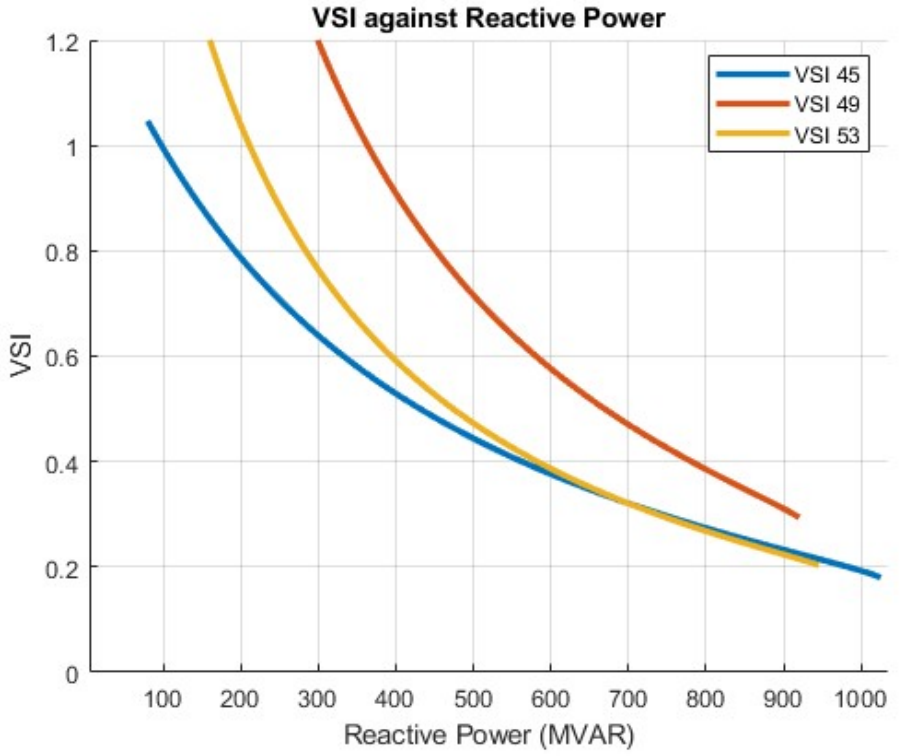

Figure 4.8: Voltage Stability Assessment of Dhalkebar Grid Division

4.1.5 Pokhara Grid Division

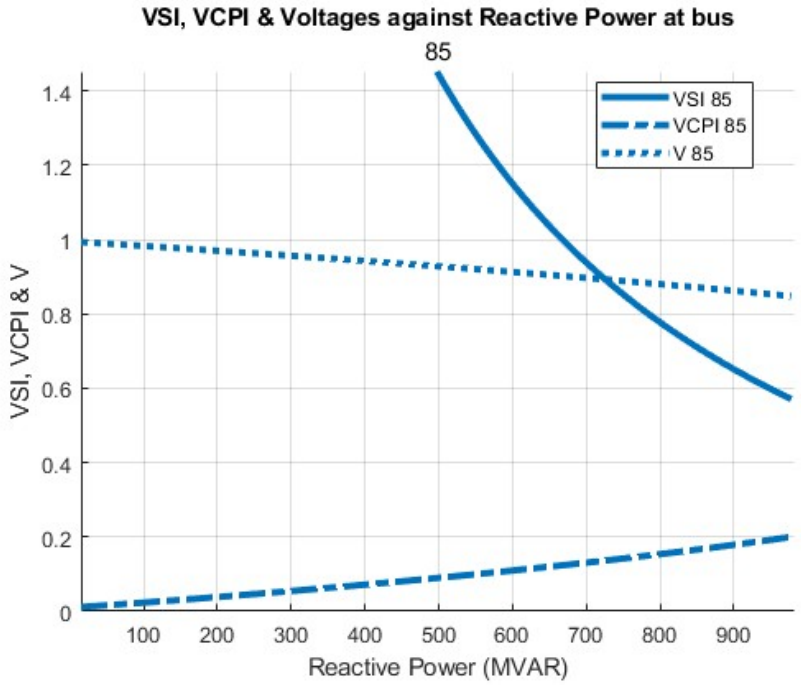

Figure 4.9: VSI, VCPI and Voltage against Reactive Power at bus 85 (Pokhara)

The Pokhara Grid Division, which includes multiple generation stations, demonstrates greater stability compared to other grid divisions. As shown in figure 4.9, the VSI reaches 1 when the loading is 668 MVAr, indicating a higher loading capability and stronger voltage stability in this region.

4.1.6 Discussions

This section conducted a detailed voltage stability assessment of the INPS using a newly developed VSI. The analysis covered all nine grid divisions, with a particular focus on Kathmandu, Hetauda, Attaria, Dhalkebar, and Pokhara. The results identified key vulnerable buses, such as Bus 14 (Matatirtha) in Kathmandu, Bus 39 in Hetauda, and Bus 104 (Lamki) in Attaria, where VSI values dropped significantly near critical loading points. For instance, at Bus 14, VSI decreased to 0.08 when the reactive power reached 1040 MVAr, indicating a high risk of voltage instability. The comparative analysis with the VCPI demonstrated that VSI provides a more computationally efficient and accurate measure of stability margins. Furthermore, the P-V curve validation confirmed that buses with lower VSI values are more prone to voltage collapse. The study underscores the importance of real-time voltage stability monitoring, with the proposed VSI offering a reliable tool for system operators to enhance grid resilience. These findings support the strategic reinforcement of Nepal's transmission network to accommodate the growing electricity demand and ensure secure and stable power supply.

4.2 Optimal Location of DPFC in IEEE 118 Test Bust System

MOGWO methodology is implemented in MATLAB in three different regions of IEEE 118 bus with objective of maximizing total VSI, minimizing total system losses, minimizing total VCPI, maximizing loadability and minimizing total voltage deviation and results obtained with total number of iterations of 1000 is discussed as below:

4.2.1 Region 1:

In the MOGWO optimization results, line 6–5 was selected by the Alpha wolf in region 1, which represents the best solution found by the algorithm. This choice reflects an optimal balance across multiple performance criteria. The Alpha solution achieved a high Voltage Stability Index (298195.33), indicating improved system stability, while also maintaining acceptable levels of real and reactive power loadability (20.31 and 29.18, respectively). Although its loss cost (7321.14) and VCPI (3.05) were higher than those in the Beta and Delta solutions, the Alpha wolf prioritized overall system robustness and voltage profile improvement. Thus, the selection of line 6–5 suggests it is a strategically important point in the network for enhancing voltage stability with minimal compromise on other performance metrics.

Table 4.1: Alpha, Beta & Delta Wolves Best Solution of Location for Region 1

	Max (+) & Min (-)	**Alpha.Best**	**Beta.Best**	**Delta.Best**
Position		4	20	32
Line		6-5	19-20	27-115
VSI.Cost	+	298195.33	297516.43	297593.54
Loss.Cost	-	7321.14	2094.73	378.25
VCPI.Cost	-	3.05	3.31	2.13
$P_{Loadability}$.Cost	+	20.31	20.31	20.31
$Q_{Loadability}$.Cost	-	29.18	50.90	28.61
$V_{deviation}$.Cost	-	2.72	3.02	2.70

Figure 4.10 shows the location of DPFC after choosing the alpha wolf position i.e. line 6-5 in region 1.

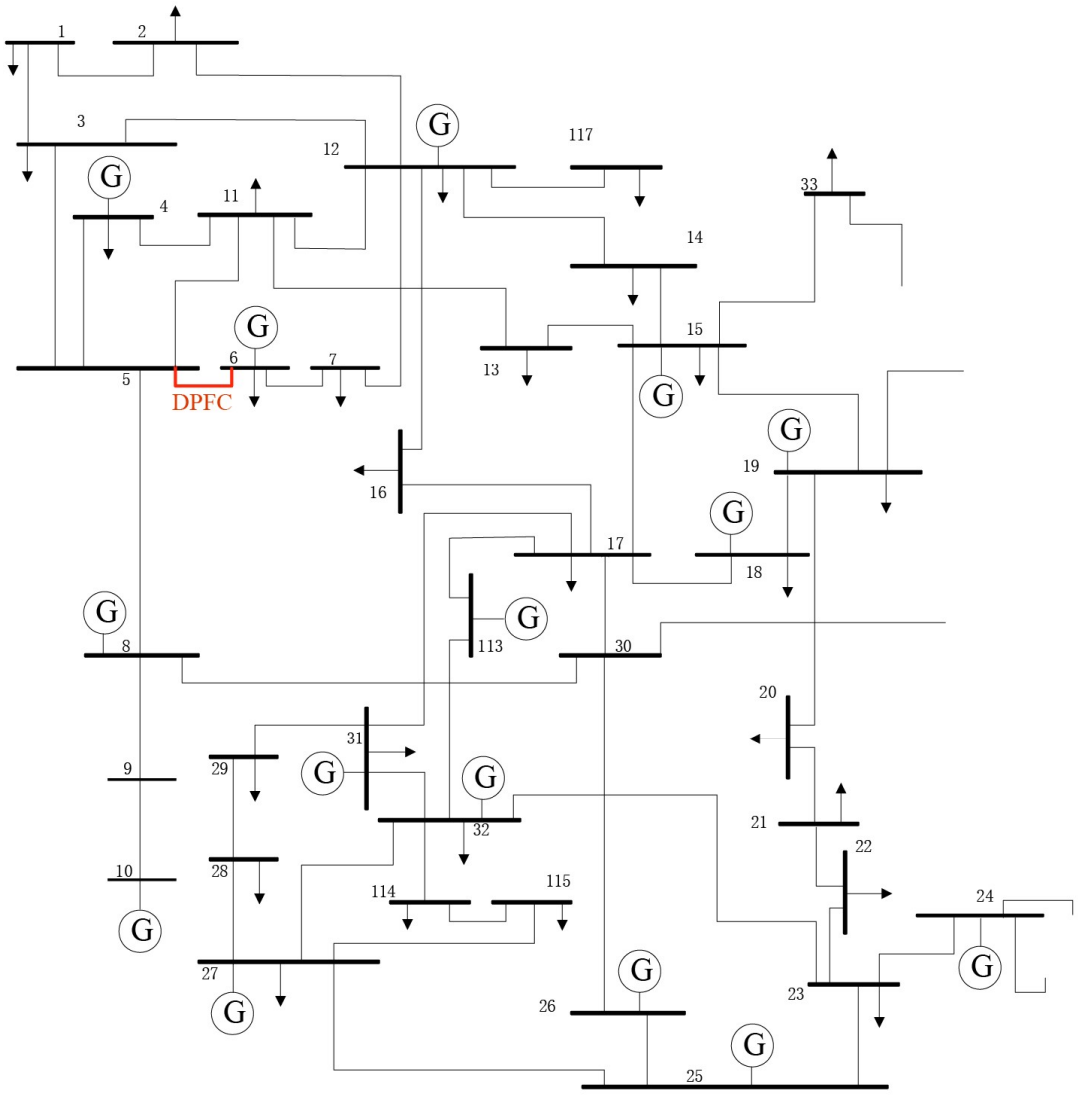

Figure 4.10: Location of DPFC in Region 1 of IEEE 118 System

4.2.2 Region 2

In region 2, line 59–60 was selected by the Alpha wolf (Position 19), indicating it as the most optimal intervention point in the network. Although the Beta wolf achieved a slightly better VSI.Cost (297733.06) and marginally lower VCPI, the Alpha solution demonstrated the lowest total Loss.Cost (-565.68) and the best voltage deviation (-2.73), showing stronger performance in minimizing losses and improving voltage regulation. The real power loadability was consistent across all top solutions (20.31), and the Alpha solution's reactive power loadability (-40.03) remained competitive. Therefore, the selection of line 59–60 reflects the Alpha wolf's ability to identify a configuration that enhances overall system efficiency and voltage quality, making it the most balanced and effective choice.

Table 4.2: Alpha, Beta & Delta Wolves Best Solution of Location for Region 2

	Max (+) & Min (-)	**Alpha.Best**	**Beta.Best**	**Delta.Best**
Position		19	9	5
Line		59-60	46-47	40-41
VSI.Cost	+	297585.55	297733.06	297585.55
Loss.Cost	-	-565.68	-564.60	-562.25
VCPI.Cost	-	-2.032	-2.04	-2.04
$P_{Loadability}$.Cost	+	20.31	20.31	20.31
$Q_{Loadability}$.Cost	-	-40.03	-40.70	-40.28
$V_{deviation}$.Cost	-	-2.73	-2.71	-2.72

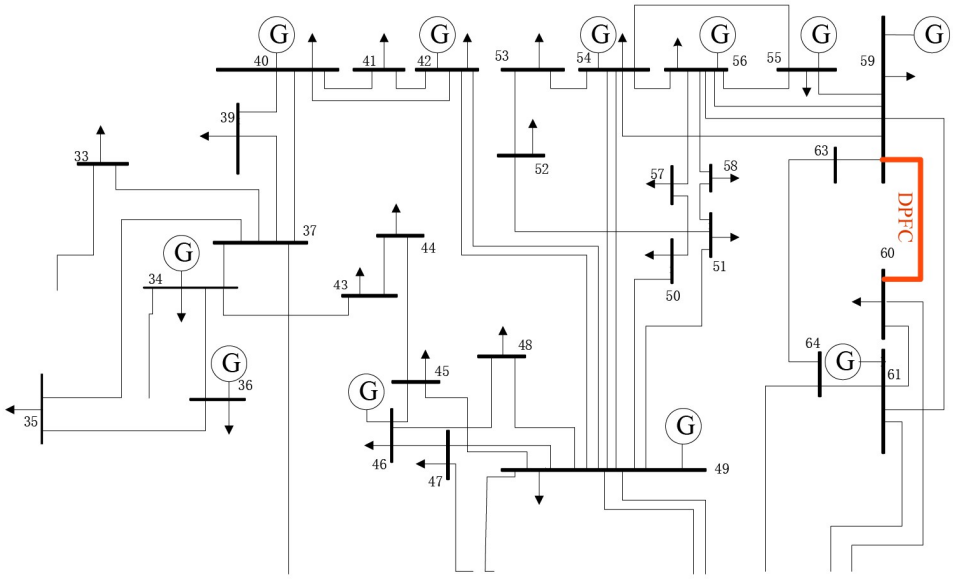

Figure 4.11: Location of DPFC in Region 2 of IEEE 118 System

4.2.3 Region 3

In Region 3, the Alpha wolf selected line 110–109 (Position 34) as the optimal location, even though the Beta and Delta wolves both favored line 80–97, which showed significantly lower Loss.Cost (-94,524.02) and VCPI (-222.85), along with better voltage deviation (-5.36). However, the Alpha solution prioritized Voltage Stability Index (VSI.Cost = 297555.22), which was the highest among all, indicating a stronger focus on improving system voltage stability over raw loss reduction. Additionally, it achieved the best reactive power loadability (-54.51), which can be critical for maintaining power quality under varying load conditions. Thus, line 110–109 was chosen by the Alpha wolf as a balanced solution that emphasizes robust system stability and reactive power performance, making it a strategically strong choice despite the Beta and Delta solutions offering better numerical values in other aspects.

Table 4.3: Alpha, Beta & Delta Wolves Best Solution of Location for Region 3

	Max (+) & Min (-)	**Alpha.Best**	**Beta.Best**	**Delta.Best**
Position		34	24	24
Line		110-109	80-97	80-97
VSI.Cost	+	297555.22	297463.34	297463.34
Loss.Cost	-	-593.67	-94524.02	-94524.02
VCPI.Cost	-	-2.49	-222.85	-222.85
$P_{Loadability}$.Cost	+	20.31	20.31	20.31
$Q_{Loadability}$.Cost	-	-54.51	-36.67	-36.67
$V_{deviation}$.Cost	-	-3.07	-5.36	-5.36

Figure 4.12 shows the location of DPFC after choosing the alpha wolf position i.e. line 110-109 in region 3.

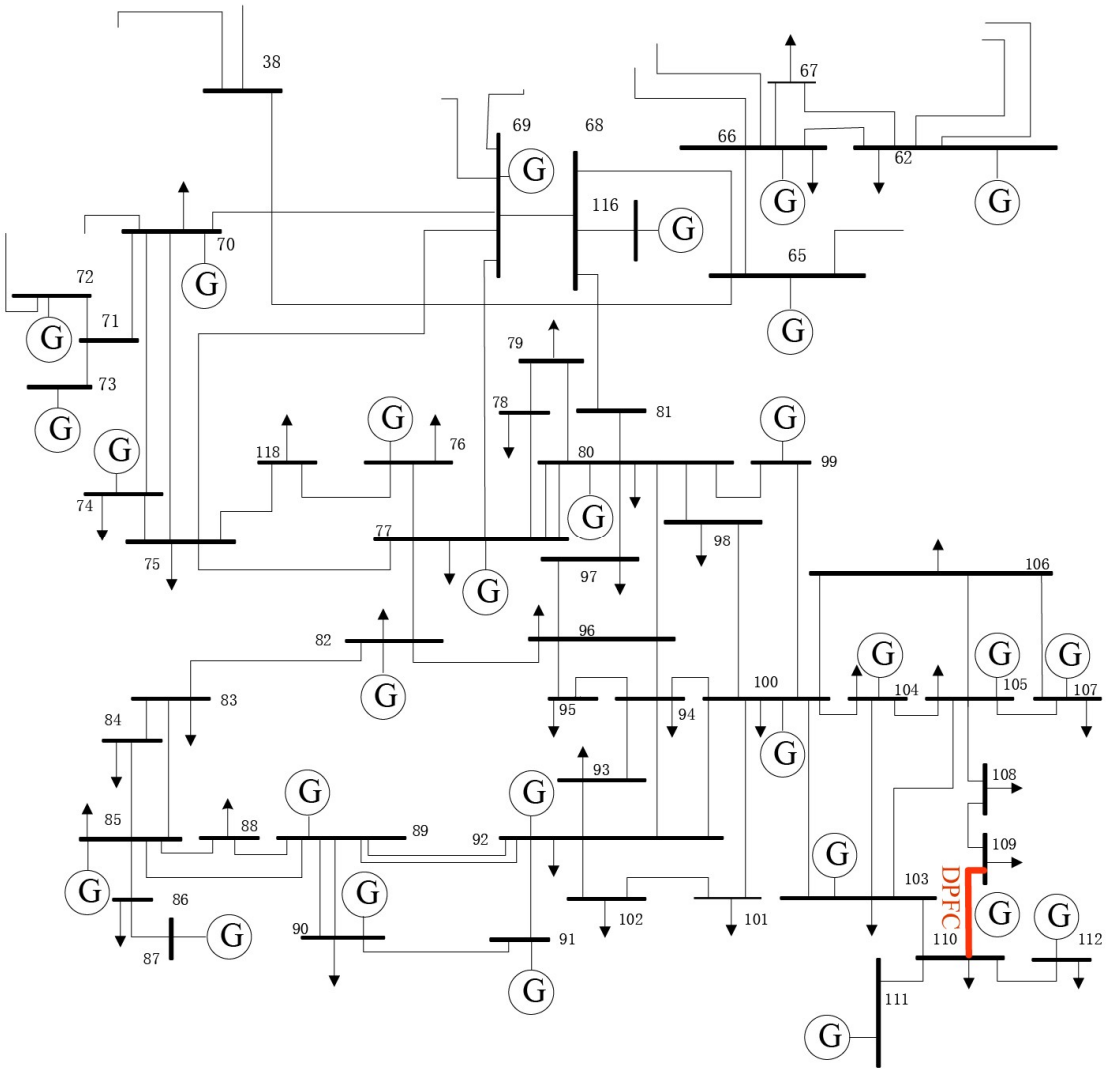

Figure 4.12: Location of DPFC in Region 3 of IEEE 118 System

So, the DPFC is optimally located in lines as 6-5, 59-60 & 110-109. Now, optimal capacity of DPFC in the selected buses is discussed in next section with results.

4.3 Optimal Capacity of DPFC on selected branches

On the three optimal locations of DPFC, the optimal size can be determined by using equations 3.76-3.84 discussed in chapter 3. MOGWO was executed with 2000 iterations to determine the optimal capacities of the series and shunt-side VSCs in the DPFC. The objective was to minimize size and third harmonic shunt voltage deviation given by equations (3.92) and (3.93).

4.3.1 Line 6-5:

Table 4.4 illustrates the best solutions obtained by the alpha, beta and delta wolves for line 6-5. The optimal configuration for line 6–5 is selected based on the alpha wolf's solution due to its minimum shunt size and lower deviation. The final optimal capacities are:

a. **Series side VSC: 212.73 MVAR**
b. **Shunt side VSC: 217.10 MVAR**

Table 4.4: Alpha, Beta & Delta Wolves Best Solution of Capacity for Line 6-5

Line 6-5				
		Alpha.Best	**Beta.Beta**	**Delta.Best**
V_{L-L}		132	132	132
I_3		5.27	12.68	14.81
S_{se}		212.73	212.73	212.73
$V_{se,3}$		23.31	9.69	8.30
$V_{sh,3}$		23.78	14.98	15.71
Objective Function				
S_{sh}	-	217.10	328.99	402.85
$V_{sh3,dev}$	-	6.22	15.02	14.29

4.3.2 Line 59-60:

Similarly choosing the best solution of alpha wolves' position from table 4.5, the optimal capacity for line 59-60 is determined as:

a. **Series side VSC: 27.28 MVAR**
b. **Shunt side VSC: 35.83 MVAR**

Table 4.5: Alpha, Beta & Delta Wolves Best Solution of Capacity for Line 59-60

Line 59-60				
		Alpha.Best	**Beta.Beta**	**Delta.Best**
V_{L-L}		220	220	220
I_3		0.83	0.83	0.96
S_{se}		27.28	27.28	27.28
$V_{se,3}$		19.00	18.94	16.33
$V_{sh,3}$		24.95	24.94	24.92
Objective Function				
S_{sh}	-	35.83	35.93	41.62
$V_{sh3,dev}$	-	5.05	5.06	5.08

4.3.3 Line 110-109:

Again, the best solution of alpha wolves' position is chosen from table 4.6 determining the optimal capacity for line 59-60 as:

a. **Series side VSC: 27.28 MVAR**
b. **Shunt side VSC: 35.83 MVAR**

Table 4.6: Alpha, Beta & Delta Wolves Best Solution of Capacity for Line 110-109

Line 110-109				
		Alpha.Best	**Beta.Beta**	**Delta.Best**
V_{L-L}		220	220	220
I_3		0.079	0.172	0.075
S_{se}		4.18	4.18	4.18
$V_{se,3}$		30.52	14.02	32.15
$V_{sh,3}$		32.14	26.03	33.54
Objective Function				
S_{sh}	-	4.40	7.75	4.36
$V_{sh3,dev}$	-	2.03	3.96	3.66

The optimal DPFC capacities determined for the selected lines using MOGWO demonstrate effective sizing for enhanced voltage stability with minimized shunt side capacity and third harmonic shunt voltage deviation.

4.4 DPFC Compensated Steady State Analysis of IEEE 118 Test Bus System

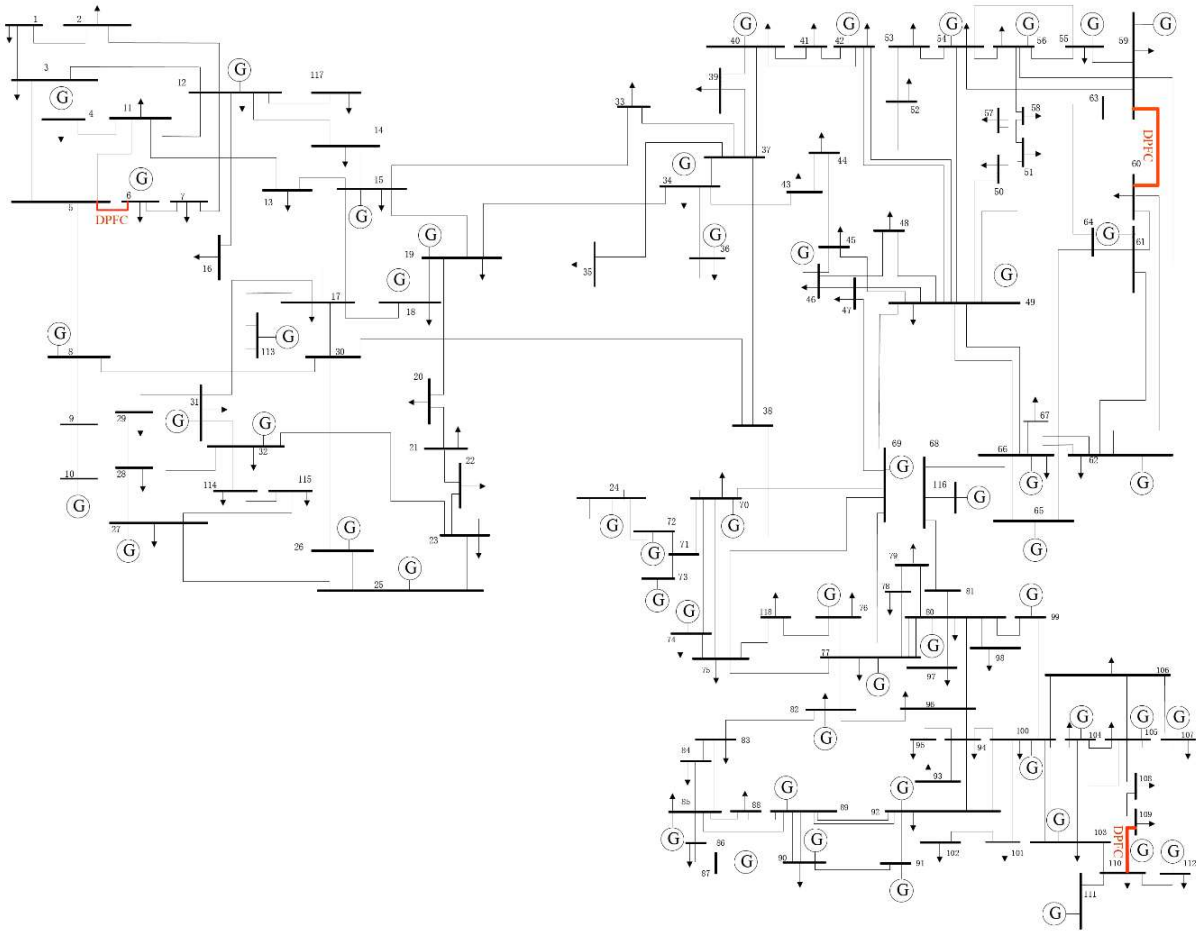

Figure 4.13: IEEE 118 Test Bus System with Optimal DPFC Placement

Based on the MOGWO methodology, DPFC devices are optimally placed on transmission lines 6-5, 59-60 and 110-109 as illustrated in figure 4.13. After incorporating DPFCs into the system, various performance indices are analyzed to assess their impact with non-linear optimal control methodology. The results, as summarized in the table below.

Table 4.7: Comparison of Uncompensated and DPFC Compensated (Optimal) IEEE 118 System

	Uncompensated	**Compensated with non-linear optimal controlled DPFC**
Active Power Loss	136.54 MW	132.19 MW
Reactive Power Loss	545.93 MVAR	572.10 MVAR
Total System Loss	562.75 MVA	587.18 MVA
Total VSI	297586.332	297739.7178
Total VCPI	2.035283918	2.0158655
$\mathbf{P_{Loadability}}$	20.3142862	20.3142862
$\mathbf{Q_{Loadability}}$	40.09076327	35.951203
Total $\mathbf{V_{deviation}}$	2.729849118 pu	2.6712162 pu

Various indices and values are compared between the uncompensated IEEE 118 test bus system and compensated non-linear optimal control of DPFC in table 4.7. The further discussion of the indices and parameters is described below:

4.4.1 Active Power Loss

The integration of a non-linearly controlled DPFC results in a reduction of active power loss from 136.54 MW to 132.19 MW. This improvement signifies better system efficiency, as less real power is dissipated in the transmission lines. The reduction in active power loss demonstrates the effectiveness of DPFC in optimizing power flow and minimizing unnecessary energy loss.

4.4.2 Reactive Power Loss

Reactive power loss increases slightly from 545.93 MVAR in the uncompensated system to 572.10 MVAR in the DPFC-compensated system. This rise can be attributed to the reactive power exchange introduced by the DPFC while regulating voltages and controlling power flow. Although the increase seems counterintuitive, it often accompanies enhanced voltage support and improved voltage profile control.

4.4.3 Total System Loss:

The total system loss, which includes both active and reactive components, increases from 562.75 MVA to 587.18 MVA after compensation. Despite the reduction in active losses, the larger reactive power flow contributes to the overall increase. This trade-off is acceptable in scenarios where voltage stability and power quality are prioritized over apparent power loss.

4.4.4 Total VSI:

The total VSI improves marginally from 297586.33 to 297739.72 with DPFC compensation. A higher VSI reflects a more stable voltage profile and a system that is better equipped to withstand disturbances or heavy loading. The improvement suggests that the DPFC contributes positively to maintaining voltage stability across the network.

4.4.5 Total VCPI:

The total VCPI decreases from 2.0353 to 2.0159, indicating that the system becomes slightly less prone to voltage collapse. A lower VCPI value implies that the system operates further from the critical point of voltage instability, showcasing the DPFC's ability to enhance the robustness of voltage support mechanisms under varying load conditions.

4.4.6 Reactive Power Loadability:

Reactive power loadability decreases from 40.09 MVAR to 35.95 MVAR with the inclusion of the DPFC. This slight reduction may result from the altered reactive power distribution in the system due to DPFC control. However, the decrease is relatively small and is outweighed by the benefits in voltage control and stability.

4.4.7 Total Voltage Deviation:

There is a reduction in total voltage deviation from 2.7298 p.u. to 2.6712 p.u., indicating that the DPFC helps maintain voltages closer to their nominal values across the system. This enhancement in voltage profile leads to improved power quality and system reliability, especially under dynamic loading conditions.

These observations collectively show that DPFC compensation enhances voltage stability and efficiency, even if it introduces slight increase in reactive power handling and apparent system losses.

4.5 Load Flow Analysis with Non-linear (Optimal) Control of DPFC on the IEEE-118 Bus Test System

A load flow analysis incorporating non-linear optimal control of a DPFC has been carried out on the IEEE 118-bus test system. The effects on bus voltages and line flows for the DPFC-compensated lines 6–5, 59–60, and 110–109 are discussed below.

4.5.1 Line 6-5

In the uncompensated case, the system operates with a power flow of 87.68 MVA from Bus 6 to Bus 5. The sending-end voltage at Bus 6 is 1.004 p.u. ∠ -14°, and the receiving-end voltage at Bus 5 is 0.99 p.u. ∠ -17°, indicating a phase angle difference of 3°, which limits power transfer.

In the DPFC compensated case, after injecting a series voltage $\left|V_{se,1}\right|, \delta_{se,1}$, the power transfer increases to 90.51 MVA. The sending-end voltage slightly improves to 1.005 p.u. ∠ -11°, and the receiving-end voltage is 0.991 p.u. ∠ -14°, effectively reducing the angle difference and improving power flow.

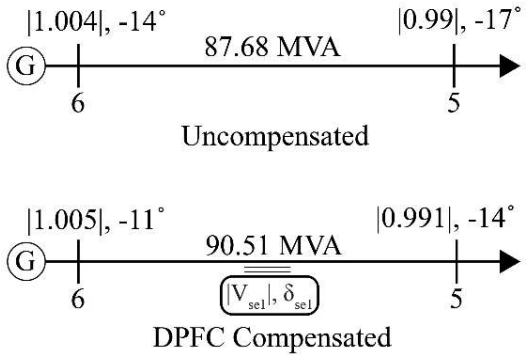

Figure 4.14: Uncompensated and DPFC Compensated (Optimal Control) power flow comparison between bus 6 and bus 5

4.5.2 Line 59-60

In the uncompensated case, the power transfer is 43.45 MVA, with a voltage of 0.985 pu at Bus 59 and 0.993 pu at Bus 60, and a power angle difference of 3.74° (from -10.5° to -6.76°), indicating a moderate mismatch.

With DPFC compensation, Bus 59 maintains a voltage of 0.985 p.u., while Bus 60 increases to 0.996 p.u. The phase angle difference is slightly adjusted to 4.05° (from -9.13° to -5.08°), and power flow rises to 46.82 MVA, demonstrating improved voltage regulation and transfer efficiency.

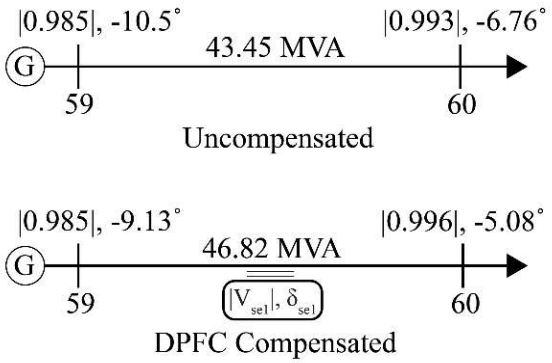

Figure 4.15: Uncompensated and DPFC compensated (optimal control) power flow comparison between bus 59 and bus 60

4.5.3 Line 110-109

In the uncompensated case, power transfer is 59.73 MVA. After DPFC compensation, the power flow is reduced and optimized to 20.4 MVA, suggesting a redistribution of power flow in the network. The voltage at Bus 110 is 0.979 p.u., and at Bus 109 it is 0.978 p.u., with a minimized phase angle difference of just 1.01°, signifying improved synchronism and reduced reactive losses.

The application of non-linear optimal control of DPFC in the IEEE 118-bus system significantly enhances system performance by optimizing power flow, reducing angle differences, improving voltage profiles, and minimizing losses. These improvements contribute to increased transmission efficiency, better voltage regulation, and improved overall stability of the power system.

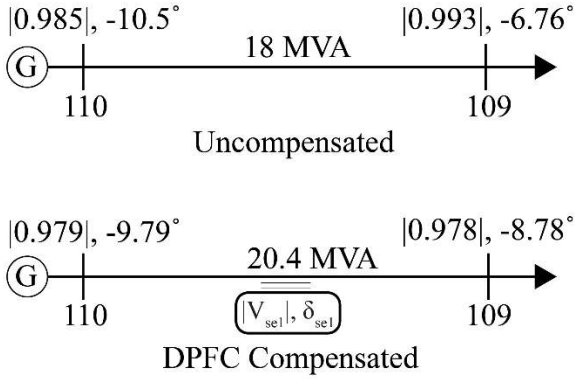

Figure 4.16: Uncompensated and DPFC compensated (optimal control) power flow comparison between bus 110 and bus 109

4.6 Steady State Analysis Non-linear (Maximum) Control of DPFC

To achieve maximum controllability of the DPFC in the IEEE 118-bus test system, the amplitude of the series voltage $V_{se,1}$ is multiplied by a factor of **6.795**. The resulting system performance indices are summarized in the table below.

Table 4.8: Comparison of Uncompensated and DPFC Compensated (Max.) IEEE 118 System

	Uncompensated	**Compensated with non-linear controlled DPFC**
Active Power Loss	136.54 MW	130.05 MW
Reactive Power Loss	545.93 MVAR	592.62 MVAR
Total System Loss	562.75 MVA	606.72 MVA
Total VSI	297586.332	297948.9365
Total VCPI	2.035283918	2.02846716
$\mathbf{P_{Loadability}}$	20.3142862	20.3142862
$\mathbf{Q_{Loadability}}$	40.09076327	21.20897962
Total $V_{deviation}$	2.729849118 pu	2.656175709

The analysis reveals that active power loss is reduced from 136.54 MW (uncompensated) to 130.05 MW (DPFC compensated), indicating improved efficiency in real power transfer. Although reactive power loss increases from 545.93 MVAR to 592.62 MVAR, the overall system performance shows improvement. The VSI increases from 297586.332 to 297948.9365, and the VCPI slightly decreases from 2.0353 to 2.0285, both suggesting enhanced voltage stability. Furthermore, total voltage deviation improves from 2.7298 p.u. to 2.6562 p.u., highlighting better voltage regulation. While active power loadability remains unchanged at 20.31 MW, the reactive power loadability shows a noticeable reduction from 40.09 MVAR to 21.21 MVAR, indicating a trade-off in reactive power support.

In conclusion, DPFC compensation plays a vital role in enhancing power system performance by improving voltage stability, reducing active power losses, and minimizing voltage deviation. The application of non-linear optimal control in DPFC further amplifies these benefits, demonstrating its effectiveness in achieving efficient and stable operation of large-scale power systems.

4.7 Load Flow Analysis with Non-linear (Maximum) Control of DPFC on the IEEE-118 Bus Test System

The load flow analysis under the condition of non-linear maximum compensation using a DPFC on the IEEE-118 Bus Test System reveals the substantial impact of DPFC in enhancing power system performance. Through the analysis of three critical transmission lines—between Buses 6–5, 59–60, and 110–109—the application of DPFC compensation demonstrates clear improvements in power transfer capability, voltage profile, and system stability.

In the uncompensated state, these lines exhibit limited power transfer and larger power angle differences, leading to inefficient power flow and potential voltage stability concerns. For instance, the power flow between Bus 110 and 109 is only 18 MVA with a significant power angle difference, while voltage levels are slightly unbalanced. After applying DPFC compensation, power flow in this line increases sharply to 60 MVA, with voltage levels becoming more controlled and power angle differences better managed.

Similarly, on the line between Buses 6 and 5, power transfer increases from 87.68 MVA to 105.32 MVA with a reversal in power angle direction, indicating a shift in flow control enabled by the DPFC. The line between Buses 59 and 60 also sees a power flow enhancement from 43.45 MVA to 65.80 MVA, along with a more favorable voltage and angle profile.

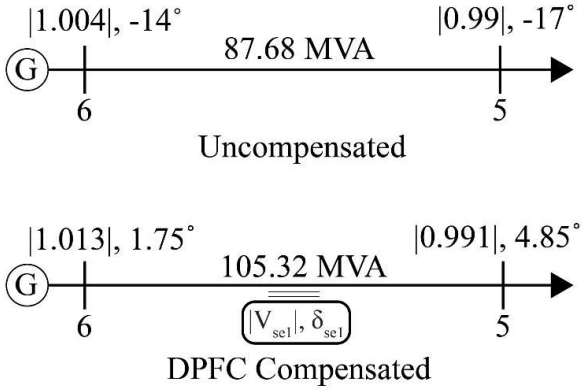

Figure 4.17: Uncompensated and DPFC compensated (maximum control) power flow comparison between bus 6 and bus 5

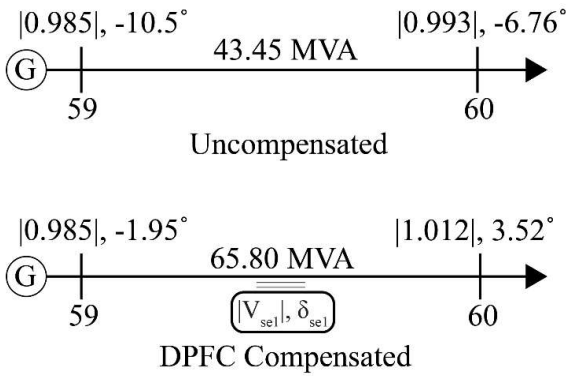

Figure 4.18: Uncompensated and DPFC compensated (maximum control) power flow comparison between bus 59 and bus 60

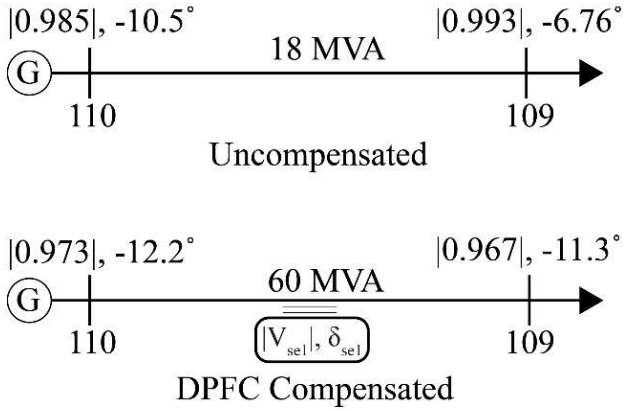

Figure 4.19: Uncompensated and DPFC compensated (maximum control) power flow comparison between bus 110 and bus 109

This analysis highlights how the DPFC's ability to inject controllable series voltage allows it to dynamically regulate power flow and mitigate the effects of system non-linearity. The results confirm that non-linear maximum compensation through DPFC not only increases the power transfer capacity of transmission lines but also contributes to better voltage regulation and enhanced overall reliability of the power system.

4.7.1 Discussions

The implementation of DPFC in the IEEE 118-bus system has led to notable improvements in system performance. The total system active and reactive power losses were reduced from 136.54 MW and 545.93 MVAR in the uncompensated case to 130.05 MW and 597.62 MVAR in the compensated case, indicating enhanced power flow control and loss minimization.

Furthermore, the total VSI increased from 297586.332 to 297948.9365, reflecting a stronger voltage profile and improved stability margins. Simultaneously, the VCPI slightly decreased from 2.035283918 to 2.02846716, suggesting a reduced risk of voltage collapse.

Overall, these results confirm that DPFC compensation enhances system stability and operational efficiency by minimizing losses, improving voltage stability, and reducing the likelihood of voltage collapse in a large-scale power system.

CHAPTER FIVE: CONCLUSION AND RECOMMENDATIONS

5.1 Conclusion

This research aimed to assess and enhance the voltage stability of the INPS using a DPFC with nonlinear control system strategies. The conclusions are drawn from IEEE 118-bus system validations and are proposed for implementation in the INPS, as outlined below:

1. **Justification for Using DPFC in INPS**

   Despite the presence of short transmission lines in INPS, the adoption of DPFC is technically justified due to its modular structure, enhanced operational reliability, cost-effectiveness, and the elimination of a DC link, which reduces insulation requirements and simplifies installation. Unlike traditional UPFCs, DPFC's distributed architecture and independent control over active and reactive power make it well-suited for Nepal's geographically diverse and economically constrained power infrastructure.

2. **Nonlinear Control through Feedback Linearization**

   Given the nonlinear dynamics of DPFC operation in a multi-machine environment, feedback linearization was employed to transform the nonlinear model into an equivalent linear form. This nonlinear control technique enables precise, decoupled control of current components in the series-side converter, ensuring fast response and robust stabilization across wide operating conditions—particularly under N-1 contingencies.

3. **Voltage Stability Assessment of INPS**

   Voltage Stability Indices (VSI and VCPI) were used to evaluate the system. The analysis revealed that bus 14 in Kathmandu, bus 39 in Hetauda, and bus 104 in Attaria are among the most vulnerable regions, exhibiting higher VSI sensitivity in between 100 MVAr and 300 MVAR. Furthermore, Kathmandu demonstrated comparatively poorer voltage stability than Pokhara, highlighting the need for localized voltage support and reactive power compensation in the central region of INPS.

4. **Optimal Location of DPFC using MOGWO**

   Using a MOGWO with five objectives—including voltage stability improvement, power loss minimization, and power flow control—the optimal DPFC locations were identified in lines 6–5, 59–60, and 110–109 in IEEE 118 test bus system. These branches are critical for managing regional voltage stress and improving grid resilience.

5. **Optimal Capacity Sizing of DPFC**

   In the second stage, MOGWO was employed with two objectives—minimization of third harmonic shunt voltage deviation and reduction in reactive compensation size. The optimal capacities were:

   a. **Line 6–5**: Series VSC – 212.73 MVAR, Shunt VSC – 217.10 MVAR
   b. **Line 59–60**: Series VSC – 27.28 MVAR, Shunt VSC – 35.83 MVAR
   c. **Line 110–109**: Series VSC – 4.18 MVAR, Shunt VSC – 4.40 MVAR

6. **Impact of DPFC on INPS Performance**

   The simulation results confirm that DPFC integration significantly improves voltage profiles, reduces system losses, and enhances power flow controllability across the INPS. Nonlinear control facilitates superior dynamic performance, ensuring better voltage regulation even under fault or overloaded conditions, particularly in regions with weak voltage support.

5.2 Recommendations

Based on the findings and conclusions of this study on *assessment of voltage stability using nonlinear control of DPFC in a multi-machine power system*, the following recommendations are proposed for practical implementation and future research:

1. **Minimize Investment Costs through Optimized DPFC Sizing**
   To enhance the affordability and feasibility of DPFC deployment in the Integrated Nepal Power System (INPS), it is recommended to reduce the investment cost by optimally minimizing the size of series and shunt-side converters. This is particularly beneficial for short transmission lines, where large converter capacities are unnecessary and economically impractical.
2. **Implement DPFC in the INPS for Voltage and Power Flow Control**
   The implementation of DPFC in the INPS is strongly recommended to address existing challenges related to voltage instability and limited power flow control. Pilot deployment at the identified optimal locations (lines 6–5, 59–60, and 110–109) will demonstrate its potential in enhancing voltage profiles, reducing losses, and improving overall system stability.
3. **Enhance Power Flow Controllability in Multi-Machine Systems**
   DPFC should be utilized to increase the controllability of power flow in Nepal's multi-machine power system. Its independent control of active and reactive power enables real-time power flow regulation, which is critical for managing grid dynamics, congestion relief, and load balancing across geographically diverse zones of the INPS.

REFERENCES

1. P. Kundur, *Power System Stability and Control*. McGraw-Hill, 1994.

2. *Nepal Electricity Authority: A Year in Review-Fiscal Year-2023/2024*, Nepal Electricity Authority.

3. Rastriya Prasaran Grid Company Limited. (2018), *Transmission System Development Plan of Nepal*, Government of Nepal, Ministry of Energy, Water Resources & Irrigation.

4. M. Haque, "A fast method for determining the voltage stability limit of a power system," *Electric Power Systems Research*, vol. 32, no. 1, pp. 35 - 43, 1995.

5. V. Balamourougan, T. Sidhu, and M. Sachdev, "Technique for online prediction of voltage collapse," Generation, Transmission and Distribution, lEE Proceedings-, vol. 151, no. 4, pp. 453-460, July 2004.

6. R. Maharjan and S. Kamalasadan, "Voltage stability index for online voltage stability assessment," *2015 North American Power Symposium (NAPS)*, Charlotte, NC, USA, 2015, pp. 1-6.

7. N.G. Hingorani and L. Gyugyi, *Understanding FACTS: Concepts and Technology of Flexible AC Transmission Systems.* New York: IEEE Press, 2000.

8. Gadal, Rabiaa & Aziz, Oukennou & Faissal, Elmariami & Belfqih, Abdelziz & Agouzoul, Naima. (2023), "Voltage Stability Assessment and Control Using Indices and FACTS: A Comparative Review," *Journal of Electrical and Computer Engineering,* 2023, 1-18.

9. Z. Yuan, S.W.H. de Haan, J.B. Ferreira and D. Cvoric, "A FACTS Device: Distributed Power-Flow Controller (DPFC)," in *IEEE Transactions on Power Electronics*, vol. 25, no. 10, pp. 2564-2572, Oct. 2010.

10. Gedam, Pradnya S. and Vijay M. Harne. "Comparison of Distributed Power Flow Controller (DPFC) with Unified Power Flow Controller (UPFC) in Power Quality Enhancement." (2018).

11. Chen, Qian & Qiu, Peng & Xiang, Zhongming & Wang, Song & Pan, Wulue & Xie, Haokai. (2021), "The application of Distributed Power Flow Controller in Gan Quan–Xiang Fu 220 kV AC lines in Hu Zhou," *Energy Reports*, 7. 210-215.

12. https://www.nrec.com/en/index.php/about/newsInfo/79.html

13. B. Reddy, "Development of Distributed Power Flow Controller for Improved Performance of the Power System Network," *Indian Journal of Science and Technology*, Vol. 8, No. 10 (2015), pp.17485.

14. Aali, S. R., & Maghouli, P. (2016), “Effect of Distributed Power-Flow Controller (DPFC) on Power System Stability,” *JEPECS*, vol. 1, NO. 3, pp. 99-106, Autumn 2016.

15. S. Nascimento and M. Gouvêa, (2017), “Voltage Stability Enhancement in Power Systems with Automatic Facts Device Allocation,” *Energy Procedia*, (2017), vol. 107, pp. 60-67.

16. Bahamani, Akhib Khan, G.M. Sreerama Reddy, and V. Ganesh, “Voltage Stability Improvement in Fourteen Bus System during Line Interruption Using DPFC,” *International Journal of Power Electronics and Drive Systems (IJPEDS),* Vol. 8, No. 2, June 2017, pp. 705.

17. J. Dai, Y. Tang, Y. Liu, *et al,* “Optimal configuration of distributed power flow controller to enhance system loadability via mixed integer linear programming,” *J. Mod. Power Syst. Clean Energy* **7**, pp. 1484–1494 (2019).

18. Godbole, P. and George, S. 2023. A Novel Algorithm for Optimal Harmonic Load Flow including Harmonic Compensation. *Engineering, Technology & Applied Science Research*. 13, 1 (Feb. 2023), 10093–10099.

19. P. Ramesh and M.D. Reddy, “Control of Power in a Transmission Line by Distributed Power-Flow Controller (DPFC),” *International Journal of Electrical Engineering*, Vol. 5, No. 4, pp. 411-425.

20. Tang, Aihong & Shao, Yunlu & Xu, Qiushi & Zheng, Xu & Huang, Yong, “Study on control method of a distributed power flow controller,” IEEJ Transactions on Electrical and Electronic Engineering, (2019) Vol. 14, No. 10, pp. 1002.

21. H. Yan, A. Tang, J. Yuan, H. Lei, X. Zheng and S. Zhao, "Nonlinear Optimal Control for Distributed Power Flow Controller," *2019 IEEE 4th Advanced Information Technology, Electronic and Automation Control Conference (IAEAC)*, Chengdu, China, 2019, pp. 160-165.

22. M. Xiao and S. Wang, “Coordination Control Method Suitable for Practical Engineering Applications for Distributed Power Flow Controller (DPFC),” *Energies* **2018**, *11*, no. 12: 3406.

23. Y. Jin, A. Tang, Y. Huang, X. Zheng and Q. Xu, "Research for Equivalent Mathematical Model of MMC-DPFC," *2017 International Conference on Industrial Informatics - Computing Technology, Intelligent Technology, Industrial Information Integration (ICIICII)*, Wuhan, China, 2017, pp. 231-236.

24. A. Tang, Z. Lu, H. Yang, X. Zou, Y. Huang and X. Zheng, "Digital/analog simulation platform for distributed power flow controller based on ADPSS and dSPACE," in *CSEE Journal of Power and Energy Systems*, vol. 7, no. 1, pp. 181-189, Jan. 2021.

25. R. Venkatesh, M. Rekha and G. Sundar, “Deciding optimal location for placing FACTS devices [UPFC, IPQC, DPFC] using Bang-Bang control technique,” *IOSR Journal of Electrical and Electronics Engineering*, (2014), Vol. 9, pp. 35-46.

26. J. Chakravorty, and J. Saraswat, “Deciding Optimal Location of DPFC in Transmission Line Using Artificial Algae Algorithm,” *Engineering, Technology & Applied Science Research*, (2019) Vol. 9, pp. 3978-3980.

27. B. Ismail, N. I. Abdul Wahab, M. L. Othman, M. A. M. Radzi, K. Naidu Vijyakumar and M. N. Mat Naain, "A Comprehensive Review on Optimal Location and Sizing of Reactive Power Compensation Using Hybrid-Based Approaches for Power Loss Reduction, Voltage Stability Improvement, Voltage Profile Enhancement and Loadability Enhancement," in *IEEE Access*, vol. 8, pp. 222733-222765, 2020.

28. Pi, Y., Tang, A., Li, J., Shan, S., Feng, Y. (2014), “A Method of the Design of DPFC System Parameters,” *In: Park, J., Pan, Y., Kim, CS., Yang, Y. (eds) Future Information Technology,* Lecture Notes in Electrical Engineering, vol 309. Springer, Berlin, Heidelberg.

29. X. Zhai, A. Tang, X. Zou, X. Zheng and Q. Xu, "Research on DPFC Capacity and Parameter Design Method," *2020 IEEE International Conference on Information Technology,Big Data and Artificial Intelligence (ICIBA)*, Chongqing, China, 2020, pp. 978-982.

30. Mirjalili, Seyedali & Saremi, Shahzad & Mirjalili, Seyed & Coelho, Leandro. (2015). Multi-objective grey wolf optimizer: A novel algorithm for multi-criterion optimization. Expert Systems with Applications.

31. *Nepal Electricity Authority, Transmission/Project Management Directorate: A Year Book – Fiscal Year 2023/2024 (2080/2081 BS),* NEA.

32. http://labs.ece.uw.edu/pstca/pf118/ieee118cdf.txt

33. Arunachalam Sundaram (2024). Load FLow Analysis For IEEE 118 Bus Sytem (https://www.mathworks.com/matlabcentral/fileexchange/170161-load-flow-analysis-for-ieee-118-bus-sytem), MATLAB Central File Exchange. Retrieved November 23, 2024.

34. Seyedali Mirjalili (2025). Multi-Objective Grey Wolf Optimizer (MOGWO) (https://www.math works.com/matlabcentral/fileexchange/55979-multi-objective-grey-wolf-optimizer-mogwo), MATLAB Central File Exchange. Retrieved April 20, 2025.

APPENDIX A.1: IOE GC CERTIFICATE

IOE Graduate Conference

Certificate of Participation

THIS CERTIFICATE IS AWARDED TO

Bimal Adhikari

in recognition of an invaluable contribution as

POSTER PRESENTER

at the 16th IOE Graduate Conference

Organized by Tribhuvan University, IOE, Thapathali Campus in association with IOE, Office of the Dean held from April 18-20, 2025 at Thapathali Campus, Kathmandu, Nepal.

Dr. Raj Kumar Chaulagain
Convener
16th IOE Graduate Conference

Dr. Khem Gyanwali
Campus Chief
Thapathali Campus

Prof. Dr. Sushil Bahadur Bajracharya
Dean
Institute of Engineering

VOLTAGE STABILITY ASSESSMENT OF INTEGRATED NEPAL POWER SYSTEM

Bimal Adhikari [a], Jeetendra Chaudhary [b]

[a, b] *Department of Electrical Engineering, Pulchowk Campus, IOE, Tribhuvan University, Nepal*
[a] 079mspse006.bimal@pcampus.edu.np [b] jeetendra@ioe.edu.np

Abstract
Voltage stability is a critical concern in rapidly expanding power grids like the Integrated Nepal Power System (INPS), where localized instability can escalate into a system-wide collapse. This study introduces a novel Voltage Stability Index (VSI) based on Thevenin equivalent theory and maximum loading capability to assess voltage collapse risks. The analysis covers all nine grid divisions of the INPS, focusing on load buses above 132 kV across five key divisions. The study identifies critical buses, such as Bus 14 in Kathmandu and Bus 104 in Attaria, where VSI drops significantly between 100-300 MVAr loading, indicating vulnerability. In Kathmandu, VSI at Bus 14 decreased to 0.08 at a reactive power loading of 1040 MVAr, while the Voltage Collapse Proximity Index (VCPI) increased to 0.12, signaling proximity to collapse. MATLAB-based simulations demonstrate that VSI provides a computationally efficient alternative to traditional methods like VCPI and P-V curves for identifying weak buses. The findings offer valuable insights for Nepal's power system operators, supporting targeted transmission reinforcement strategies and real-time voltage stability monitoring.

Keywords
Power System Stability, Voltage Instability, Reactive Power Management, Critical Bus Identification, Transmission Network Analysis, Voltage Collapse Prediction, Power Flow Study, Online Stability Monitoring, Phasor Measurement Unit (PMU).

1. Introduction

Nepal Electricity Authority (NEA) has been fulfilling its obligation of generating, transmitting, and distributing reliable, high-quality, and affordable power to consumers for the past 39 years. The demand for electricity has been growing steadily, with the number of consumers reaching 5.46 million in the fiscal year (FY) 2023/24, reflecting a 6.33% increase from the previous year's 5.14 million. In response to the increasing demand, the total length of transmission lines expanded from 5,742 circuit kilometers (circuit km) to 6,508 circuit km, while total substation capacity increased from 8,867 MVA to 13,050 MVA in the same period. Despite these expansions, the existing transmission infrastructure in major cities is anticipated to be insufficient to meet both rising energy consumption and peak power demand in the coming years [1].

The Integrated Nepal Power System (INPS) is Nepal's primary electricity network comprising generation, transmission, and distribution systems. The INPS is managed by the NEA and is organized into several grid divisions, each responsible for overseeing the transmission and distribution of electricity within specific regions. These divisions ensured efficient power delivery across Nepal's diverse topography. [1]

The INPS is organized into nine grid divisions: Kathmandu Grid Division, Hetauda Grid Division, Dhalkebar Grid Division, Duhabi Grid Division, Butwal Grid Division, Pokhara Grid Division, Attaria Grid Division, Khimti Grid Section, and Kohalpur Grid Section. INPS comprises a vast transmission network, including 514.46 circuit km of 66 kV, 3,967.87 circuit km of 132 kV, 1,105 circuit km of 220 kV, and 384 circuit km of 400 kV transmission lines. These are distributed among 17, 50, 10, and 2 transmission lines, respectively. Under these divisions, there are 83 high-voltage grid substations, with a total of 271 transformers of various voltage ratings, contributing to a combined capacity of 13,050 MVA in the fiscal year 2080/81. [1]

Voltage stability remains a critical concern in power system operation, as voltage instability, though primarily a localized phenomenon, can escalate into a system-wide voltage collapse. A progressive voltage decline in buses may lead to cascading outages, tripping of transmission lines and protective elements, and, ultimately, the loss of synchronism among generators [2]. Several factors

contribute to voltage collapse, including increased system loading, reactive power limits of generators and compensating devices, the action of tap-changing transformers, load recovery dynamics, and the tripping of transmission lines or generator outages [3].

To assess the proximity to voltage collapse, voltage stability indices (VSIs) serve as effective analytical tools. A VSI is a scalar quantity that predicts the likelihood of voltage instability, enabling system operators to take corrective measures before a critical event occurs. An ideal VSI should exhibit a smooth and predictable behavior, with fast computation for real-time applications [3]. Various methodologies have been proposed to develop such indices, each employing different mathematical approaches to determine the system's vulnerability to voltage instability.

In this paper, a VSI is developed based on the maximum loading capability and Thevenin equivalent theory [4]. Unlike existing indices such as those proposed in [5], [6], which are applicable only to distribution feeders, the proposed VSI is specifically formulated for transmission networks. The methodology involves reducing the transmission network into an equivalent two-node system using a fast computational approach as described in [9]. This VSI can be applied using both power flow analysis and Phasor Measurement Unit (PMU) data, making it a versatile tool for assessing system stability under varying operating conditions.

This study presents a comprehensive voltage stability assessment for five grid divisions within the INPS. The computed VSI results provide insights into the stability margins across various grid divisions, highlighting potential vulnerabilities and areas requiring reinforcement. The findings aim to assist in strategic decision-making for transmission system planning and real-time voltage stability monitoring.

The paper is divided into four sections. Section 1 discusses Nepal's growing electricity demand and voltage stability challenges. Section 2 introduces the proposed VSI, comparing it with VCPI and P-V curves. Section 3 explains the MATLAB-based methodology for computing VSI across INPS grid divisions. Section 4 presents results, identifying vulnerable buses like Matatirtha (Bus 14) and Lamki (Bus 104), confirming VSI's effectiveness for online stability monitoring.

2. Methodology

2.1 Thevenin Equivalent Methodology

The no-load or Thevenin equivalent voltage V_{th} of load bus r can be obtained from the load flow solution. The voltage and impedance of the Thevenin equivalent circuit are obtained by slightly modifying the load flow solution and the diagonal elements of the Z-matrix in order to nullify the effects of load impedance at the candidate bus.

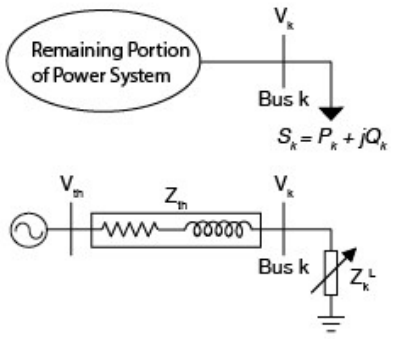

Figure 1: Thevenin Equivalent of Power System

Schematic diagram of Thevenin equivalent of a power system is shown in figure 1. The load impedance of bus k for constant power can be written as [7]

$$Z_k^L = \frac{|V_k|^2}{P_k - jQ_k} \quad (1)$$

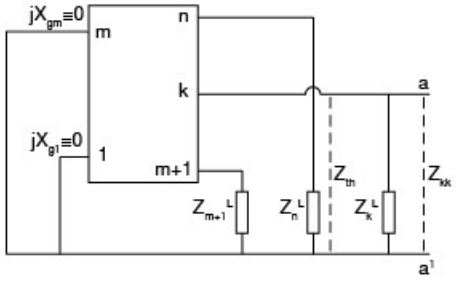

Figure 2: Generator model and Thevenin impedance of load bus

Figure 2 is the schematic diagram of generator model in power system with constant terminal voltage and series reactance X_g of internal voltage source equal to zero. Here buses 1 to m are the generator buses and buses m+1 to n are the load buses. If Z_{kk} is the kth diagonal element of the Z matrix when all loads are considered, then Thevenin impedance can be obtained as:

$$Z_{th} = \left(\frac{1}{Z_{kk}} - \frac{1}{Z_k^L}\right)^{-1} \quad (2)$$

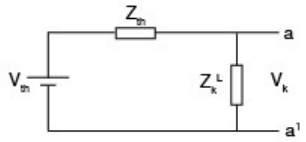

Figure 3: Calculation of Thevenin equivalent of bus k

Figure 3 shows the schematic diagram for calculation of Thevenin equivalent of bus k. Thevenin voltage is given as:

$$V_{th} = \left(1 + \frac{Z_{th}}{Z_k^L}\right) V_k \tag{3}$$

Obtaining values of parameters from Newton Raphson load flow analysis, a voltage stability index of bus *k* for determining proximity to the voltage collapse based on maximum loading capability [4] is derived in appendix A which is given as:

$$VSI = \frac{-b \pm \sqrt{b^2 - 4ac}}{2a} \tag{4}$$

where,

$$a = 4Y_{kk}^2 \left[(P_k \cos\theta - Q_k \sin\theta)^2 - \left(P_k^2 + Q_k^2\right)\right] \tag{5}$$

$$b = 4V_{th}^2 Z_{th}^{-2} Y_{kk} (P_k \cos\theta - Q_k \sin\theta) \tag{6}$$

$$c = V_{th}^4 Z_{th}^{-4} \tag{7}$$

2.2 Voltage Collapse Proximity Index

In a power system network, for a bus k; voltage collapse proximity index (VCPI) [8] is given as:

$$VCPI_{kth\ bus} = \left| 1 - \frac{\sum_{\substack{m=1 \\ m \neq k}}^{N} V_m'}{V_k} \right| \leq 1 \tag{8}$$

where,

$$V_m' = \frac{Y_{km}}{\sum_{\substack{j=1 \\ j \neq k}}^{N} Y_{kj}} \tag{9}$$

2.3 Power-Voltage Curve

For $\tan\phi = \frac{P_k}{Q_k}$, a relation for power-voltage curve equation [2] is obtained as:

$$p = -v^2 \sin\phi \cos\phi + v \cos\phi \sqrt{1 - v^2 \cos^2\phi} \tag{10}$$

where,

$$p = \frac{P_k}{(V_{th}^2/Z)} \tag{11}$$

$$v = \frac{V_k}{V_{th}} \tag{12}$$

2.4 Flowchart

Figure 4 outlines a stepwise process for voltage stability assessment. It starts with load flow analysis to calculate load impedance (Z_L) and extracts the diagonal element (Z_{kk}) of the impedance matrix. Then, Thevenin impedance (Z_{th}) and voltage (V_{th}) are computed. Using these values, VSI is determined, followed by recalculating VSI and VCPI for stability assessment.

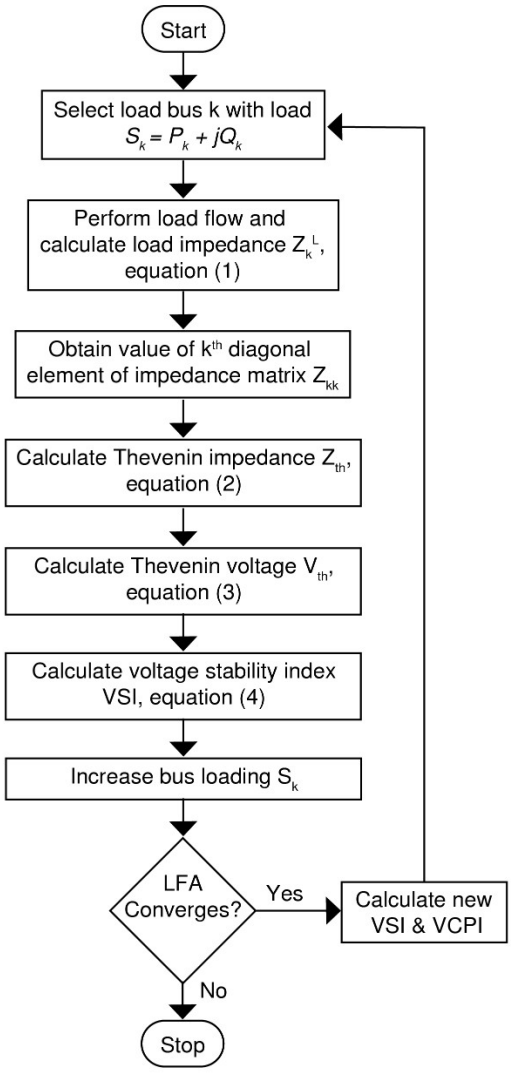

Figure 4: Flowchart for Online Voltage Assessment

2.5 Methodology

Taking Muzzafarpur as a reference bus in INPS, voltage stability assessment for all nine grid divisions of INPS is conducted in MATLAB by progressively increasing the load on each bus (buses above 132 kV) until it reaches its critical loading point, leading to system collapse. This approach evaluates the loading capacity of different buses and their ability to sustain increasing demand. A significant

3. Results and Discussions

variation in the magnitude of the proposed VSI indicates buses that are more susceptible to voltage instability. Additionally, the characteristics of the P-V curve provide insights into system loading behavior, while the VCPI quantifies the proximity of buses to voltage collapse.

Voltage stability assessment of nine grid division is conducted and results and discussions of five grid division is presented in this paper as:

3.1 Kathmandu Grid Division

Kathmandu Grid Division located at Minbhawan, Kathmandu has sixteen substations namely Balaju, Banepa, Baneshwor, Bhaktapur, Chapali, K3, Lainchaur, Matatirtha, New Chabahil, New Patan, Panchkhal, Siuchatar, Teku, Malekhu, Grang, and Samundratar. 66 kV and higher voltage transmission lines inside the Kathmandu Valley are connected mainly from Chilime, Devighat, Khimti, Marsyangdi, Trishuli, Trishuli 3A, and Kulekhani. [9]

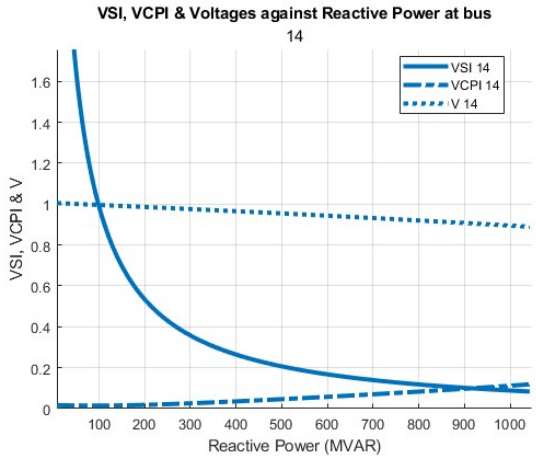

Figure 5: VSI, VCPI & Voltage against Reactive Power at bus 14

Figure 5 compares VSI with VCPI. When reactive power reaches 200 MVAr, VSI is 0.54, and its slope sharply decreases, while VCPI rises to 0.02. The bus's maximum loading is determined to be 1040 MVAr, where VSI drops to 0.08, VCPI increases to 0.12, and the critical voltage is 0.89. Beyond this loading point, the system collapses with no further steady-state solution.

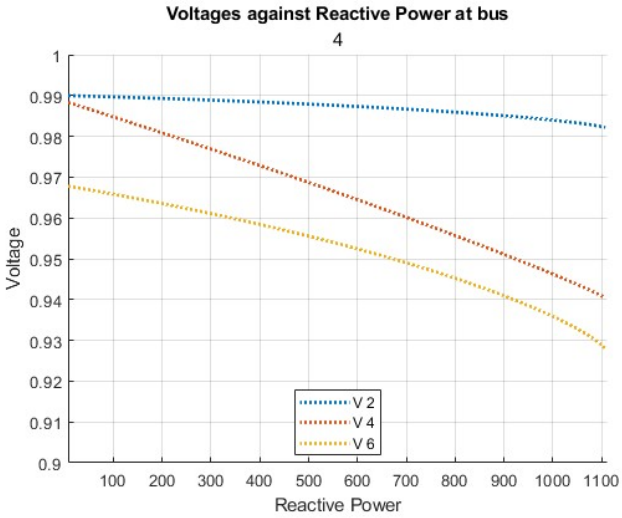

Figure 6: Voltages against Reactive Power at bus 4 (Suichatar)

Figure 6 presents the voltages at surrounding buses—bus 2, bus 4, and bus 6—when the reactive power at bus 4 is varied, while Figure 7 illustrates the VSI at these buses. Despite a sharp voltage drop at bus 6, its corresponding VSI remains constant well above 0, indicating that the bus is not near voltage collapse. This demonstrates that voltage monitoring alone may not provide sufficient information for predicting voltage collapse.

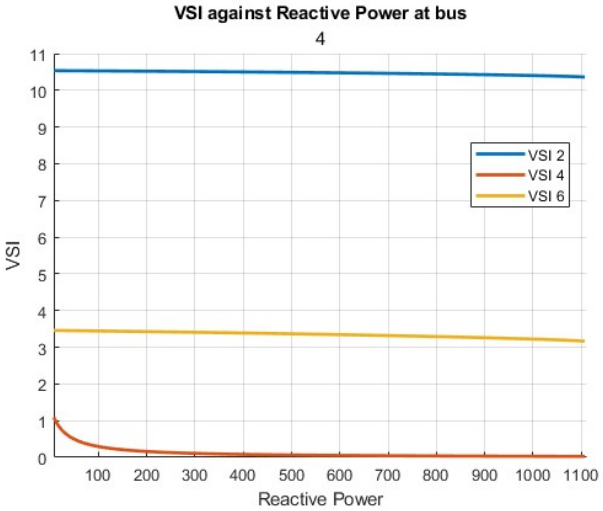

Figure 7: VSI against Reactive Power at bus 4

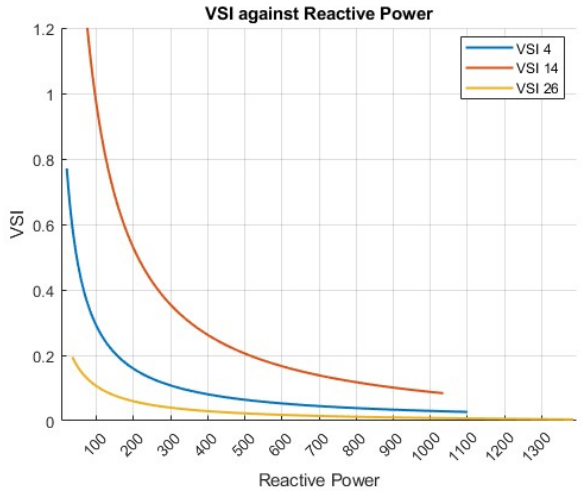

Figure 8: Comparison of VSI for load buses of Kathmandu Grid Division

By separately increasing the load at each bus to its maximum loading and plotting the results in MATLAB, figure 8 presents a comparison of the VSI for load buses 4, 14, and 26 in the Kathmandu Grid Division. Based on their proximity to voltage instability, the buses are ranked as 14, 4, and 26 for a load variation ranging from 100 MVAr to 300 MVAr. The VCPI and the maximum loading approach yield the same ranking, as shown in figure 9.

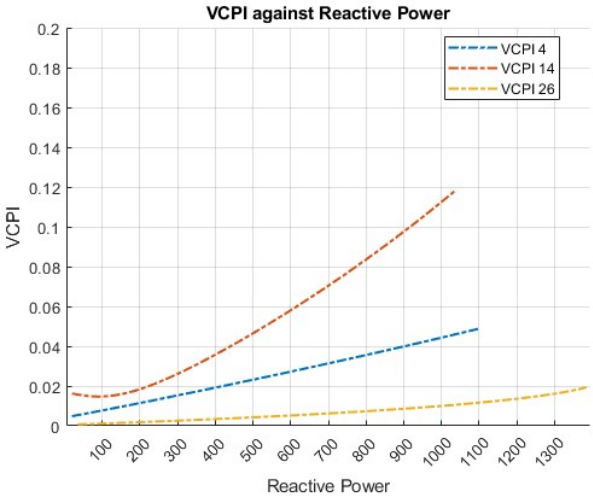

Figure 9: Comparison of VCPI for load buses of Kathmandu Grid Division

3.2 Hetauda Grid Division

Hetauda Grid Division is located at Chowkitole, Hetauda. Ten substations namely at Amlekhgunj, Bharatpur, New Bharatpur (Aaptari), Birgunj, Hetauda, Kamane, New Parwanipur, Piluwa, Purbi Chitwan (Hardi), and Simara are supervised, operated and maintained by this division. [9]

Similar to figure 8, figure 10 presents the plot of VSI and voltages for various load buses in the Hetauda Grid Division with changing reactive power load. Within the range of 100 MVAr to 300 MVAr, VSI ranks the buses based on proximity to voltage instability as 39, 38 and 33.

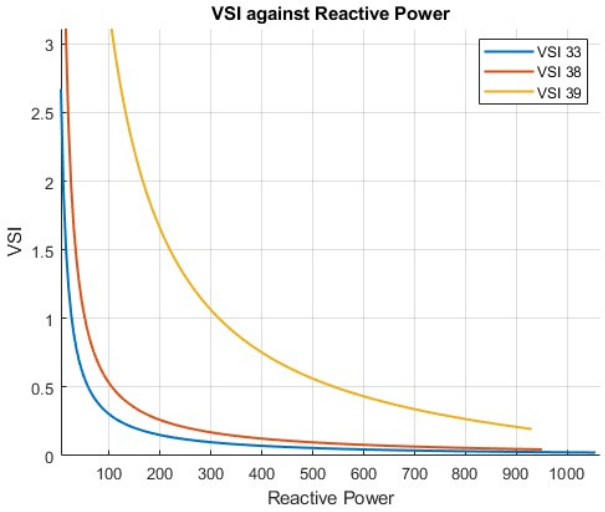

Figure 10: Comparison of VSI for load buses of Hetauda Grid Division

3.3 Attaria Grid Division

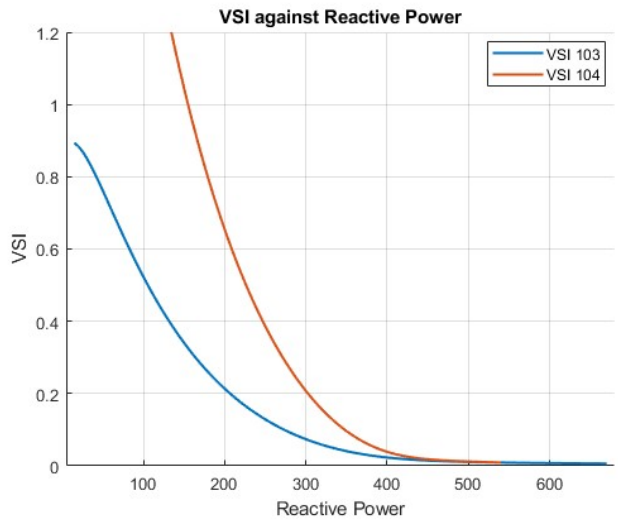

Figure 11: Comparison of VSI for load buses of Attaria Grid Division

Attaria Grid Division is located at Attaria, Kailali. This division has five substations namely Attaria, Lalpur (Mahendranagar), Lamki, Pahalmanpur, and Syaule. [9]

Figure 11 shows that bus 104 (Lamki) is the most vulnerable bus than bus 103 in Attaria Grid Division.

3.4 Dhalkebar Grid Branch

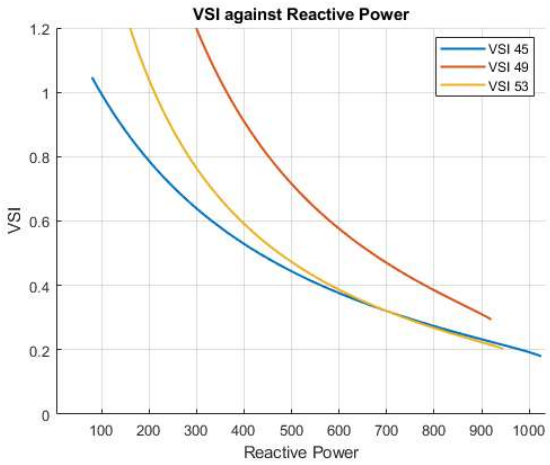

Figure 12: Voltage Stability Assessment of Dhalkebar Grid Division

Chapur, Dhalkebar, Lahan, Mirchaiya, Rupani, Tingla, and Nawalpur are major substations of the Dhalkebar Grid Division, operating at 132 kV, 220 kV, and 400 kV. This division is crucial for domestic power transmission and cross-border exchange with India. Figure 12 indicates that bus 45 (Dhalkebar bus) is the stable bus to the change in reactive power loading compared to other substation buses in the Dhalkebar Grid Division.

3.5 Pokhara Grid Division

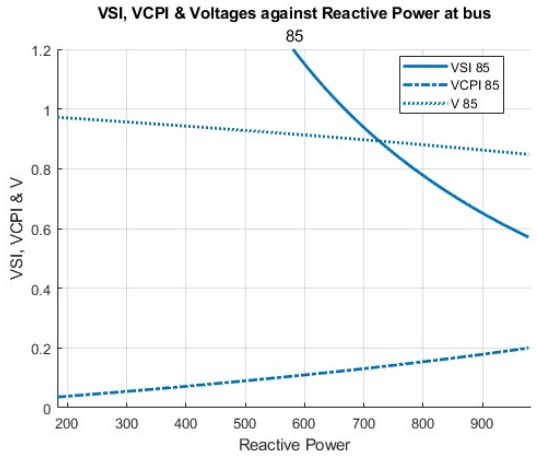

Figure 13: VSI, VCPI and Voltage against Reactive Power at bus 85 (Pokhara)

The Pokhara Grid Division, which includes multiple generation stations, demonstrates greater stability compared to other grid divisions. As shown in Figure 13, the Voltage Stability Index (VSI) reaches 1 when the loading is 668 MVAr, indicating a higher loading capability and stronger voltage stability in this region.

4. Conclusion

This study conducted a detailed voltage stability assessment of the INPS using a newly developed VSI. The analysis covered all nine grid divisions, with a particular focus on Kathmandu, Hetauda, Attaria, Dhalkebar, and Pokhara. The results identified key vulnerable buses, such as Bus 14 (Matatirtha) in Kathmandu, Bus 39 in Hetauda, and Bus 104 (Lamki) in Attaria, where VSI values dropped significantly near critical loading points. For instance, at Bus 14, VSI decreased to 0.08 when the reactive power reached 1040 MVAr, indicating a high risk of voltage instability. The comparative analysis with the Voltage Collapse Proximity Index (VCPI) demonstrated that VSI provides a more computationally efficient and accurate measure of stability margins. Furthermore, the P-V curve validation confirmed that buses with lower VSI values are more prone to voltage collapse. The study underscores the importance of real-time voltage stability monitoring, with the proposed VSI offering a reliable tool for system operators to enhance grid resilience. These findings support the strategic reinforcement of Nepal's transmission network to accommodate the growing electricity demand and ensure secure and stable power supply.

Acknowledgement

The authors extend their sincere gratitude to the NEA for providing crucial data, technical insights, and operational information on the INPS.

References

[1] *Nepal Electricity Authority: A Year in Review-Fiscal Year-2023/2024*, NEA.

[2] P. Kundur. Power System Stability and Control. McGraw-Hill. 1994.

[3] Ajjarapu, Venkataramana, Computational Techniques for Voltage Stability Assessment and Control. Springer US, 2007.

[4] R. Maharjan and S. Kamalasadan, "Voltage stability index for online voltage stability assessment," *2015*

North American Power Symposium (NAPS), Charlotte, NC, USA, 2015, pp. 1-6.

[5] B. Venkatesh, "Dynamic voltage collapse index - wind generator application," in Power Engineering Society General Meeting, 2007. IEEE, June 2007, pp. I-I.

[6] B. Singh and S. N. Singh, "Voltage stability assessment of grid connected offshore wind farms," Wind Energy, vol. 12, no. 2, pp. 157 169, 2009.

[7] M. Haque, "A fast method for determining the voltage stability limit of a power system," Electric Power Systems Research, vol. 32, no. 1, pp. 35 - 43, 1995.

[8] V. Balamourougan, T. Sidhu, and M. Sachdev, "Technique for online prediction of voltage collapse," Generation, Transmission and Distribution, IEE Proceedings-, vol. 151, no. 4, pp. 453-460, July 2004.

[9] *Nepal Electricity Authority, Transmission/Project Management Directorate: A Year Book – Fiscal Year 2023/2024 (2080/2081 BS),* NEA.

[10] Arunachalam Sundaram (2024). Load Flow Analysis For IEEE 118 Bus System (https://www.mathworks.com/matlabcentral/fileexchange/170161-load-flow-analysis-for-ieee-118-bus-sytem), MATLAB Central File Exchange. Retrieved November 23, 2024.

Appendices

Appendix A.1

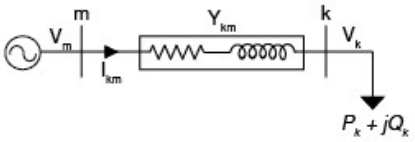

Figure A: Two bus network

The active and reactive power at a bus in a power system network can be represented as:

$$P_k = \sum_{m=1}^{n} |V_k||V_m||Y_{km}| \cos(\delta_m - \delta_k + \theta_{km}) \quad \text{(I)}$$

$$Q_k = -\sum_{m=1}^{n} |V_k||V_m||Y_{km}| \sin(\delta_m - \delta_k + \theta_{km}) \quad \text{(II)}$$

The power equations for two bus network as shown in Figure A can be obtained from (I) as following.

$$P_k = V_k^2 Y_{kk} \cos\theta_{kk} + V_k V_m Y_{km} \cos(\delta_m - \delta_k + \theta_{km}) \quad \text{(III)}$$

$$P_k - V_k^2 Y_{kk} \cos\theta_{kk} = V_k V_m Y_{km} \cos(\delta_m - \delta_k + \theta_{km}) \quad \text{(IV)}$$

Similarly, reactive power equations will be as following.

$$Q_k = -V_k^2 Y_{kk} \sin\theta_{kk} - V_k V_m Y_{km} \sin(\delta_m - \delta_k + \theta_{km}) \quad \text{(V)}$$

$$V_k^2 Y_{kk} \sin\theta_{kk} + Q_k = -V_k V_m Y_{km} \sin(\delta_m - \delta_k + \theta_{km}) \quad \text{(VI)}$$

Squaring (IV) gives,

$$P_k^2 + V_k^4 Y_{kk}^2 \cos^2\theta_{kk} - 2V_k^2 Y_{kk} \cos\theta\, P_k = (V_k V_m Y_{km})^2 \cos^2(\delta_m - \delta_k + \theta_{km}) \quad \text{(VII)}$$

Squaring (VI) gives,

$$V_k^4 Y_{kk}^2 \sin^2\theta_{kk} + Q_k^2 + 2V_k^2 Y_{kk} \sin\theta\, Q_k = (V_k V_m Y_{km})^2 \sin(\delta_m - \delta_k + \theta_{km}) \quad \text{(VIII)}$$

Adding (VII) and (VIII),

$$V_k^4 Y_{kk}^2 + P_k^2 + Q_k^2 - 2V_k^2 Y_{kk}(P_k \cos\theta - Q_k \sin\theta) = (V_k V_m Y_{km})^2 \quad \text{(IX)}$$

Rearranging,

$$V_k^4 Y_{kk}^2 - V_k^2\big((V_m Y_{km})^2 + 2Y_{kk}(P_k \cos\theta - Q_k \sin\theta)\big) + \big(P_k^2 + Q_k^2\big) = 0 \quad \text{(X)}$$

$$Y_{kk}^2\big(V_k^2\big)^2 - V_k^2\big((V_m Y_{km})^2 + 2Y_{kk}(P_k \cos\theta - Q_k \sin\theta)\big) + \big(P_k^2 + Q_k^2\big) = 0 \quad \text{(XI)}$$

Solution for voltage V_k at bus k, is expressed as:

$$V_k^2 = \frac{-b \pm \sqrt{(b^2 - 4ac)}}{2a} \quad \text{(XII)}$$

Where,

$$a = Y_{kk}^2 \quad \text{(XIII)}$$

$$b = -(V_m^2 Y_{km}^2 + 2Y_{kk}(P_k \cos\theta - Q_k \sin\theta) \quad \text{(XIV)}$$

$$c = \big(P_k^2 + Q_k^2\big) \quad \text{(XV)}$$

To get real solution of V_k^2, $(b^2 - 4ac) \geq 0$ should be true. Replacing a, b and c in $(b^2 - 4ac) \geq 0$

$$[-\big(V_m^2 Y_{km}^2 + 2Y_{kk}(P_k \cos\theta - Q_k \sin\theta)\big]^2 - 4Y_{kk}^2(P_k^2 + Q_k^2) \geq 0 \quad \text{(XVI)}$$

Assuming constant power factor, $P_k + jQ_k$ is replaced by $VSI * (P_k + jQ_k)$ where VSI is voltage stability index which represent the closeness to voltage collapse. VSI is tends to 0 when the line is reaching its maximum power transfer limit i.e. $Z_{th} = Z_L$. The slope of VSI shows the closeness to the voltage collapse.

$$[V_m^2 Y_{km}^2 + 2Y_{kk}(P_k \cos\theta\, VSI - Q_k \sin\theta\, VSI)]^2 - 4Y_{kk}^2 VSI^2\big(P_k^2 + Q_k^2\big) = 0 \quad \text{(XVII)}$$

$$V_m^4 Y_{km}^4 + 4V_m^2 Y_{km}^2 Y_{kk} VSI(P_k \cos\theta - Q_k \sin\theta) + 4Y_{kk}^2 VSI^2 (P_k \cos\theta - Q_k \sin\theta)^2 - 4Y_{kk}^2 VSI^2 \left(P_k^2 + Q_k^2\right) = 0 \quad \text{(XVIII)}$$

$$4VSI^2 Y_{kk}^2 \left[(P_k \cos\theta - Q_k \sin\theta)^2 - \left(P_k^2 + Q_k^2\right)\right] + VSI\ 4V_m^2 Y_{km}^2 Y_{kk} (P_k \cos\theta - Q_k \sin\theta) + V_m^4 Y_{km}^4 = 0 \quad \text{(XIX)}$$

Where,

$$VSI = \frac{-b \pm \sqrt{b^2 - 4ac}}{2a} \quad \text{(XX)}$$

$$a = 4Y_{kk}^2 [\left(P_k Cos(\theta) - Q_k Sin(\theta)\right)^2 - (P_k^2 + Q_k^2 \quad \text{(XXI)}$$

$$b = 4V_m^2 Y_{km}^2 Y_{kk} \left(P_k Cos(\theta) - Q_k Sin(\theta)\right) \quad \text{(XXII)}$$

$$c = V_m^4 Y_{km}^4 \quad \text{(XXIII)}$$

Equation (XX) is the derived voltage stability index (VSI) for the system which predicts proximity to the voltage collapse. For a large power network, on replacing V_m with V_{th} and Y_{km} with Z_{th} for a bus k, we can get the a, b, and c parameters as below:

$$a = 4Y_{kk}^2 \left[(P_k \cos\theta - Q_k \sin\theta)^2 - \left(P_k^2 + Q_k^2\right)\right] \quad \text{(XXIV)}$$

$$b = 4V_{th}^2 Z_{th}^{-2} Y_{kk} (P_k \cos\theta - Q_k \sin\theta) \quad \text{(XXV)}$$

$$c = V_{th}^4 Z_{th}^{-4} \quad \text{(XXVI)}$$

Appendix A.2

Bus naming for the purpose of load flow analysis in MATLAB are Bus 2 – Balaju; Bus 4 – Siuchatar; Bus 6 – Patan; Bus 14 – Matatirtha; Bus 26 – Mulpani; Bus 33 – New Bharatpur; Bus 38 – Pathlaiya; Bus 39 – Purbi Chitwan; Bus 45 – Dhalkebar; Bus 49 – Nawalpur; Bus 53 – Chandranigah; Bus 85 – Pokhara; Bus 103 – Attariya & Bus 104 – Lumki.

APPENDIX B: INPS BUS & LINE DATA

TABLE B.1: INPS BUS DATA

S.N.	Bus Type	Voltage	Phase Angle	Active Power Demand	Reactive Power Demand	Active Power Generated	Q Generated	Q min	Q max	Q shunt		Bus Voltage	Bus Name
% A. KATHMANDU GRID DIVISION													
1	0	1	0	0	0	0	0	0	0	0	%	132	BALAJU
2	0	1	0	58.787	19.322	0	0	0	0	0	%	66	BALAJU 112
3	0	1	0	61.139	20.095	0	0	0	0	0	%	132	CHAPALI
4	0	1	0	21.947	7.214	0	0	0	0	0	%	132	SIUCHATR
5	0	1	0	23.515	7.729	0	0	0	0	0	%	66	SIUCHATAR
6	0	1	0	53.301	17.519	0	0	0	0	0	%	66	PATAN
7	0	1	0	39.192	12.882	0	0	0	0	0	%	66	BANESHWOR
8	2	1	0	0	0	2.4	0	-0.6	1.2	0	%	11	BHAKTAPUR
9	0	1	0	53.301	17.519	0	0	0	0	0	%	132	BHAKTAPUR 123
10	0	1	0	18.808	6.182	0	0	0	0	0	%	66	BHAKTAPUR 124
11	0	1	0	15.677	5.153	0	0	0	0	0	%	66	BANEPA
12	2	1	0	3.919	1.288	14	0	-3.5	7	0	%	66	PANCHKHAL
13	0	1	0	0	0	0	0	0	0	0	%	220	MATATIRTHA
14	0	1	0	23.515	7.729	0	0	0	0	0	%	132	MATATIRTHA 107
15	2	1	0	0	0	9	0	0	0	0	%	132	SAMUNDRATAR
16	0	1	0	0	0	0	0	0	0	0	%	220	TRISHULI3B
17	2	1	0	0	0	60	0	-15	30	0	%	132	TRISHULI3B 86
18	2	1	0	9.404	3.091	28.94	0	-7.235	14.47	0	%	66	TRISHULI
19	2	1	0	0	0	22.1	0	-5.526	11.05	0	%	66	CHILIME
20	2	1	0	9.404	3.091	20	0	-5	10	0	%	66	DEVIGHAT
21	2	1	0	0	0	10.05	0	-2.5125	5.025	0	%	66	SUNKOSHI
22	2	1	0	0	0	60	0	-15	30	0	%	66	K.KHANI1
23	2	1	0	0	0	68	0	-17	34	0	%	132	K.KHANI2
24	0	1	0	0	0	0	0	0	0	0	%	132	CHANGU
25	0	1	0	0	0	0	0	0	0	0	%	132	PHUTUNG
26	0	1	0	37.616	12.364	0	0	0	0	0	%	132	MULPANI
27	0	1	0	0	0	0	0	0	0	0	%	132	NALAGUMBA
% B. HETAUDA GRID DIVISION													
28	2	1	0	0	0	6.6	0	-1.65	3.3	0	%	132	HETAUDA
29	0	1	0	19.596	6.441	0	0	0	0	0	%	66	HETAUDA 106

30	0	1	0	32.921	10.821	0	0	0	0	0	%	132	KAMANE
31	0	1	0	59.571	19.58	0	0	0	0	0	%	132	BHARATPUR
32	0	1	0	0	0	0	0	0	0	0	%	220	BHARATPUR 116
33	0	1	0	7.838	2.576	0	0	0	0	0	%	132	NEW_BHARATPU
34	2	1	0	39.192	12.882	80	0	0	0	0	%	132	PARWANIPUR
35	0	1	0	98.473	32.367	0	0	0	0	0	%	66	PARWANIPUR 73
36	0	1	0	7.838	2.576	0	0	0	0	0	%	66	SIMRA_76
37	0	1	0	0.784	0.258	0	0	0	0	0	%	66	AMLEKHGUNJ
38	0	1	0	5.487	1.803	0	0	0	0	0	%	132	PATHALAIYA
39	0	1	0	17.244	5.668	0	0	0	0	0	%	132	PURBI CHITWAN
40	0	1	0	0	0	0	0	0	0	0	%	132	NEW HETAUDA
41	0	1	0	143.359	47.12	0	0	0	0	0	%	220	NEW HETAUDA
42	0	1	0	0	0	0	0	0	0	0	%	220	NEWMARSYS 68
% C. DHALKEBAR GRID BRANCH													
43	2	1	0	0	0	7	0	-1.75	3.5	0	%	33	LAHAN
44	0	1	0	27.969	9.193	0	0	0	0	0	%	132	LAHAN 128
45	0	1	0	86.222	28.34	0	0	0	0	0	%	132	DHALKEBAR
46	0	1	0	0	0	0	0	0	0	0	%	400	DHALKEBAR 85
47	0	1	0	0	0	0	0	0	0	0	%	220	DHALKEBAR 28
48	0	1	0	18.028	5.926	0	0	0	0	0	%	132	MIRCHAIYA
49	0	1	0	27.434	9.017	0	0	0	0	0	%	132	NAWALPUR
50	0	1	0	25.867	8.502	0	0	0	0	0	%	132	RUPANI
51	0	1	0	0	0	0	0	0	0	0	%	132	OKHALDHUNGA
52	1	1	0	0	0	-160.991	0	0	0	0	%	400	MUZZAFURPUR1
53	0	1	0	35.273	11.594	0	0	0	0	0	%	132	CHANDRANIGAH
% D. DUHABI GRID DIVISION													
54	2	1	0	18.812	6.183	23.5	0	-5.875	11.75	0	%	132	TINGLA
55	0	1	0	180.282	59.256	0	0	0	0	0	%	132	DUHABI
56	2	1	0	0	0	11.23	0	-2.807	5.615	0	%	33	DUHABI 58
57	0	1	0	70.545	23.187	0	0	0	0	0	%	132	ANARMANI
58	0	1	0	36.056	11.851	0	0	0	0	0	%	132	DAMAK
59	2	1	0	41.844	5.153	109	0	-27.25	54.5	0	%	132	GODAK
60	2	1	0	5.197	1.708	54.95	0	-13.737	27.475	0	%	132	PHIDIM
61	2	1	0	5.197	1.708	49.8	0	-12.5	25	0	%	132	KABELI
62	2	1	0	0	0	50	0	-12	25	0	%	132	KUSAHA
63	0	1	0	29.786	9.79	0	0	0	0	0	%	132	INARUWA
64	0	1	0	243.709	80.103	0	0	0	0	0	%	220	INARUWA 92
65	2	1	0	8.369	5.153	3	0	0	0	0	%	220	TUMLINGTAR
66	2	1	0	8.369	4.184	4	0	0	0	0	%	220	BANESHWOR 113
67	2	1	0	0	0	12.5	0	-3	6.25	0	%	220	BASANTAPUR

68	2	1	0	0	0	21.9	0	-5.475	10.95	0	%	132	MAI_KHOLA
69	0	1	0	77.498	25.472	0	0	0	0	0	%	220	DHARAN
% E. BUTWAL GRID DIVISION													
70	2	1	0	117.575	38.645	1	0	0	0	0	%	132	BUTWAL
71	0	1	0	23.515	7.729	0	0	0	0	0	%	132	BARDAGHAT
72	0	1	0	0	0	0	0	0	0	0	%	220	BARDAGHAT 35
73	2	1	0	23.515	7.729	2.3	0	-0.575	1.15	0	%	132	KAWASOTI
74	2	1	0	35.273	11.594	15	0	-3.75	7.5	0	%	132	GANDAK
75	0	1	0	30.093	9.891	0	0	0	0	0	%	132	MOTIPUR
76	2	1	0	7.055	2.319	3.2	0	-0.8	1.6	0	%	132	SANDHIKHARKA
77	0	1	0	18.808	6.182	0	0	0	0	0	%	132	MAINAHAIYA
78	0	1	0	0	0	0	0	0	0	0	%	132	NEW_BUTWAL
79	0	1	0	0	0	0	0	0	0	0	%	220	NEW_BUTWAL 118
80	0	1	0	0	0	0	0	0	0	0	%	132	SUNAWAL
81	2	1	0	0	0	144	0	-36	72	0	%	132	KALIGANDAKI
82	0	1	0	0	0	0	0	0	0	0	%	220	NEWKALIG
83	0	1	0	15.677	5.153	0	0	0	0	0	%	132	NEWMARSYS
% F. POKHARA GRID DIVISION													
84	2	1	0	10.19	3.349	10.6	0	-2.65	5.3	0	%	132	DAMAULI
85	0	1	0	39.192	12.882	0	0	0	0	0	%	132	POKHARA
86	2	1	0	11.758	3.865	75	0	-18.25	37.5	0	%	132	LEKHNATH
87	2	1	0	7.838	2.576	9.4	0	-2.35	4.7	0	%	132	SYANGJA
88	2	1	0	0	0	16.2	0	0	0	0	%	220	DANA
89	0	1	0	0	0	0	0	0	0	0	%	220	KUSMA
90	0	1	0	0	0	0	0	0	0	0	%	132	KUSMA 88
91	2	1	0	0	0	15.8	0	-3	7	0	%	132	LAHACHOWK
92	2	1	0	0	0	7.6	0	-1.9	3.8	0	%	132	KIRTIPUR
93	2	1	0	0	0	70	0	-17.5	35	0	%	132	MIDDLE_MARSY
94	2	1	0	0	0	50	0	12.5	25	0	%	132	UPPER_MARSY
95	2	1	0	15.677	5.153	69	0	-17.25	34.5	0	%	132	MARSYANGDI
96	0	1	0	0	0	0	0	0	0	0	%	220	UDIPUR
97	2	1	0	0	0	63.43	0	-15.856	31.712	0	%	132	UDIPUR 55
98	2	1	0	0	0	14.8	0	-3.438	6.875	0	%	132	MODI_KHOLA
99	0	1	0	0	0	0	0	0	0	0	%	220	RAHUGHAT
100	2	1	0	0	0	10	0	-5	10	0	%	132	LOWER MK
101	0	1	0	0	0	0	0	0	0	0	%	132	NEWMODI
102	2	1	0	18.808	6.182	30	0	-7.5	15	0	%	220	KHUDI
% G. ATTARIA GRID DIVISION													
103	0	1	0	18.028	5.926	0	0	0	0	0	%	132	ATTARIYA
104	0	1	0	13.325	4.38	0	0	0	0	0	%	132	LUMKI

105	2	1	0	18.028	5.926	100	0	-25	50	0	%	132	MAHENDRANAGA
106	0	1	0	4.703	1.546	0	0	0	0	0	%	132	PAHALMANPUR
107	2	1	0	6.271	2.061	22.5	0	-5.625	11.25	0	%	132	SYAULE
108	2	1	0	0	0	30	0	-7.5	15	0	%	132	CHAMELIYA
109	2	1	0	18.808	6.182	16.5	0	-4.125	8.25	0	%	132	BALANCH
% H. KHIMTI GRID SECTION													
110	0	1	0	124.775	41.012	0	0	0	0	0	%	220	NEWKHIMTI
111	2	1	0	0	0	79.1	0	-19.775	39.55	0	%	132	NEWKHIMTI 101
112	2	1	0	0	0	60	0	-15	30	0	%	132	KHIMTI
113	2	1	0	0	0	58	0	-11.25	22.5	0	%	132	SINGATI
114	2	1	0	0	0	24.2	0	0	0	0	%	132	GARJYANG
115	2	1	0	0	0	5	0	-1.25	2.5	0	%	66	INDRAWATI
116	0	1	0	0	0	0	0	0	0	0	%	132	LAMSANGHU_2
117	2	1	0	18.808	6.182	81.3	0	-20.325	40.65	0	%	132	LAMOSANGHU
118	2	1	0	0	0	52.4	0	-13.1	26.2	0	%	132	LIKHU
119	2	1	0	0	0	45	0	-11.25	22.5	0	%	132	BHOTEKOSHI
120	2	1	0	0	0	456	0	-114	228	0	%	220	U.TAMAKOSHI
% I. KOHALPUR GRID SECTION													
121	0	1	0	39.192	12.882	0	0	0	0	0	%	132	KOHALPUR
122	0	1	0	1.568	0.515	0	0	0	0	0	%	132	BHURIGAON
123	0	1	0	1.568	0.515	0	0	0	0	0	%	132	KUSUM
124	0	1	0	14.893	4.895	0	0	0	0	0	%	132	HAPURE
125	0	1	0	21.947	7.214	0	0	0	0	0	%	132	LAMAHI
126	0	1	0	31.353	10.305	0	0	0	0	0	%	132	GHORAHI
127	2	1	0	0	0	12.5	0	-3.125	6.25	0	%	132	JHIMRUK
128	0	1	0	31.353	10.305	0	0	0	0	0	%	132	SHIVAPUR

TABLE B.2: INPS LINE DATA

Sending End	Receiving End	Resistance	Reactance	Susceptance	Tap Ratio
1	2	0	0.031635	0	0.935
2	18	0.0034286	0.0125434	0.043918705	1
4	14	0.060349	0.1268505	0.007539778	1
4	1	0.120698	0.253701	0.003769889	1
4	5	0	0.031635	0	0.985
5	22	0.014567	0.030619025	0.007279785	1
6	7	0.027053	0.0568639	0.003359901	1
6	5	0.0309781	0.0463938	0.011359665	1
7	10	0.01548905	0.0231969	0.005679832	1
9	10	0	0.0475	0	0.935
10	11	0.067969	0.091311	0.005719831	1
10	8	0	0.095	0	0.935
11	12	0.049432	0.066408	0.004159877	1
12	21	0.179191	0.240729	0.015079555	1
13	16	0.000905	0.0122	0.059902233	1
13	42	0.001765	0.02385	0.11663656	1
13	14	0	0.0475	0	0.96
14	23	0.0112212	0.0410508	0.035918941	1
15	17	0.0081	0.02965	0.025999233	1
16	17	0	0.0475	0	0.96
18	20	0.0018702	0.0068418	0.023959293	1
19	18	0.162318	0.341184	0.020279402	1
22	29	0.0112212	0.0410508	0.143675763	1
24	26	0.0003117	0.0011403	0.000999971	1
24	9	0.0003117	0.0011403	0.000999971	1
25	1	0.00171435	0.00627165	0.005479838	1
25	3	0.00171435	0.00627165	0.005479838	1
26	3	0.0043638	0.0159642	0.013979588	1
27	117	0.0118446	0.0433314	0.037918882	1
27	9	0.003117	0.011403	0.009979706	1
28	30	0.00402	0.0147	0.003219905	1
28	38	0.0237	0.0867	0.01899944	1
28	39	0.0261828	0.0957852	0.020959382	1
28	23	0.002495	0.0091	0.007979765	1
28	29	0	0.0475	0	0.935
30	38	0.0049872	0.0182448	0.003989882	1
30	53	0.018702	0.068418	0.014969558	1
31	33	0.0023346	0.00711	0.001439958	1

31	84	0.0243126	0.0889434	0.019459426	1
31	95	0.01362	0.05813	0.012259638	1
32	33	0	0.0475	0	0.96
34	35	0	0.0475	0	0.935
35	36	0.0196128	0.0837072	0.070597918	1
37	36	0.166905	0.266829	0.013199611	1
37	29	0.0116536	0.0244952	0.001439958	1
38	53	0.0236892	0.0866628	0.018959441	1
38	34	0.0056	0.02055	0.01795947	1
39	33	0.0174552	0.0638568	0.013969588	1
40	28	0.0006234	0.0022806	0.001999941	1
41	32	0.00291	0.02045	0.113756645	1
41	40	0	0.0475	0	0.985
42	32	0.00101	0.00775	0.038806855	1
42	83	0	0.095	0	0.985
44	43	0	0.095	0	0.935
45	48	0.0103	0.03765	0.032999027	1
45	49	0.0130914	0.0478926	0.041918764	1
46	47	0	0.031635	0	0.985
47	110	0.00299	0.021	0.117356539	1
47	45	0	0.031635	0	0.96
48	51	0.014	0.068	0.108796791	1
48	44	0.0084	0.0308	0.026999204	1
50	62	0.0109095	0.0399105	0.03491897	1
50	44	0.0084159	0.0307881	0.026939205	1
52	46	0.000363	0.004045	0.047043413	1
53	49	0.0087276	0.0319284	0.027939176	1
54	51	0.00273166	0.01501435	0.018859444	1
55	58	0.0134	0.04905	0.042998732	1
55	63	0.00535	0.0195	0.017079496	1
55	56	0	0.095	0	0.935
58	57	0.0168	0.0616	0.013499602	1
58	59	0.0218	0.0798	0.017499484	1
58	60	0.046755	0.171045	0.037428896	1
59	68	0.00686	0.0251	0.005489838	1
59	60	0.0218	0.0798	0.017499484	1
60	61	0.0046755	0.0171045	0.014959559	1
62	63	0.0075	0.02735	0.023999292	1
64	67	0.00238636	0.0642727	0.053598819	1
64	63	0	0.031635	0	0.985

66	65	0.000215	0.00291	0.01425558	1
67	66	0.000452	0.0061	0.029951117	1
69	64	0.0025	0.071388889	0.0203394	1
69	67	0.00375	0.106944444	0.0305271	1
70	80	0.003117	0.011403	0.009979706	1
70	81	0.0157992	0.067431	0.056878322	1
70	77	0.0068574	0.0250866	0.021959352	1
70	75	0.0118446	0.0433314	0.037918882	1
71	78	0.0037404	0.0136836	0.011979647	1
71	74	0.0043638	0.0159642	0.013979588	1
72	32	0.00299	0.021	0.117356539	1
72	79	0.000835	0.0059	0.032759034	1
72	71	0	0.0475	0	0.96
73	71	0.0357972	0.10902	0.022079349	1
73	31	0.0225678	0.06873	0.013919589	1
76	75	0.0115329	0.0421911	0.036918911	1
79	78	0	0.0475	0	0.985
80	78	0.003117	0.011403	0.009979706	1
81	87	0.0313815	0.0659622	0.000979971	1
82	89	0.001645	0.01265	0.063214136	1
82	79	0.001645	0.01265	0.063214136	1
83	84	0.0305	0.112	0.024499277	1
83	93	0.029923	0.109469	0.023949294	1
83	95	0.001395485	0.00767015	0.009639716	1
84	93	0.0287	0.105	0.022999322	1
85	98	0.0108659	0.0397509	0.008699743	1
86	85	0.0230658	0.0843822	0.018459456	1
86	84	0.0049872	0.0182448	0.003989882	1
87	86	0.0468045	0.108936	0.021079378	1
89	99	0.002361111	0.018055556	0.032615038	1
89	90	0	0.0475	0	0.985
90	101	0.0068574	0.0250866	0.005489838	1
91	86	0.0074808	0.0273672	0.023959293	1
91	101	0.0040521	0.0148239	0.012979617	1
93	94	0.0139548	0.0767016	0.02407929	1
95	4	0.002762	0.010103	0.002209935	1
96	42	0.00131	0.01005	0.050254518	1
96	102	0.00066	0.00409	0.019223433	1
96	97	0	0.095	0	0.985
97	92	0.0059	0.02165	0.018959441	1

98	100	0.0139548	0.0767016	0.02407929	1
99	88	0.0004305	0.0058	0.028511159	1
100	90	0.0068574	0.0250866	0.005489838	1
103	106	0.01095	0.04015	0.035198962	1
103	107	0.0209	0.0765	0.06679803	1
104	122	0.0106	0.0387	0.033799003	1
105	103	0.01155	0.0422	0.036998909	1
106	104	0.009	0.033	0.028799151	1
107	109	0.0209	0.0765	0.06679803	1
109	108	0.00324	0.0119	0.002589924	1
110	111	0	0.0475	0	0.96
111	112	0.0012468	0.0045612	0.000999971	1
112	117	0.00305466	0.0111749	0.002449928	1
113	116	0.01245	0.0456	0.03999882	1
114	111	0.0096627	0.0353493	0.030939088	1
115	12	0.0006234	0.0022806	0.001999941	1
116	117	0	0.0475	0	0.935
118	111	0.005075	0.02465	0.039438837	1
119	117	0.00965	0.03535	0.030999086	1
120	110	0.00097	0.0131	0.064150108	1
121	123	0.0151	0.055	0.048198578	1
122	121	0.01725	0.063	0.055198372	1
123	125	0.015585	0.057015	0.049898528	1
123	124	0.00685	0.0251	0.021999351	1
125	128	0.0157	0.0575	0.050198519	1
125	126	0.0021875	0.010625	0.016999499	1
125	127	0.0128	0.04675	0.040998791	1
128	75	0.0071691	0.0262269	0.022959323	1

APPENDIX C: NEUTRAL INSULATION FACTOR & CONVERTER EFFICIENCY

TABLE C.1: NEUTRAL INSULATION FACTOR ACCORDING TO GROUNDING TYPE

Grounding Type	k (Insulation Factor)	$V_{n.max}$ Formula	Approx. $V_{n1.max}$
Solidly Grounded	1.1	$1.1 \times \frac{V_{LL}}{\sqrt{3}}$	$0.8 - 0.9 \times V_{n.max}$
Impedance Grounded	1.5	$1.5 \times \frac{V_{LL}}{\sqrt{3}}$	$0.8 - 0.95 \times V_{n.max}$
Ungrounded	1.73	$1.73 \times \frac{V_{LL}}{\sqrt{3}}$	$0.9 - 1.0 \times V_{n.max}$

TABLE C.2: TYPICAL MINIMUM EFFICIENCY REQUIREMENTS BY CONVERTER TYPE

Converter Type	Typical Efficiency (%)	Minimum Efficiency Requirement (%)
AC-DC (Rectifier) (Diode Bridge, Phase-Controlled)	80% - 90%	≥ 80%
DC-AC (Inverter) (SPWM, Square Wave)	85% - 98%	≥ 85%
AC-AC (Cycloconverter, Matrix Converter)	70% - 95%	≥ 70%
DC-DC (Buck, Boost, Buck-Boost, Flyback, Forward, Push-Pull, Full-Bridge, Half-Bridge, LLC Resonant)	85% - 97%	≥ 85%

Bimal Adhikari

Assessment of voltage stability using non-linear control of distributed power flow controller in mul

Tribhuvan University

Document Details

Submission ID
trn:oid:::3117:451730924

Submission Date
Apr 23, 2025, 11:57 AM GMT+5:45

Download Date
Apr 23, 2025, 11:59 AM GMT+5:45

File Name
Assessment of voltage stability using non-linear control of distributed power flow controller in ....pdf

File Size
4.5 MB

80 Pages

17,767 Words

95,315 Characters

12% Overall Similarity

The combined total of all matches, including overlapping sources, for each database.

Match Groups

- **205** Not Cited or Quoted 12%
  Matches with neither in-text citation nor quotation marks
- **6** Missing Quotations 0%
  Matches that are still very similar to source material
- **0** Missing Citation 0%
  Matches that have quotation marks, but no in-text citation
- **0** Cited and Quoted 0%
  Matches with in-text citation present, but no quotation marks

Top Sources

6% Internet sources
11% Publications
0% Submitted works (Student Papers)

Integrity Flags

0 Integrity Flags for Review

No suspicious text manipulations found.

Our system's algorithms look deeply at a document for any inconsistencies that would set it apart from a normal submission. If we notice something strange, we flag it for you to review.

A Flag is not necessarily an indicator of a problem. However, we'd recommend you focus your attention there for further review.

Match Groups

- 205 Not Cited or Quoted 12%
  Matches with neither in-text citation nor quotation marks
- 6 Missing Quotations 0%
  Matches that are still very similar to source material
- 0 Missing Citation 0%
  Matches that have quotation marks, but no in-text citation
- 0 Cited and Quoted 0%
  Matches with in-text citation present, but no quotation marks

Top Sources

6% Internet sources
11% Publications
0% Submitted works (Student Papers)

Top Sources

The sources with the highest number of matches within the submission. Overlapping sources will not be displayed.

1	Internet	
documents.mx		<1%
2	Publication	
Aihong Tang, Yunlu Shao, Qiushi Xu, Xu Zheng, Yong Huang. "Study on control m...		<1%
3	Internet	
jestr.org		<1%
4	Internet	
pdfcoffee.com		<1%
5	Publication	
Xiaohui Zhai, Aihong Tang, Xingpeng Zou, Xu Zheng, Qiushi Xu. "Research on DPF...		<1%
6	Internet	
journals.tubitak.gov.tr		<1%
7	Publication	
"Swarm, Evolutionary, and Memetic Computing", Springer Nature, 2013		<1%
8	Publication	
H. Shayeghi, Y. Hashemi. "Technical–economic analysis of including wind farms a...		<1%
9	Publication	
"Advances in Electrical and Computer Technologies", Springer Science and Busine...		<1%
10	Internet	
journal.esrgroups.org		<1%

11 Publication

"Power System Dynamic Modelling and Analysis in Evolving Networks", Springer ... <1%

12 Publication

Alfaris, Faris Ebrahem. "Modular Static Transmission and Distribution Controller f... <1%

13 Internet

www.mdpi.com <1%

14 Publication

Yuan, Zhihui, Sjoerd W. H. de Haan, Jan Braham Ferreira, and Dalibor Cvoric. "A F... <1%

15 Internet

www.scribd.com <1%

16 Internet

open.metu.edu.tr <1%

17 Publication

Vijay Kumar, Jitender Kumar Chhabra, Dinesh Kumar. "Grey Wolf Algorithm-Base... <1%

18 Internet

dokumen.pub <1%

19 Publication

Qian Chen, Peng Qiu, Zhongming Xiang, Song Wang, Wulue Pan, Haokai Xie. "The... <1%

20 Internet

www.researchgate.net <1%

21 Publication

Xi-Fan Wang, Yonghua Song, Malcolm Irving. "Modern Power Systems Analysis", ... <1%

22 Publication

Abubakar Siddique, Yonghai Xu, Waseem Aslam, Muhammad Rasheed. "A Compr... <1%

23 Publication

Junfeng Liu, Zhe Yang, Dingfang Li. "A multiple search strategies based grey wolf ... <1%

24 Publication

Kayode E. Adetunji, Ivan Hofsajer, Adnan M. Abu-Mahfouz, Ling Cheng. "A Review... <1%

25 Internet
www.int-arch-photogramm-remote-sens-spatial-inf-sci.net <1%

26 Internet
www.ijrat.org <1%

27 Publication
"Modeling of FACTS-Devices in Optimal Power Flow Analysis", Power Systems, 2006 <1%

28 Publication
Lashkar Ara, A., A. Kazemi, and S. A. Nabavi Niaki. "Multiobjective Optimal Locati... <1%

29 Publication
Pérez-Londoño, S., L.F. Rodríguez, and G. Olivar. "A Simplified Voltage Stability In... <1%

30 Publication
Yule Wang, Wanliang Wang. "Quantum-Inspired Differential Evolution with Grey ... <1%

31 Publication
Adel Ali Abou El-Ela, Mohamed T. Mouwafi, Adel A. Elbaset. "Modern Optimization... <1%

32 Publication
Ting, Tiew On. "Development of hybrid constrained genetic algorithm and particl... <1%

33 Internet
rabida.uhu.es <1%

34 Publication
Altaf Q. H. Badar. "Evolutionary Optimization Algorithms", CRC Press, 2021 <1%

35 Publication
Chunying Wu, Jianzhou Wang, Xuejun Chen, Pei Du, Wendong Yang. "A novel hybr... <1%

36 Publication
Gopisetti Manikanta, Ashish Mani, Hemender Pal Singh, Devendra Kumar Chatur... <1%

37 Publication
Handbook of Mathematics, 2015. <1%

38 Publication
Power Systems, 2014. <1%

39 Internet
dergipark.org.tr <1%

40 Internet
fa.ee.sut.ac.ir <1%

41 Publication
Burak Ozpineci. "AC vs. DC distribution: Maximum transfer capability", 2008 IEEE ... <1%

42 Publication
C.D. Vournas. "Voltage stability and controllability indices for multimachine powe... <1%

43 Publication
Mirjalili, Seyedali, Shahrzad Saremi, Seyed Mohammad Mirjalili, and Leandro dos ... <1%

44 Publication
Said Ouhssain, Hamid Chojaa, Yahya Aljarhizi, Elmehdi Al Ibrahmi, Alfian Maarif, ... <1%

45 Publication
Turan Gonen. "Modern Power System Analysis", CRC Press, 2019 <1%

46 Publication
Imran Rahman, Junita Mohamad-Saleh. "Hybrid bio-Inspired computational intell... <1%

47 Internet
vdoc.pub <1%

48 Publication
A.F. Mohammed. "Voltage stability and reactive power compensation on the T an... <1%

49 Publication
Katarina Kecojevic, Ognjen Lukacevic, Martin Calasan, Sasa Mujovic. "Minimizing ... <1%

50 Publication
Shenhang Wang, Qi Xu, Ruishi Lin, Mingjun Yang, Wei Zheng, Zhaolei Wang. "Fee... <1%

51 Publication
Xuebin Li, Zhao Jin, Shengqun Li, Daiwei Yu, Jun Zhang, Wenjin Zhang. "Li-ion batt... <1%

52 Internet
dissertations.mak.ac.ug <1%

53 Internet
lib.buet.ac.bd:8080 <1%

54 Internet
www.utko.fekt.vut.cz <1%

55 Publication
F. R. Zaro, M. A. Abido. "Multi-objective particle swarm optimization for optimal p... <1%

56 Publication
Mohammad Mohammadi. "Bacterial foraging optimization and adaptive version f... <1%

57 Publication
Syed A. Nasar, F.C. Trutt. "Electric Power Systems", CRC Press, 2018 <1%

58 Internet
businessdocbox.com <1%

59 Internet
shodhganga.inflibnet.ac.in <1%

60 Internet
worldwidescience.org <1%

61 Internet
www.ijmer.com <1%

62 Internet
www.semanticscholar.org <1%

63 Publication
"Computational Science and Its Applications — ICCSA 2003", Springer Science and... <1%

64 Publication
Alonso, M.. "A multiobjective approach for reactive power planning in networks ... <1%

65 Publication
Jinghang Lu, Ming Zhao, Saeed Golestan, Tomislav Dragicevic, Xuewei Pan, Josep ... <1%

66 Publication
Joong-Rin Shin. "<![CDATA[A New Optimal Routing Algorithm for Loss Minimizatio... <1%

67 Publication
R. Sirjani, A. Mohamed, H. Shareef. "An improved harmony search algorithm for o... <1%

68 Internet
core.ac.uk <1%

69 Internet
jfas.info <1%

70 Internet
libratez.cu.edu.tr <1%

71 Internet
vbook.pub <1%

72 Internet
5dok.net <1%

73 Publication
A. Abdelaziz. "Voltage Stability Assessment of Multi-Machine Power Systems Usin... <1%

74 Publication
A. Lashkar Ara, A. Kazemi, S.A. Nabavi Niaki. "Modelling of Optimal Unified Power... <1%

75 Publication
Akula N. V. V. Rajasekhar, Mamidi. Naveen Babu. "Harmonics reduction and powe... <1%

76 Publication
Ban H. Alajrash, Mohamed Salem, Mahmood Swadi, Tomonobu Senjyu, Mohamad... <1%

77 Publication
Brian J. Cory. "Phasor measurement application for power system voltage stabilit... <1%

78 Publication
Das, Debrup, Rajendra Prasad Kandula, Javier A. Munoz, Deepak Divan, Ronald G. ... <1%

79 Publication
F.G.M. Lima, F.D. Galiana, I. Kockar, J. Munoz. "Phase shifter placement in large-sc... <1%

80 Publication
G. Verbic, F. Gubina. "A New Concept of Voltage-Collapse Protection Based on Loc... <1%

81	Publication	Hasan, Md. Shamim. "Optimization and Control of Transmission and Distribution ... <1%
82	Publication	Jinling Feng, Song Han, Yuhang Pan, Xiao Hu. "Steady-state modelling of Extende... <1%
83	Publication	Maolin Shi, Liye Lv, Wei Sun, Xueguan Song. "A multi-fidelity surrogate model bas... <1%
84	Publication	Rajasangu, K., and N. Kumarappan. "Wavelet Transform Based Fault Classificatio... <1%
85	Publication	Ren Hongtao. "Analysis on Withstand Voltage of DC bias Device at 500kV Transfor... <1%
86	Publication	Saad Belgana, Handy Fortin-Blanchette. "A Novel Neural Network-Based Droop C... <1%
87	Publication	Seon-Ju Ahn. "Structure and operation strategies of an automatic supervisory con... <1%
88	Publication	Sotirios G. Liliopoulos, George S. Stavrakakis, Konstantinos S. Dimas. "Linear and ... <1%
89	Publication	YOUNG-ILL LEE, CHEE-MUN ONG. "PROXIMITY INDEX FOR PREDICTING VOLTAGE ... <1%
90	Internet	human-competitive.org <1%
91	Internet	ijsart.com <1%
92	Internet	ir.jkuat.ac.ke <1%
93	Internet	mdpi-res.com <1%
94	Internet	pure.rug.nl <1%

95 Internet
www2.mdpi.com <1%

96 Internet
Egea-Àlvarez, Agustí, Fekriasl, Sajjad, Prieto-Araujo, Eduardo. "Improved droop co... <1%

97 Publication
M.S. Sachdev. "<![CDATA[A simulation technique for studying real and reactive po... <1%

98 Publication
Martin Ćalasan, Tatjana Konjić, Katarina Kecojević, Lazar Nikitović. "Optimal Alloc... <1%

99 Publication
Neeraj Kumar Singh, Vasundhara Mahajan. "Fuzzy Logic for Reducing Data Loss d... <1%

100 Publication
R. Thirunavukarasu, I.A. Chidambaram. "PI2 controller based coordinated control... <1%

101 Publication
J.G. Vlachogiannis, K.Y. Lee. "Reactive Power Control based on Particle Swarm Mul... <1%

102 Publication
Mahmoud A. Attia, Hany M. Hasanien, Almoataz Y. Abdelaziz. "Performance enha... <1%

103 Publication
Nakarmi, Upama. "Reliability Analysis of Power Grids and its Interdependent Infr... <1%

104 Publication
O. D. Lyantsev, T. V. Breikin, G. G. Kulikov, V. Y. Arkov. "Optimal multi-variable con... <1%

105 Publication
Sen, . "Analysis of Voltage Stability of Longitudinal Power Supply System Using an... <1%

106 Publication
Zhaowen Luan. "Power Transmission Paths Based Voltage Stability Assessment", ... <1%

107 Publication
Özmüslüman, Ahmet Talat. "Modified Forward Backward Sweep Power Flow Solut... <1%